



UNIVERSITY OF
LEICESTER

**Modelling Urban Visual Walkability of Leicester with Street
View Images Using Deep Learning and Unsupervised
Learning Techniques**

By

Adhib Hussain Syed

2023

In submitting this thesis, I confirm that it is my own work.

**A thesis submitted to the School of Geography, Geology and the
Environment, University of Leicester in partial fulfilment of the
requirements for the degree of Master of Science**

Abstract

This dissertation presented an application of deep learning and unsupervised learning techniques to model the visual walkability of Leicester based on Google Street View Images. The adapted Integrated Visual Walkability (IVW) framework quantified walkability by extracting perceptual features through semantic segmentation of street-level images using the SegFormer-B5 model. Four visual subindicators were derived: psychological greenery, visual crowdedness, outdoor enclosure, and visual pavement. The IVW index revealed localised variations in walkability, with high scoring streets situated in proximity to lower scoring ones. This reflects the complexity of interactions between fine-grained attributes that distinguish nuanced pedestrian experiences. Insufficient greenery emerged as the subindicator disproportionately limiting overall visual walkability. To uncover additional insights, cluster analysis was applied to identify latent relationships and spatial groupings among the subindicators across the city using the unsupervised K-Means and Fuzzy C-Means algorithms. Incorporating amenity diversity data highlighted correlations between urban vibrancy and greenery levels. However, limitations in accurately distinguishing pavement pixels impacted interpretability of the visual pavement subindicator. Overall, the results demonstrate the potential of computer vision and unsupervised learning techniques to advance walkability modelling through multidimensional assessment.

Acknowledgments

First and foremost, I would like to express my deepest gratitude to my supervisor, Dr. Stefano De Sabbata, for their invaluable guidance, encouragement, and support throughout my research. This dissertation is the culmination of everything I have learned from them during the past year. Their extensive expertise and insightful feedback at every stage were instrumental to the completion of this work. I am sincerely grateful for their dedication and commitment to my academic and professional growth.

Second, I wish to thank the outstanding faculty in the Department of Geography, especially Dr. Nick Tate, for their steadfast support and direction this past year. The fundamental concepts and techniques I learned during the MSc provided the essential building blocks for this dissertation.

Third, I am tremendously grateful to my dear friends and fellow residents of the G25 lab – Mridul, Naya, Nidhika, Razi, and Steven. Their presence made the long days and nights in the lab enjoyable and memorable. Without them, the past year would have been rather dull, so I thank them wholeheartedly.

Last but not least, I would like to thank my friends and family for their unconditional love, patience, and encouragement throughout this journey. I could not have done this without their unyielding belief in me.

Table of Contents

Abstract	i
Acknowledgments.....	ii
Table of Contents	iii
List of Figures.....	vi
List of Tables.....	x
List of Abbreviations.....	xi
Chapter 1. Introduction.....	1
1.1. Aims and Objectives.....	1
1.2. Dissertation Structure	2
Chapter 2. Literature Review	3
2.1. Concept of Walkability	3
2.2. Walkability Assessment.....	4
2.3. Computer Vision to Assess Walkability	5
2.4. Integrated Visual Walkability Framework.....	6
2.5. Urban Vibrancy and 15-minute Cities	7
2.6. Research Gaps	8
Chapter 3. Methodology	9
3.1. Defining the Study Area	11
3.2. Data Acquisition	13
3.2.1. Points Along the Street Network	13
3.2.2. Downloading the Street View Images	13
3.3. Semantic Segmentation of the Images	15
3.4. Data Preparation	19
3.4.1. Data Pre-processing	19

3.4.2. Data Processing	20
3.4.2.1. Developing the Visual Walkability Subindicators.....	20
3.4.2.2. Standardisation and Transformation	24
3.4.2.3. Categorisation of the Subindicators Data	27
3.4.2.4. Mean Subindicators per Hexagon	27
3.5. Developing the IVW Index.....	28
3.6. Cluster Analysis	29
3.6.1. K-Means Clustering Algorithm	29
3.6.2. Fuzzy C-Means Clustering Algorithm	30
3.6.3. Cluster Analysis with Points of Interest (POI) Diversity Data.....	31
Chapter 4. Results and Analysis	33
4.1. Visual Walkability Profile of Leicester	33
4.2. Cluster Analysis of the Visual Walkability Subindicators	47
4.2.1. K-Means Clustering	49
4.2.2. Fuzzy C-Means Clustering	54
4.2.2.1. Filtering Weak Membership Clusters.....	59
4.2.3. Cluster Analysis with the POI Diversity Data.....	62
4.2.3.1. K-Means Clustering	64
4.2.3.2. Fuzzy C-Means Clustering	69
4.2.3.2.1. Filtering Weak Membership Clusters.....	73
Chapter 5. Discussion	79
5.1. Model Limitations	79
5.2. IVW Framework Results	80
5.3. Cluster Analysis Results.....	82
5.3.1. With Visual Walkability Subindicators	82
5.3.2. With Visual Walkability Subindicators and POI Diversity Index.....	82

Chapter 6. Conclusion	84
List of References	86
Appendices	90
Appendix A: Python Code.....	91
Appendix B: Mean Subindicator Values per Hexagon	103
Appendix C: OpenStreetMap Amenities	105

List of Figures

Figure 2.1: Hierarchy of walking needs and their relevant associated visual factor (Alfonzo, 2005; Li, Yabuki and Fukuda, 2022).	3
Figure 3.1: Overview of the research methodology.	10
Figure 3.2: Map of the study area – Leicester, with a reference map inset highlighting the geolocation (Map scale: 1:60000).	12
Figure 3.3: An example SVI set (Heading 0, 120, 240 respectively) from the downloaded dataset. Contains Google Street View data © Google © 2023.	14
Figure 3.4: Overview of the SegFormer model – the input image is passed through the hierarchical transformer encoder to extract multi-scale features. These features are aggregated by the MLP decoder to produce the pixel-wise segmented output (Adapted from Xie et al. (2021), Contains Google Street View data © Google © 2023).	16
Figure 3.5: Reclassification process done to obtain the final categories.	20
Figure 3.6: SVI at University Road (52.62728, -1.12156). Contains Google Street View data © Google © 2023.	22
Figure 3.7: Histograms of the IVW subindicators.	24
Figure 3.8: Histograms of the standardised IVW subindicators.	25
Figure 3.9: Histograms of the standardised IVW subindicators without outliers.	26
Figure 3.10: Histograms of the transformed IVW subindicators.	26
Figure 3.11: Histogram of the POI Diversity Index.....	32
Figure 3.12: Map showing the Mean POI Diversity Index per hexagon (Map scale: 1:60000).	32
Figure 4.1: Integrated Visual Walkability Index for Leicester (Map Scale: 1:65000).....	34
Figure 4.2: Histogram showing the distribution of the Integrated Visual Walkability Index. .	35
Figure 4.3: Greenery Index for Leicester (Map Scale: 1:65000).	36
Figure 4.4: Visual Crowdedness Index for Leicester (Map Scale: 1:65000).	37
Figure 4.5: Outdoor Enclosure Index for Leicester (Map Scale: 1:65000).	38
Figure 4.6: Visual Pavement Index for Leicester (Map Scale: 1:65000).	39
Figure 4.7: The distribution of the categorised IVW Subindicators.....	42
Figure 4.8: Street View Imagery with an IVW score of 100. Contains Google Street View data © Google © 2023.....	43

Figure 4.9: Street View Imagery with an IVW score of 85. Contains Google Street View data © Google © 2023.....	43
Figure 4.10: Street View Imagery with an IVW score of 65. Contains Google Street View data © Google © 2023.....	44
Figure 4.11: Street View Imagery with an IVW score of 45. Contains Google Street View data © Google © 2023.....	44
Figure 4.12: Street View Imagery with an IVW score of 25. Contains Google Street View data © Google © 2023.....	45
Figure 4.13: Mean Integrated Visual Index per Hexagon (Map Scale: 1:60000).....	46
Figure 4.14: Pair plot visualising relationships between the visual walkability subindicators.	47
Figure 4.15: Elbow plot showing the optimal number of clusters for the walkability subindicators.....	49
Figure 4.16: Silhouette plot showing the optimal number of clusters for the walkability subindicators.....	49
Figure 4.17: Pair plot showing the four clusters of the walkability subindicators data obtained via K-Means.....	50
Figure 4.18: Heatmap showing the K-Means cluster averages for the visual walkability subindicators.....	51
Figure 4.19: Map of Leicester showing the visual walkability clusters from K-Means (Map Scale: 1: 60000).....	53
Figure 4.20: Elbow plot showing the optimal number of FCM clusters for the visual walkability subindicators.....	54
Figure 4.21: Silhouette plot showing the optimal number of FCM clusters for the visual walkability subindicators.....	54
Figure 4.22: Pair plot showing the four clusters of the walkability subindicators data obtained via FCM.....	55
Figure 4.23: Heatmap showing the FCM cluster averages for the visual walkability subindicators.....	56
Figure 4.24: Map of Leicester showing the visual walkability clusters from FCM (Map Scale: 1: 60000).....	58

Figure 4.25: Bar plot comparing the size of FCM clusters before and after filtering.....	59
Figure 4.26: Pair plot showing the four clusters of the walkability subindicators data obtained via FCM after filtering.....	60
Figure 4.27: Map of Leicester showing the visual walkability clusters from FCM after filtering (Map Scale: 1: 60000).....	61
Figure 4.28: Alluvial diagram representing the flow of cluster assignment of the hexagons between the two clustering techniques.	62
Figure 4.29: Pair plot visualising relationships between the visual walkability subindicators and the POI diversity index.	63
Figure 4.30: Elbow plot showing the optimal number of clusters for the walkability subindicators and the POI diversity.	64
Figure 4.31: Silhouette plot showing the optimal number of clusters for the walkability subindicators and POI diversity data.	64
Figure 4.32: Pair plot showing the four clusters of the walkability subindicators and POI diversity data obtained via K-Means.....	65
Figure 4.33: Heatmap showing the K-Means cluster averages for the walkability subindicators and POI diversity.	66
Figure 4.34: Map of Leicester showing the walkability clusters from K-Means (Map Scale: 1: 60000).....	68
Figure 4.35: Elbow plot showing the optimal number of FCM clusters for the walkability subindicators and the POI diversity.	69
Figure 4.36: Silhouette plot showing the optimal number of FCM clusters for walkability subindicators and POI diversity.....	69
Figure 4.37: Pair plot showing the four clusters of the walkability subindicators and POI diversity data obtained via FCM.....	70
Figure 4.38: Heatmap showing the FCM cluster averages for the walkability subindicators and POI diversity.	71
Figure 4.39: Map of Leicester showing the walkability clusters from FCM (Map Scale: 1: 60000).....	72
Figure 4.40: Bar plot comparing the size of FCM clusters before and after filtering.	73

Figure 4.41: Pair plot showing the four clusters of the walkability subindicators and POI data obtained via FCM after filtering.....	74
Figure 4.42: Map of Leicester showing the walkability clusters from FCM after filtering (Map Scale: 1: 60000).....	75
Figure 4.43: Alluvial diagram representing the flow of cluster assignment of the hexagons between the two clustering technique for the walkability subindicators and POI diversity. .	76
Figure 4.44: Map of Leicester showing the visual walkability clusters from K-Means (Map Scale: 1: 60000).	77
Figure 4.45: Map of Leicester showing the visual walkability clusters from FCM (Map Scale: 1: 60000).....	77
Figure 4.46: Map of Leicester showing the walkability clusters from K-Means (Map Scale: 1: 60000).....	78
Figure 4.47: Map of Leicester showing the walkability clusters from FCM (Map Scale: 1: 60000).....	78
Figure 5.1: SVI with inaccurate road/pavement segmentation (IVW:70, gi:4, Ci:4, Ei:4, Pi:2), (Road: Orange, Pavement: Yellow). Contains Google Street View data © Google © 2023....	79
Figure 5.2: SVI with inaccurate road/pavement segmentation (IVW:65, Gi:4, Ci:4, Ei:4, Pi:1), (Road: Orange, Pavement: Yellow). Contains Google Street View data © Google © 2023....	80
Figure B-1: Mean Psychological Greenery per Hexagon (Map scale: 1:60000).....	103
Figure B-2: Mean Visual Crowdedness per Hexagon (Map scale: 1:60000).....	103
Figure B-3: Mean Outdoor Enclosure per Hexagon (Map scale: 1:60000).....	104
Figure B-4: Mean Visual Pavement per Hexagon (Map scale: 1:60000)	104
Figure C-1: Points of Interest in Leicester (Map scale: 1:60000).....	110

List of Tables

Table 3.1: Pseudocode highlighting a simplified version of the process used to obtain SVI.	.15
Table 3.2: Pseudocode highlighting a simplified version of the process used to segment SVI.	
.....	18
Table 3.3: Categorisation of the subindicators based on the Jenks classes. 27
Table 4.1: Cluster counts before and after removing hexagons with membership degrees below 0.5. 60
Table 4.2: FCM Cluster counts before and after removing hexagons with membership degrees below 0.5. 73

List of Abbreviations

IVW	Integrated Visual Walkability
SVI	Street View Images
FCM	Fuzzy C-Means
IMD	Indices of Multiple Deprivation
Gi	Greenery Index
Ci	Crowdedness Index
Ei	Enclosure Index
Pi	Pavement Index

Chapter 1. Introduction

Walkability refers to the extent to which the built environment promotes and supports walking (Southworth, 2005). It is an important concept in urban planning and design, as highly walkable neighbourhoods can encourage physical activity, social interactions, sustainable transportation, economic development, and overall better quality of life (Litman, 2003). Assessing and measuring walkability has been an active area of research, with studies utilising various data sources and methodologies. Recently, computer vision techniques applied to street-level imagery have emerged as a promising approach to evaluate the fine-grained visual features of the walking environment (Hasan, Oh and Kwigizile, 2021).

This dissertation focuses on modelling the visual walkability of Leicester utilising deep learning and unsupervised learning techniques. Specifically, it employs a pre-trained semantic segmentation model called SegFormer-B5 to extract perceptual features from Google Street View Images (SVI) sampled along the street network. These features are used to quantify visual walkability according to an adapted version of the Integrated Visual Walkability (IVW) framework proposed by Zhou *et al.* (2019). The study also applies cluster analysis methods, including K-Means and Fuzzy C-Means (FCM) clustering, to gain additional insights into the patterns and structure of visual walkability indicators. Furthermore, points of interest (POI) data measuring amenity diversity are incorporated to relate visual walkability to accessibility and vibrancy principles of the 15-minute city.

1.1. Aims and Objectives

The overarching aim of this dissertation is to apply the aforementioned computational techniques to evaluate and analyse the walkability of Leicester based on visual environment attributes. The specific research questions are:

- 1) What is the visual walkability profile of Leicester according to the adapted IVW framework?
 - 2) What additional insights does cluster analysis, in particular the K-Means and Fuzzy C-Means clustering techniques, provide into visual walkability patterns beyond the IVW framework?
-

- 3) What additional insights into visual walkability and service access are provided by including amenity diversity data in the clustering analysis?
- 4) How does visual walkability compare and relate to accessibility-focused walkability as measured by amenity diversity in the context of 15-minute city principles?

This research builds upon recent work utilising street-level imagery and deep learning for urban analysis, while also exploring novel applications of unsupervised learning techniques for understanding walkability. The results aim to provide urban planners and designers with enhanced computational tools to evaluate and improve walkability in support of healthy, sustainable, and vibrant neighbourhoods.

1.2. Dissertation Structure

This dissertation will be presented in the following structure:

Chapter 1 Introduction: This chapter will provide insight into the chosen research topic as well as highlight the main aim and key objectives of the project.

Chapter 2 Literature Review: This chapter reviews the relevant literature on walkability assessment, the use of deep learning to evaluate urban environments, the integrated visual walkability framework, and principles of urban vibrancy and 15-minute neighbourhoods.

Chapter 3 Methodology: This chapter details the methods used in this research, including the acquisition and processing of data, the calculation of the visual walkability subindicators and the development of the IVW index, and the application of the cluster analysis techniques.

Chapter 4 Results and Analysis: This chapter presents the results of the visual walkability analysis and cluster analysis. It analyses and discusses key findings, including the visual walkability profile of Leicester.

Chapter 5 Discussion: This chapter discusses the implications of the results concerning the research aim, objectives, and questions. It also highlights limitations and areas for further research.

Chapter 6 Conclusion: The final chapter summarises the overall conclusions of the dissertation and provides recommendations based on the research findings.

Chapter 2. Literature Review

2.1. Concept of Walkability

While there are various operational definitions for walkability, Southworth (2005) provides an influential conceptualisation, defining walkability as the degree to which the physical environment promotes walking by ensuring pedestrian safety, comfort, and access to diverse destinations within a reasonable amount of time, while also providing sufficient visual interest. This multifaceted definition incorporates key factors identified as shaping walkability and walking behaviour, including feasibility, accessibility, safety, comfort, and pleusability, as shown in the hierarchy of walking needs in Figure 2.1 (Alfonzo, 2005).

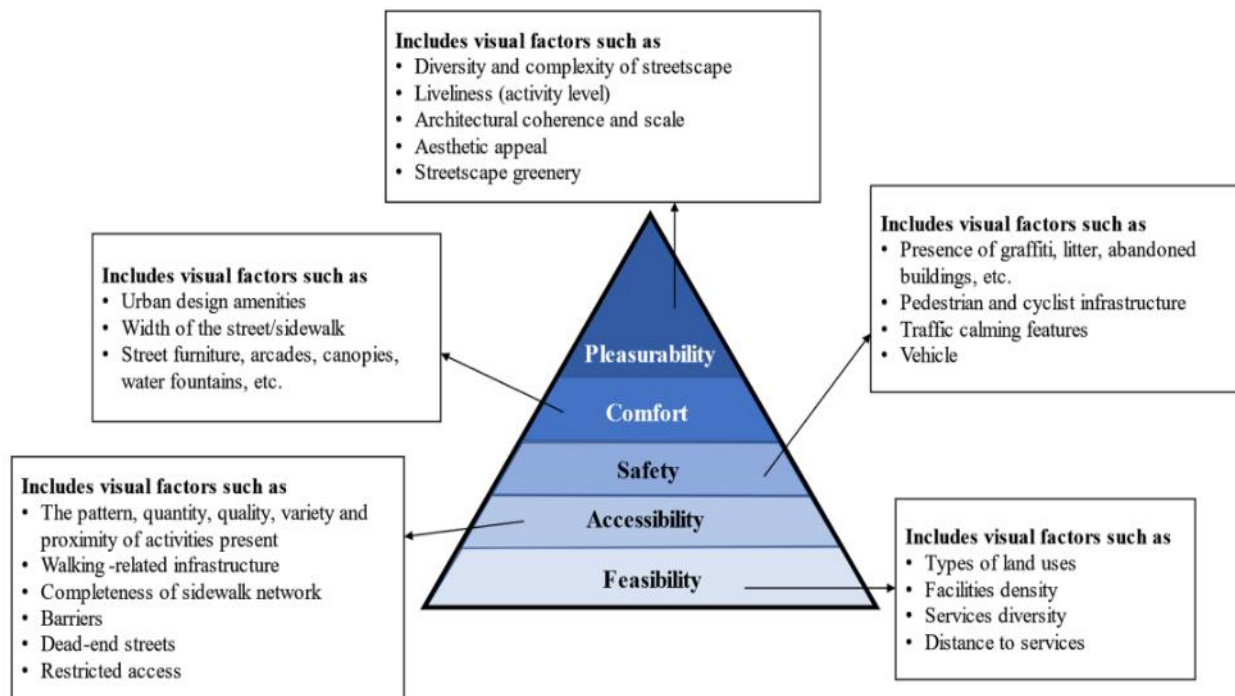


Figure 2.1: Hierarchy of walking needs and their relevant associated visual factor (Alfonzo, 2005; Li, Yabuki and Fukuda, 2022).

These factors operate at different scales, with some relating to the wider neighbourhood environment such as connectivity and proximity to amenities, while others focus on the finer-grained street-level walking experience encompassing pavement quality, enclosure, and street greenery. There are thus different conceptual lenses on walkability, and various

methodological approaches have been used to measure attributes at the neighbourhood (macroscale) versus street (mesoscale-microscale) level. The subsequent section will provide an overview of common walkability assessment methods and data sources, spanning macroscale audits and indicators to mesoscale-microscale perceptual surveys and computer vision techniques.

2.2. Walkability Assessment

Walkability assessment approaches can be broadly categorised into three – perception-based methods relying on surveys and subjective judgements, measurement-based methods using systematic audits and indicators, and hybrid methods combining subjective and objective techniques (Hasan, Oh and Kwigizile, 2021). These vary in their ability to capture macroscale factors associated with overall neighbourhood walkability versus mesoscale-microscale factors shaping street-level walking experiences.

Perception-based methods gather insights directly from residents or experts regarding the walking environment. Surveys record perceived walkability attributes like safety, comfort, and visual appeal (Kelly *et al.*, 2011). For instance, Park, Deakin and Lee (2014) conducted surveys in Mountain View, California to develop a perception-based walkability index incorporating microlevel environmental qualities. Respondents evaluated factors like pavement facilities, street enclosure, and pedestrian infrastructure. Kelly *et al.* (2011) used multiple survey techniques in Leeds, UK to assess pedestrian route preferences. This included an on-street survey to rate attributes along a given route, and a mobile interview to capture live experiences while walking. Key factors highlighted were pavement cleanliness, safe crossings, connectivity, and security. Such perception-based approaches provide first-hand insights into experiential walkability factors that enhance or detract from walking. However, surveys are limited in scale and reliant on subjective assessments.

Measurement-based methods use audits, GI systems, and physical tools to objectively gauge built environment variables. For instance, Frank *et al.* (2010) developed a walkability index for the Neighbourhood Quality of Life Study in Atlanta integrating parcel-level data on residential density, land use mix, street connectivity, and retail floor area ratio. Lefebvre-Ropars and Morency (2018) tested various walkability indices against observed trip data in Montreal to identify the optimal built environment predictors and spatial scales. Meanwhile, Erath, van

Eggermond and Ordóñez Medina (2016) created an open-source GIS tool to calculate accessibility indicators calibrated to pedestrian route preferences where users could weight destination attractiveness and simulate infrastructure changes. Such measurement-based approaches provide standardised, scalable ways to quantify walkability components. They can also be utilised to assess walkability factors relevant to both macroscale and mesoscale-microscale level indicators. However, they rely on available spatial data and cannot be easily generalised to use on different areas that may have a different urban form.

Traditionally, street-level attributes relied on labour-intensive in-person audits with limited coverage. However, emerging computer vision techniques applied to readily available streetscape imagery can objectively measure perceptual features at citywide scales (Yin and Wang, 2016). Deep learning methods like semantic segmentation automate fine-grained audits, unlocking new mesoscale-microscale walkability insights. This can complement the established macroscale GI system indicators for a hybrid approach to assessing walkability. The next section reviews key developments in using computer vision and deep learning for walkability assessment.

2.3. Computer Vision to Assess Walkability

The proliferation of street level imagery through sources like Google Street View has enabled new computer vision approaches to evaluate walkability, complementing traditional methods based on surveys, audits, and GIS data (Hasan, Oh and Kwigizile, 2021). Advancements in deep learning have allowed for the analysis of visual attributes related to walkability at much larger scales than previously feasible. Semantic segmentation techniques can label objects like buildings, trees, pavements, and roads in streetscape images, thus providing a means to quantify the built environment enabling walkability assessment (Nagata *et al.*, 2020). Other methods have measured visual enclosure, greenery, and other factors with SVI.

Pliakas *et al.* (2017) compared foot-based and virtual audits in 17 British towns, finding good agreement and that virtual audits effectively captured more objective features. Lu (2018) used SVI and the PSPNet model to relate eye-level greenness exposure to resident's walking behaviours. Villeneuve *et al.* (2018) analysed street view greenery in Ottawa, Canada along with survey data to assess links between greenness, recreational physical activity, and health. Yin and Wang (2016) applied machine learning techniques to SVI in New York to generate

visual enclosure measures associated with observed pedestrian volumes. These examples demonstrate the value of street-level imagery for built environment analysis, with computer vision techniques enabling large-scale standardised measurement of experiential attributes relevant to walkability.

Building on these precedents showing the value of street-level imagery for built environment analysis, recent research demonstrates the potential for computer vision and deep learning to directly quantify walkability from streetscape images. Nagata *et al.* (2020) applied semantic segmentation to model streetscape walkability previously scored by audits in Tokyo. Koo, Guhathakurta and Botchwey (2022) used computer vision to extract mesoscale factors from Atlanta streetscapes associated with walking. Jeon and Woo (2023) measured neighbourhood greenery and openness in Seoul to evaluate walkability in areas with public housing. Such examples showcase automated extraction of specific urban design attributes relevant to walkability enabled by advances in computer vision.

Other recent studies have directly measured a more complete concept of perceptual walkability using streetscape visual data. Li, Yabuki and Fukuda (2023) integrated computer vision with other urban data sources to evaluate physical and perceived walkability criteria. Notably, Zhou *et al.* (2019) proposed the Integrated Visual Walkability (IVW) framework, which is utilised in this study, and employed deep learning on streetscapes to quantify visual features related to experiential walkability in Shenzhen. This emerging research demonstrates that computer vision and deep neural networks enable standardised quantification of complex experiential attributes from street-level scenes, advancing walkability assessment.

2.4. Integrated Visual Walkability Framework

An influential conceptual framework for understanding visual walkability was proposed by Zhou *et al.* (2019), termed the Integrated Visual Walkability (IVW) framework. This framework views walkability as an indicator of psychological and visual comfort for pedestrians. It incorporates four key dimensions derived from urban design and environmental psychology literature: 1) Psychological Greenery, reflecting the visibility of vegetation which can positively influence mood; 2) Visual Crowdedness, representing obstacles and clutter negatively impacting the walking experience; 3) Outdoor Enclosure, characterising the room-like quality

of outdoor spaces framed by vertical elements; and 4) Visual Pavement, capturing the balance of roads versus pavements influencing perceptions.

To quantify these dimensions, Zhou *et al.* (2019) utilised computer vision and deep learning to semantically segment street view imagery into different features. The proportion of pixels belonging to each class was used to calculate the visual walkability subindicators for the four dimensions, which were then standardised into 1-5 ordinal scales. More details about how these walkability subindicators are computed is provided in Section 3.4.2.1. Finally, an integrated visual walkability index summing these subindicators was proposed to represent overall visual walkability. This framework demonstrates how emerging computer vision capabilities can extract perceptual features from streetscape images to model complex experiential concepts like walkability relatively easily when compared with prior methods.

2.5. Urban Vibrancy and 15-minute Cities

Urban Vibrancy refers to the level of activity and vitality in a neighbourhood, capturing how dynamic, lively, and socially engaging an area is (Botta and Gutiérrez-Roig, 2021). Research has linked vibrancy to the diversity of amenities and destinations present locally, as measured by entropy indices of amenity types based on data sources like OpenStreetMap. Areas with more amenities encourage social interactions and promote foot traffic. Thus, amenity diversity provides an accessibility-focused measure of walkability complementary to visual walkability.

The emerging 15-minute city concept prioritises proximity, envisioning urban neighbourhoods where daily needs are accessible within a short walk (Allam *et al.*, 2022). This aligns with visual walkability's focus on experiential factors that attract pedestrians to streets. While amenity diversity provides a utilitarian measure of walkable access, visual walkability captures the living experience of a place. Cluster analysis incorporating both these perspectives can reveal relationships between them, exploring whether visually appealing streets also offer functional access to amenities. This demonstrates how computational methods enable multifaceted walkability measurement, linking 15-minute city principles to subjective qualities of real urban spaces. The goal is neighbourhood environments which are visually engaging and vibrant, while also offering proximity to the diversity of destinations needed for everyday life.

2.6. Research Gaps

While prior work has explored visual walkability using street view imagery, a specific computational walkability analysis of the city of Leicester is still lacking. Currently, there is no established visual walkability index for Leicester. Furthermore, the existing visual walkability framework relies on subjective scoring to categorise subindicators. This research takes an alternative approach by developing the subindicators statistically to quantify them more objectively. The study then employs a modified IVW framework with these enhanced subindicators. Additionally, instead of just aggregating the subindicators into a composite index, cluster analysis is also utilised to preserve nuanced relationships between distinct visual attributes. Moreover, amenity diversity data is incorporated alongside visual walkability to relate accessibility considerations in line with 15-minute city principles. The multi-method analysis linking visual appeal and proximity to amenities provides new multifaceted insights into walkability. Thus, this dissertation helps address gaps by: 1) performing the first computational walkability study specific to Leicester using SVI, 2) developing an objective IVW framework using statistical subindicators, 3) applying cluster analysis to uncover patterns within the subindicators, and 4) relating visual walkability and amenity diversity to capture experiential and utilitarian aspects of place.

Chapter 3. Methodology

This chapter presents the methodology followed to develop the Integrated Visual Walkability (IVW) index for Leicester. Firstly, Section 3.1 defines the study area and its spatial extent in detail. Following this, Section 3.2 describes the process of acquiring the necessary datasets and downloading the Street View Images (SVI) required for the analysis from Google Street View. The process used to run the semantic segmentation model on the downloaded SVI and generate pixel-level outputs is then explained in Section 3.3.

Subsequently, Section 3.4 elaborates on the data preparation techniques employed, which includes the development of the walkability variables and formulation of the visual walkability subindicators, standardisation and transformation of variables, categorisation of data, and aggregation of subindicators to a hexagonal level.

Section 3.5 then describes the development of the IVW index from the walkability subindicators, following a modified version of the approach utilised by Zhou *et al.* (2019). An alternative approach of aggregating the subindicators based on cluster analysis is presented in Section 3.6, which is divided into two subsections for the cluster analysis of the walkability subindicators, which is then again divided into two subsections - K-Means and Fuzzy C-Means (FCM) clustering techniques, and the cluster analysis of the walkability subindicators and the Points of Interest (POI) Diversity Data. The clustering aims to identify nuanced patterns among the visual walkability subindicators that may be obscured during the simplified aggregation process of the IVW framework.

Excluding the use of SVI, the adopted methodology made use of open-source datasets and tools to ensure reproducibility. The entire project was done utilising Python 3.9, and the required libraries, along with the pseudocode and the complete code is available in the Appendix A.

In summary, this chapter delineates the key phases in developing a visual walkability index from data acquisition to index creation and cluster analysis. Figure 3.1 presents a general overview of the methodology adopted to complete this study.

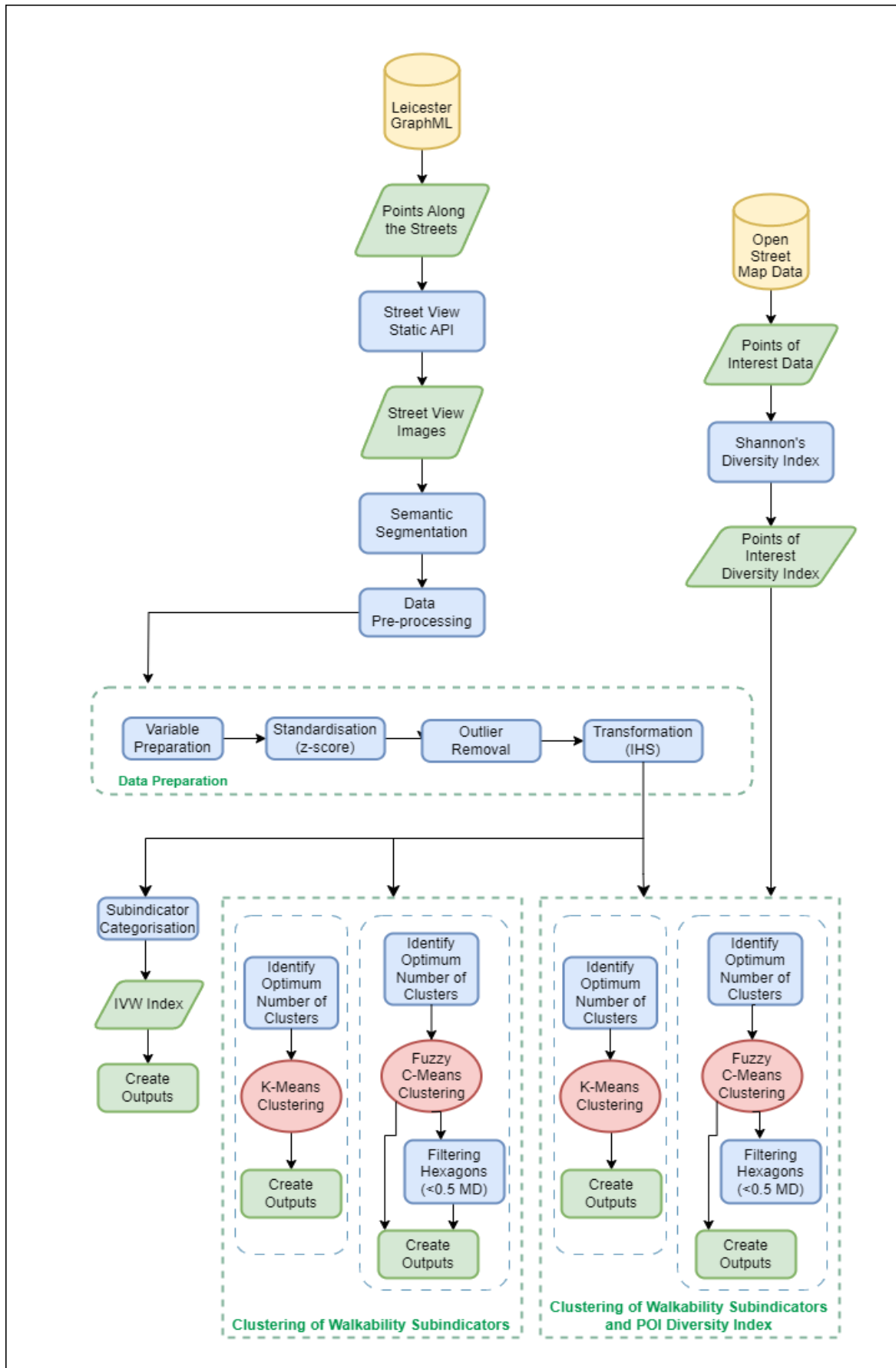


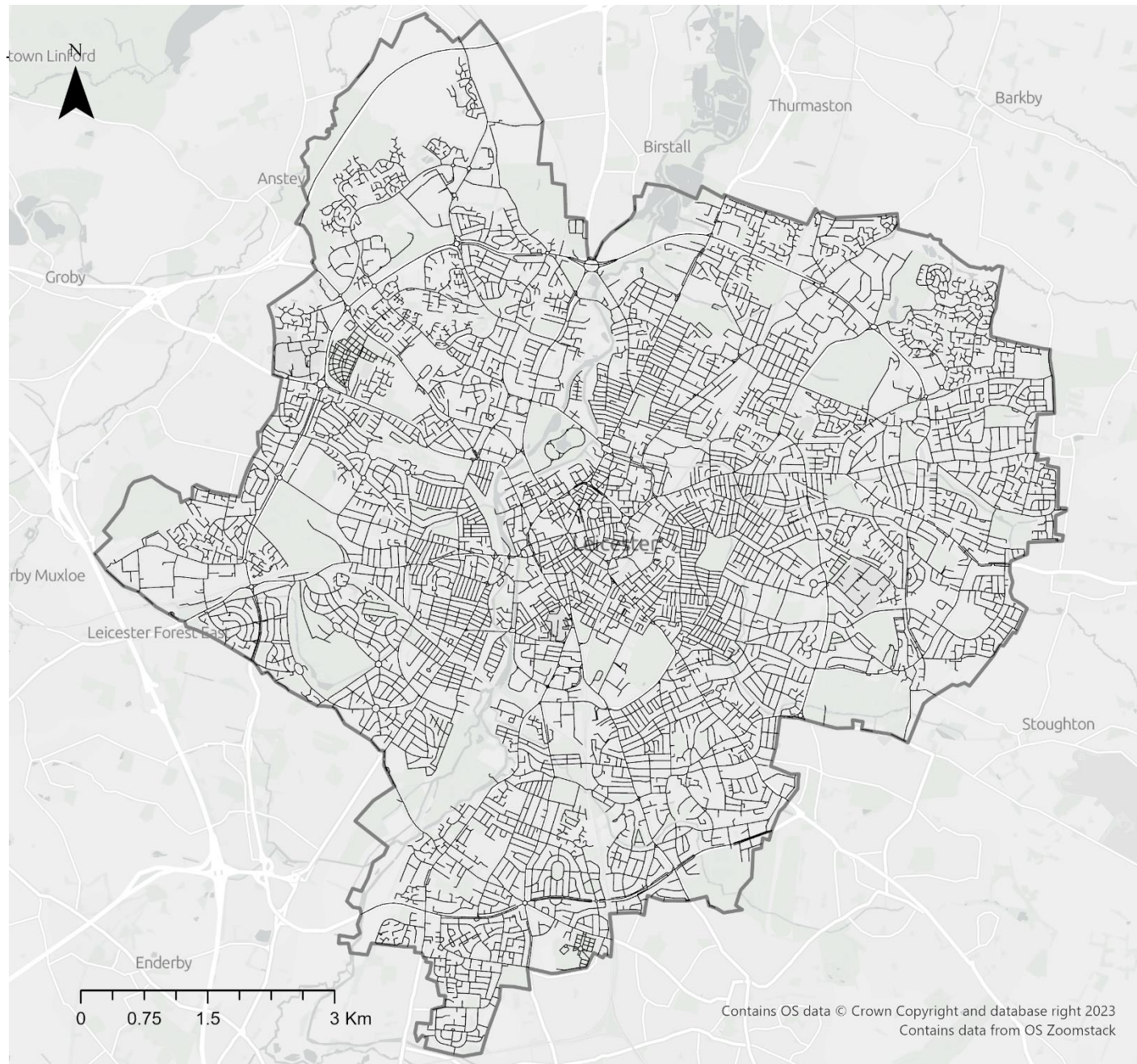
Figure 3.1: Overview of the research methodology.

3.1. Defining the Study Area

The study area for this project is the city or unitary authority area of Leicester, situated in the East Midlands region of England. With a population of 368,600 in 2021, it is the largest city in the East Midlands region (ONS, 2022), and has an extensive network of roads and a diverse variety of streets spanning approximately 940 kilometres, as seen in Figure 3.2. However, no previous studies have quantitatively assessed the walkability or visual walkability of Leicester's street network.

With the city centre containing the retail heart of the city clustered around the High Cross, and with economic hubs outside the city centre along various roads such as Belgrave Road, London Road, Narborough Road, and Queens Road, the suburban streets in the city are well-connected to various amenities offering great accessibility for pedestrians (Leicester City Council, 2020). Home to two universities – the University of Leicester and the De Montfort University, countless young professionals take up residence in the many Victorian terraces and modern developments encircling the city centre area. The city also has a ring road encircling it, the A563, in addition to the other major roads and streets in the city.

Through the Connecting Leicester initiative launched by the Leicester City Council, the city has undergone many changes including the opening of new public squares, improvement of cycling and walking infrastructure, and increased pedestrianisation of the city (Leicester City Council, 2020). Given ongoing pedestrianisation efforts and the reliance on walking for transportation, developing pleasant and walkable streets is a priority for Leicester. A visual walkability index can aid these efforts by quantitatively assessing patterns of visual walkability and identifying streets needing improvement. Focusing on Leicester's dense urban core allows an in-depth examination of fine-grained visual elements affecting the pedestrian experience within the city.



Study Area



Legend

- England
- Road Network
- Boundary of Leicester

Data Source: Ordnance Survey

Figure 3.2: Map of the study area – Leicester, with a reference map inset highlighting the geolocation (Map scale: 1:60000).

3.2. Data Acquisition

3.2.1. Points Along the Street Network

As a prerequisite to downloading the SVI, it was necessary to obtain points along the street network of Leicester. For this purpose, the street network data for Leicester was downloaded as a GraphML file originally sourced from (Boeing, 2020), which contained 13,293 nodes. Pre-processing was done on this raw network in Python using the OSMnx (Boeing, 2016) library to remove duplicate nodes and edges, and then converted to a cityseer format to utilise functions provided by the cityseer library (Simons, 2023). The streets were then segmented at 50 meter intervals along each street to generate point locations that would serve as locations for extracting SVI, similar to the approach by Li, Yabuki and Fukuda (2022). Segmenting at regular intervals allows for a consistent spatial sampling of the streetscape. The cityseer data was then converted to a GeoDataFrame containing the node geometries in British National Grid coordinates, then transformed to longitude/latitude for integration with the Street View Application Programming Interface (API). To facilitate batched downloads, the point dataset was split into four subsets containing between 8037-8039 points each. This process resulted in around 32,150-point locations distributed across Leicester's Street network for extracting SVI, with roughly one point per 50 meters along each street. The code for this section of the methodology is provided in Appendix A.

3.2.2. Downloading the Street View Images

To download the SVI, the Static Street View API provided by Google was utilised (Google, 2023). This API allows downloading of images closest to specified latitude and longitude coordinates that match configured parameters. The Python library google_streetview (Wen, 2019) provided a convenient interface to access the API and its functions.

The API was configured to download 640x640 pixel images at a 120° field of view. This resolution was selected as the image quality would be sufficiently high enough to capture relevant streetscape elements while maintaining manageable file sizes for processing. For each point location obtained in section 3.2.1, the API was called three times with compass headings of 0°, 120° and 240° to acquire three different perspectives of the streetscape at each location, obtaining panorama data with 360° coverage. The downloading process was executed in four batches corresponding to the four subsets of point locations generated

previously. The algorithm loops through each heading and point in a given batch to generate API calls with the required latitude, longitude, and heading parameters. Unique panorama IDs (pano ID) were tracked to avoid duplicating images. A multi-threaded approach using Python's ThreadPoolExecutor enabled 10 images to be downloaded in parallel per batch, improving efficiency.

The downloaded metadata and images were saved in separate systematic folder structures organised by heading and batch number. Comprehensive JSON files containing all metadata returned by the API were consolidated for each heading and batch. In total, 90,742 SVI were successfully downloaded covering Leicester's entire street network. This substantial image dataset provides extensive coverage of the urban streetscape from three angles, enabling accurate assessment of visual walkability in subsequent steps. Simplified pseudocode of the process is highlighted in Table 3.1 below, while the full Python code for this process is presented in Appendix A. An example of a downloaded Street View Image is shown in Figure 3.3.



Figure 3.3: An example SVI set (Heading 0, 120, 240 respectively) from the downloaded dataset. Contains Google Street View data © Google © 2023.

Table 3.1: Pseudocode highlighting a simplified version of the process used to obtain SVI.**Algorithm 1:** Download Street View Images

Data: Point location batches (batch_1, batch_2, batch_3, batch_4)

Input: Headings (0, 120, 240)

Output 1: Street view images saved in /images_{heading}/ folder

Output 2: Metadata JSON files saved in /metadata_{heading}_{batch}.json

```

1  metadata_list ← empty list
2  For batch in Data do
3      For heading in Input do
4          For point in batch do
5              params ← {location: point.lat,point.lon, size: 640x640, fov: 120,
6                  heading: heading}
7              response ← call_streetview_api(params)
8              If response.metadata.status == 'OK' then
9                  save_image(response.image, f'Output 1
10                     folder/{response.pano_id}.jpg')
11                 Extract metadata from response
12                 Append metadata to metadata_list
13             End if
14         End for
15     End for
16     save_json(metadata_list, f'Output 2 folder_{heading}_{batch}.json')
17 
```

3.3. Semantic Segmentation of the Images

As highlighted in section 2.3, semantic segmentation is an active research area in computer vision with many applications for urban planning and walkability assessments (Nagata *et al.*, 2020; Li, Yabuki and Fukuda, 2022). Semantic segmentation involves assigning a class label such as ‘road’ or ‘car’ to each relevant pixel in an image, which allows for the parsing of images into semantically meaningful regions (Hao, Zhou and Guo, 2020). Recent advances in semantic segmentation models have enabled their application for parsing SVI to quantify walkability. One such state-of-the-art model is SegFormer, proposed by Xie *et al.* (2021).

SegFormer adopts a hierarchical transformer-based encoder-decoder architecture (Figure 3.4) and achieves exceptional accuracy on semantic segmentation tasks while being highly efficient. The transformer encoder extracts multi-scale features from the input image using self-attention layers arranged in a hierarchical structure. This generates both high-resolution coarse features and low-resolution fine-grained features. The lightweight multilayer perceptron (MLP) decoder aggregates information from the different levels to produce a pixel-wise segmentation mask.

Compared to prior approaches involving convolutional or attention modules, SegFormer demonstrates considerably higher accuracy and efficiency on semantic segmentation benchmarks (Xie *et al.*, 2021). For instance, SegFormer-B5 attains 84% mean intersection of union (mIoU) on the Cityscapes dataset, while being 5 times faster than previous methods. Additionally, the model does not need fixed positional encodings, making it robust to varied image sizes. This combination of accuracy, speed, and flexibility makes SegFormer highly appealing for segmenting complex street scenes to quantify visual walkability.

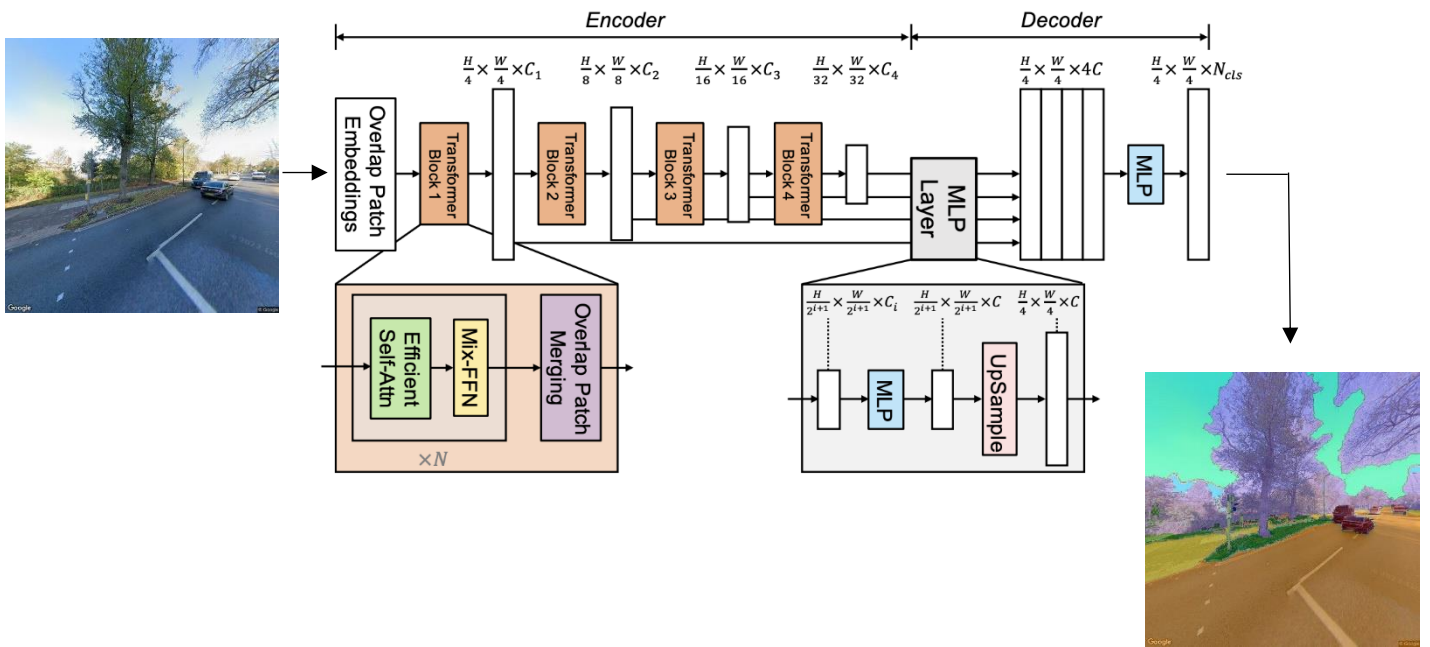


Figure 3.4: Overview of the SegFormer model – the input image is passed through the hierarchical transformer encoder to extract multi-scale features. These features are aggregated by the MLP decoder to produce the pixel-wise segmented output (Adapted from Xie *et al.* (2021), Contains Google Street View data © Google © 2023).

For this study, the SegFormer-B5 model from the HuggingFace Transformers library was utilised. This model has been trained on the ImageNet-1K dataset for the initial pretraining and later finetuned on street view imagery from the Cityscapes dataset (Cordts *et al.*, 2016) at 1024x1024 resolution. The pretrained model was loaded and set to run on a GPU using PyTorch for improved performance. As mentioned in the previous section, the images that would be run through the model were organised into three batches based on the heading. An image generator function was defined to iteratively load the images from each batch in smaller segmented batches of 50-75 images to optimise memory usage. This function also parsed relevant metadata including latitude, longitude, and unique panorama ID from each image filename using a defined regular expression pattern.

These segmented image batches were input into a robust process_images pipeline designed to efficiently execute semantic segmentation at scale. Simplified pseudocode of this process is highlighted in Table 3.3, while the complete code is presented in Appendix A. The images were passed through the SegFormer model in evaluation mode with PyTorch no_grad enabled to reduce computational overhead by disabling gradient calculation. This generated pixelwise semantic segmentation logit outputs for each 640x640 pixel image.

Post-processing was applied to transform the raw logits into usable walkability metrics. The number and percentage of pixels belonging to each of the 20 Cityscapes semantic classes was calculated by thresholding the logits and normalising to account for varied object proportions. These percentages and pixel counts were compiled alongside the latitude, longitude, and panorama ID into dictionaries for each image and saved in dataframes.

Additionally, the predicted labels were resized to the original image dimensions and utilised to generate coloured masks corresponding to each semantic class based on a predefined qualitative colour palette. These masks were overlayed onto the original images with 50% transparency to produce composite visualisations that clearly revealed the semantic segmentation results. The composited images were saved to disk to enable manual verification and quality checks.

Several optimisation techniques were employed to enhance performance and ensure scalability. The GPU memory cache was cleared periodically and processing was intentionally paused for 30 seconds after every 15 batches to prevent out-of-memory failures. In total, this

robust batched pipeline efficiently parsed 90,742 SVI using SegFormer, facilitating the development of precise semantic segmentation statistics and composite images for quantifying the walkability-related features.

Table 3.2: Pseudocode highlighting a simplified version of the process used to segment SVI.

Algorithm 2: Semantic Segmentation of the SVI Utilising the SegFormer-B5 Model

Data:

- SVI Dataset
- Label names and colour palette

Input 1: Images folder path (*images_folder*)

Input 2: Overlayed images folder path (*overlaid_images_folder*)

Input 3: Results DataFrame (*df_results*)

Input 4: Segmentation batch size (*seg_batch_size*)

Output 1: Updated Results DataFrame (*df_results*)

- 1 Initialise an empty list **results_list** to store the segmentation results.
 - 2 Initialise a **batch_counter** to keep track of the number of processed batches.
 - 3 List **image_files** contain the names of all image files in the *images_folder*.
 - 4 Loop over image batches using the *image_generator* function:
 - 5 Initialise **batch_images** and **batch_metadata** lists.
 - 6 For each **image_file** in the batch, extract **latitude**, **longitude**, and **pano_id** from the filename using regular expressions.
 - 7 Load the **image** from *images_folder*.
 - 8 Append the **image** to **batch_images** and **metadata** to **batch_metadata**.
 - 9 If the batch size exceeds **seg_batch_size**, yield **batch_images** and **batch_metadata**, and reset **batch_images** and **batch_metadata**.
 - 10 For each batch of **images** and **metadata**:
 - 11 Initialise **batch_logits** to store model logits for each **image** in the batch.
 - 12 Loop over **batch_images**:
 - 13 Extract image features using the **feature_extractor** and move them to the GPU.
 - 14 Set the model to evaluation mode and make predictions for the **image**.
 - 15 Append the **logits** to **batch_logits**.
 - 16 Get the image height and width for later use.
-

```
17 Loop over batch_metadata:  
18     Try the following for each image:  
19         Retrieve the image and logits.  
20         Calculate the percentage and pixel count for each segmented object.  
21         Normalise the percentages based on the total percentage.  
22         Obtain the predicted labels with the highest probability.  
23         Create a colour mask for each label and blend it with the original image.  
24         Save the overlaid image with the format  
25             overlay_latitude_longitude_pano_id.jpg.  
26         Create result dictionaries for both percentage and pixel count data.  
27         Append the combined dictionary to results_list.  
28         If an error occurs during processing, print an error message and continue to the  
29             next image.  
30         Clear the GPU memory.  
31         Increment batch_counter by 1.  
32         If batch_counter is a multiple of 15, pause for 30 seconds to prevent GPU memory  
33             exhaustion.  
34     Compile results into Output 1
```

3.4. Data Preparation

3.4.1. Data Pre-processing

After obtaining the segmentation results, pre-processing was undertaken to transform the labels into categories more directly relevant to visual walkability. Some of the labels were used as is, but some were combined together into new composite variables – ‘greenery’, ‘obstacles’, and ‘built area’. The reclassification that was done is highlighted below in Figure 3.5. The original constituent categories were then dropped. The final categories that would be utilised for the development of the visual walkability subindicators include road, sidewalk, greenery, built area, fence, sky, and obstacles. The pixel counts across the categories were then summed up to obtain the total pixels for each image.

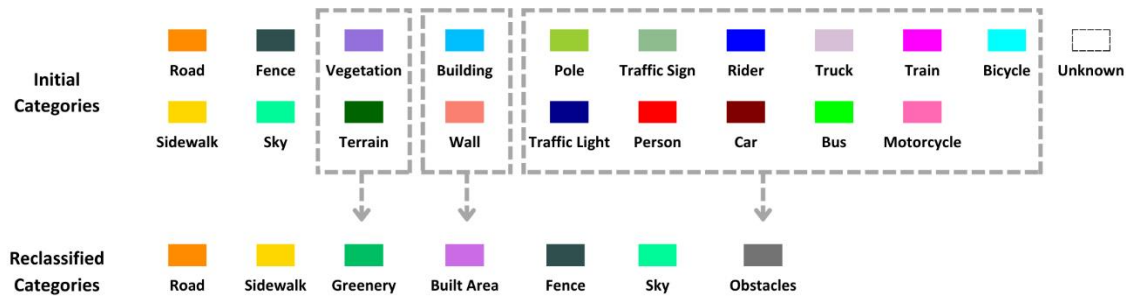


Figure 3.5: Reclassification process done to obtain the final categories.

The dataframes for the three headings were then merged and filtered to only retain the images with panorama IDs present across all headings for consistency. The data was grouped by latitude, longitude, and panorama ID before being aggregated through summation. Further filtering was applied to remove anomalous panorama IDs. This pre-processing condensed the various categories into a smaller set of interpretable features relevant to visual walkability, while aggregating the data to a single record per geographic point for analysis. The final categories follow similar groupings used in prior work for the IVW index development by Zhou *et al.* (2019). The dataset following this pre-processing contained 27,696 records.

3.4.2. Data Processing

3.4.2.1. Developing the Visual Walkability Subindicators

Visual walkability subindicators represent different dimensions of the pedestrian walking experience that can be quantified from streetscape images. As outlined in Section 2.4, four key subindicators were utilised in this study – psychological greenery, visual crowdedness, outdoor enclosure, and visual pavement, adopted from the IVW framework developed by Zhou *et al.* (2019).

a) Psychological Greenery:

The psychological greenery subindicators denote the prominence of vegetation which can positively influence pedestrian feeling. Street greenery not only enhances the aesthetic appeal of urban landscapes but also plays a pivotal role in alleviating adverse psychological symptoms, contributing to more visually pleasing and psychologically uplifting streetscapes (Nutsford, Pearson and Kingham, 2013; Zhou *et al.*, 2019). This subindicator is measured as

the ratio of greenery pixels to total pixels (Greenery Index or Gi) in each image, as illustrated in the equation below.

$$Gi = \frac{\sum_1^3 G_n}{\sum_1^3 Sum_n}$$

Here, G_n is the total number of pixels in the Greenery variable and Sum_n is the total pixel number per image. The Gi for a point is calculated after aggregating the three images at the point. Higher values indicate better psychological greenery.

b) Visual Crowdedness:

The Visual Crowdedness subindicator captures the extent to which vehicles, objects, and other obstructions negatively impact pedestrian perceptions and comfort. Crowded streets not only deter pedestrians from walking but also generate noise and erode feelings of comfort (Lee, He and Sohn, 2017; Zhou *et al.*, 2019). This subindicator serves to quantify these adverse effects and is measured as the ratio of obstacle pixels to total pixels (Crowdedness Index or Ci) in each street view image, as illustrated in the equation below.

$$Ci = \frac{\sum_1^3 C_n}{\sum_1^3 Sum_n}$$

Here, C_n is the total number of pixels in the Obstacles variable and Sum_n is the total pixel number per image. The Ci for a point is calculated after aggregating the three images at the point. A higher value indicates more cluttered elements that can deter visual walkability, and those lower visual crowdedness values would be better for visual walkability.

c) Outdoor Enclosure:

The Outdoor Enclosure subindicator denotes the visual definition of street space provided by vertical elements like buildings and trees versus horizontal features like roads and sidewalks. This subindicator can act as a quantifier for how safe a pedestrian would feel when walking through the street. It was calculated as the ratio of the built area pixels and the greenery pixels

to the total pixels of the sidewalk, the road, and the fence (Enclosure Index or Ei), as shown in the equation below.

$$Ei = \frac{\sum_1^3 B_n + \sum_1^3 G_n}{\sum_1^3 S_n + \sum_1^3 R_n + \sum_1^3 F_n}$$

Here, B_n is the total number of pixels for the Built Area variable, G_n for Greenery, S_n for Sidewalk, R_n for Road, and finally, F_n for the Fence variable. Similar to Gi and Ci , the Ei for a point is calculated after aggregating the three images at the point.

For the outdoor enclosure subindicator, the values that wouldn't be too high or too low would have the best positive impacts on visual walkability, providing feelings of adequate safety (Baran *et al.*, 2018). To account for this, an optimal value of 1.062 was defined representing the ideal balance of vertical to horizontal features based on a selected streetscape with good enclosure (Figure 3.6). This point is situated on the University Road and is the point between New Walk and Upper New Walk. The street is characterised by ideal levels of enclosure due to the abundance of greenery in the area, while not being too open.



Figure 3.6: SVI at University Road (52.62728, -1.12156). Contains Google Street View data © Google © 2023.

The absolute difference between the calculated outdoor enclosure ratio (Ei) and this optimal value was then derived for each record as a transformed version of the enclosure subindicator. This transformed the enclosure values such that the records closer to the optimal ratio were assigned lower distance values, while those further away had higher distance values. In this way, lower transformed enclosure values represent streetscapes closer to the ideal outdoor enclosure balance. This properly accounts for the non-linear relationship between outdoor

enclosure and visual walkability, where both too high and too low values degrade the pedestrian walking experience. The optimal value and transformation align the subindicator with literature guidelines on appropriate enclosure for pedestrians.

d) Visual Pavement:

Lastly, the Visual Pavement subindicator represents the balance and proportion of road space compared to pavement and pedestrian areas, which serves as an indicator of walkability priorities and the pedestrian-friendliness of street design (Zhou *et al.*, 2019). A higher proportion of space allocated to pedestrians reflect greater consideration for walkability. This subindicator was measured as the ratio of sidewalk and fence pixels to road pixels (Visual Pavement or P_i) for each image, as illustrated in the equation below.

$$P_i = \frac{\sum_1^3 S_n + \sum_1^3 F_n}{\sum_1^3 R_n}$$

Here, S_n is the total number of pixels in the sidewalk variable, F_n is the total number of pixels for the fence variable, and R_n is the total number of pixels for the road variable per image. The P_i for a point is calculated after aggregating the three images at the point. A higher P_i ratio indicates a greater share of pixels associated with pedestrian use relative to vehicular space, thus being better for visual walkability.

The distribution of values for each visual walkability subindicator is shown through histograms in Figure 3.7. Psychological greenery, visual crowdedness, and visual pavement all demonstrate right-skewed distributions, with most images having low values and a long tail at higher values. However, the outdoor enclosure subindicator does not follow a similar trend, most likely due to the transformation done to make it more linear based on the optimal enclosure value.

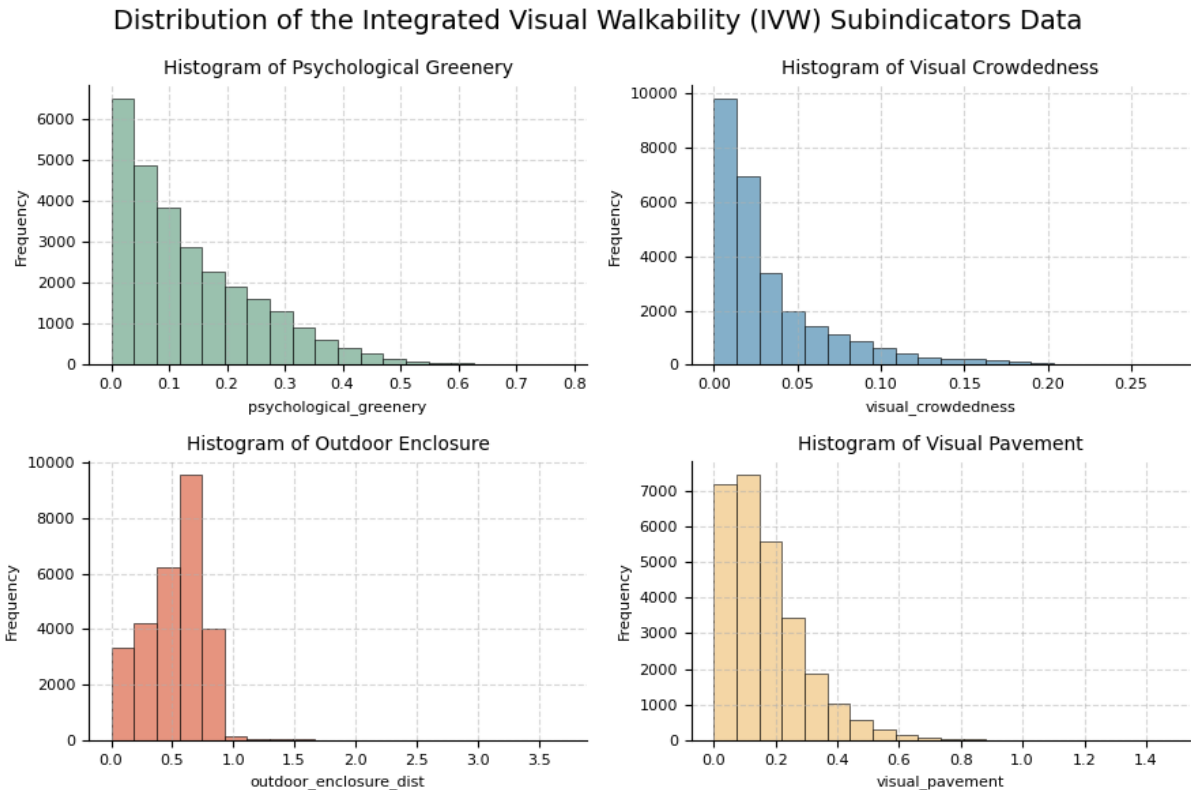


Figure 3.7: Histograms of the IVW subindicators.

3.4.2.2. Standardisation and Transformation

The subsequent data processing steps deviate from the methodology established by Zhou *et al.* (2019) for developing the IVW index. In their study, the IVW was formulated after manually dividing the raw subindicator data into five categorical levels based on value thresholds. However, systematically standardising and transforming the subindicators is a more rigorous approach that provides several benefits. Firstly, it enables consistent statistical analysis and machine learning techniques that assume standardised data, like the cluster analysis conducted later on in this study. Secondly, manually categorising the dataset into levels can introduce subjective cut-offs and thresholds. Standardisation converts the subindicators to a common scale regardless of their units and distributions, enabling a statistics-based categorisation that will be done in the subsequent section.

Although different standardisation and transformation techniques were tested on the subindicators data, the z-score technique and the inverse hyperbolic sine (IHS) technique were determined to be the most suitable for this analysis. The z-score standardisation method

transforms the data to a distribution with a mean of 0 and a standard deviation of 1 by subtracting the mean and dividing by the standard deviation. Firstly, the IVW subindicators were standardised with z-score and now have a standardised scale although skewness persists, as seen in the histograms in Figure 3.8.

Distribution of the Standardised Integrated Visual Walkability (IVW) Subindicators Data

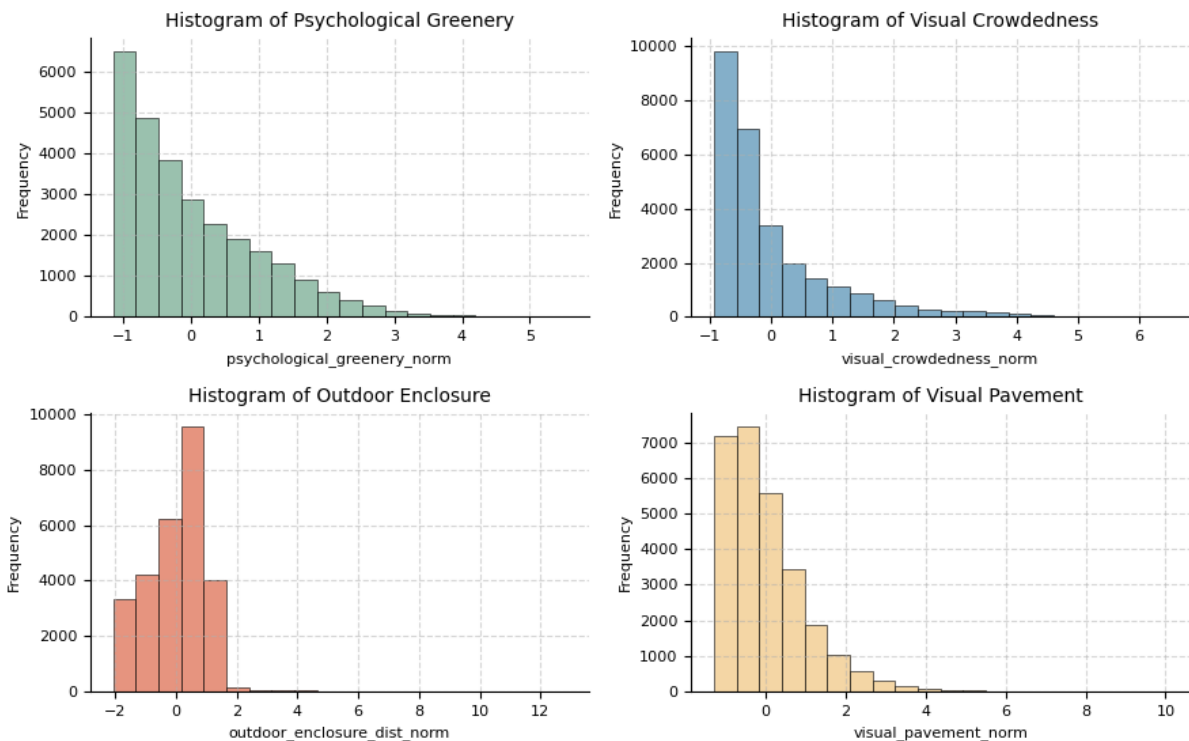


Figure 3.8: Histograms of the standardised IVW subindicators.

To mitigate the influence of outliers that can distort results, values exceeding 3 standard deviations from the mean were removed, a conventional threshold for z-score standardised data. However, as evident in Figure 3.9, psychological greenery, visual crowdedness, and visual pavement remain right-skewed, although there is a significant improvement in the overall distributions. To correct the skew further, the IHS transformation technique developed by Johnson (1949) was attempted on the dataset as it can normalise distributions while handling zeroes and negative values by applying a nonlinear logarithmic-based conversion. The distribution of the final visual walkability subindicators is illustrated in Figure 3.10. This dataset will now be categorised statistically utilising the Jenks classification method to the develop the IVW index, while it will be used as it is, albeit, at a hexagonal level after aggregation, for the subsequent cluster analysis.

Distribution of the Integrated Visual Walkability (IVW) Subindicators Data Without Outliers

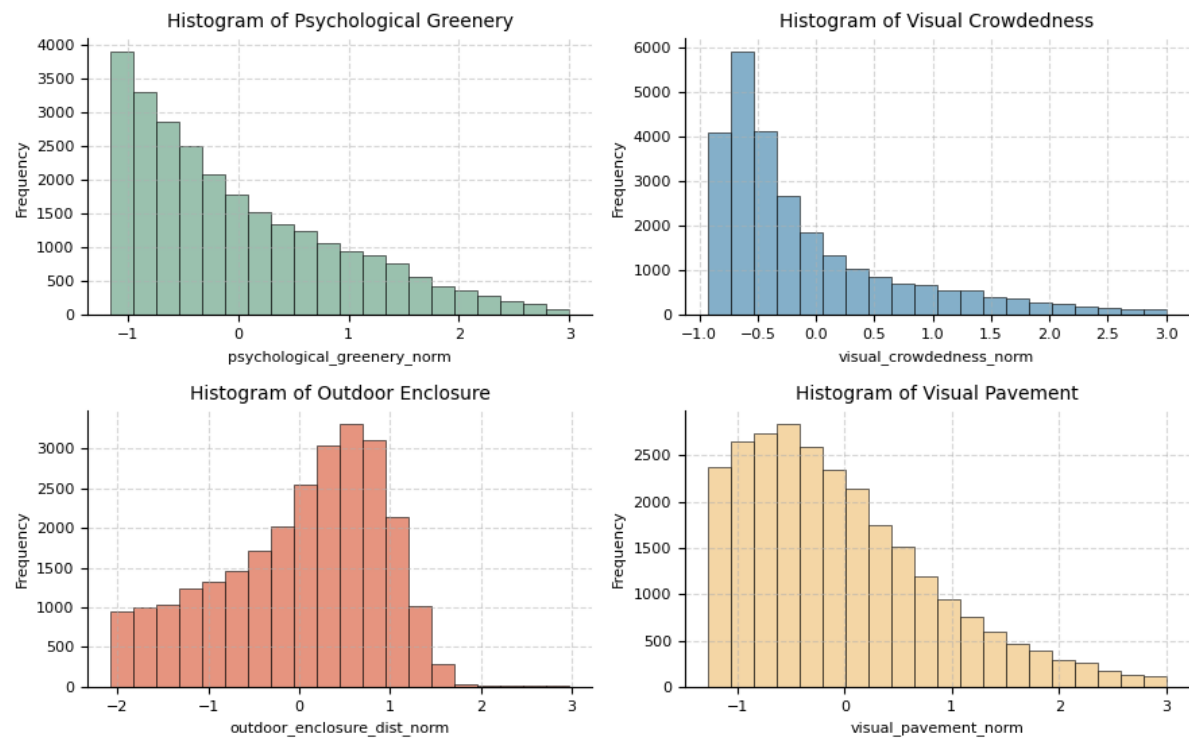


Figure 3.9: Histograms of the standardised IVW subindicators without outliers.

Distribution of the Transformed Integrated Visual Walkability (IVW) Subindicators Data

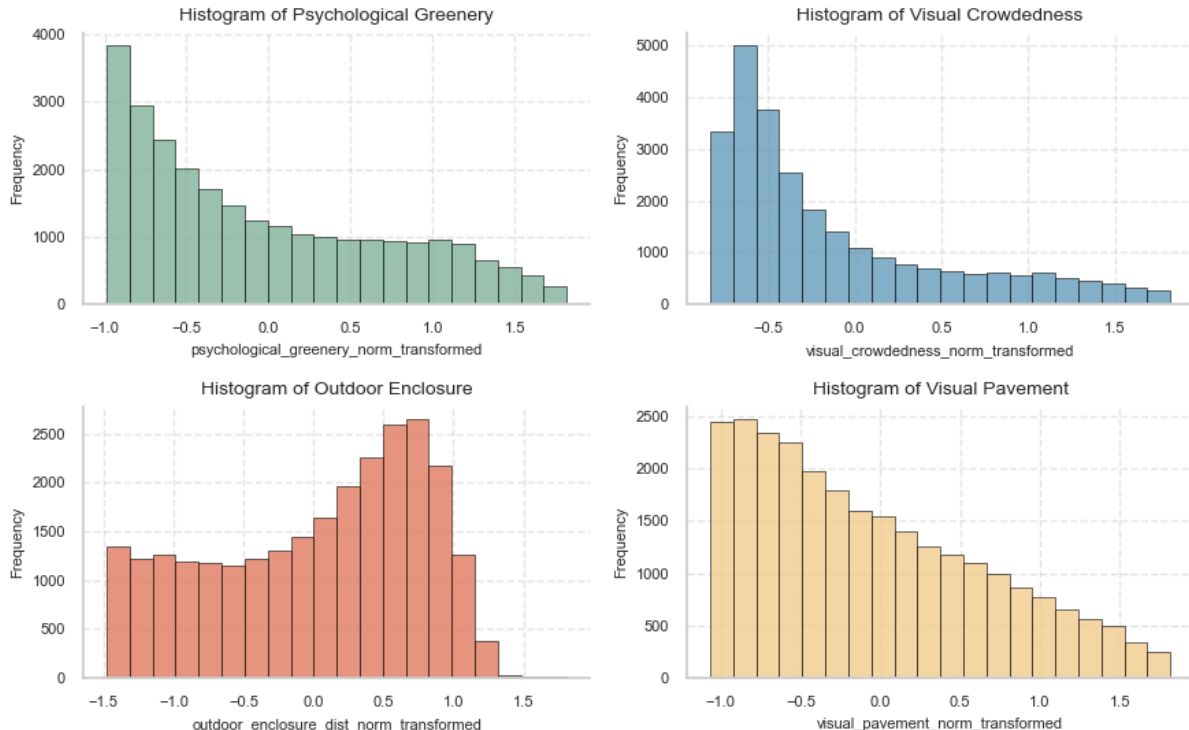


Figure 3.10: Histograms of the transformed IVW subindicators.

3.4.2.3. Categorisation of the Subindicators Data

To develop the IVW index, the standardised and transformed subindicators were categorised into discrete levels using statistical classification. The Jenks natural breaks optimisation method, also called the Jenks optimisation technique, was applied to classify the continuous subindicator data into 5 bins using the `jenkspy` Python library. This classification method determines the best arrangement of values into classes by minimising in-class variance and maximising between-class variance (Jenks, 1967). The output provides data-driven class break points that categorise the subindicators into levels aligned with their inherent distribution rather than arbitrary thresholds.

Table 3.3 displays the Jenks class bins identified for each visual walkability subindicator. The categorised subindicator level will enable formulation of the IVW index through a simplified aggregation process, as explained in section 3.5. Figure 4.7 in section 4.1 visualises the final categorised subindicator distributions. By systematically classifying the subindicators using an optimised statistical method, this process enables a rigorous categorisation minimising subjective thresholds while aligning with the overall IVW methodology formulated by (Zhou *et al.*, 2019).

Table 3.3: Categorisation of the subindicators based on the Jenks classes.

Category	Jenks Class Bins			
	Psychological Greenery	Visual Crowdedness	Outdoor Enclosure	Visual Pavement
1	-0.9874 < Gi < -0.5893	1.0891 < Ci < 1.8184	0.6988 < Ei < 1.8089	-1.0660 < Pi < -0.6292
2	-0.5893 < Gi < -0.1001	0.4808 < Ci < 1.0891	0.2335 < Ei < 0.6988	-0.6292 < Pi < -0.1504
3	-0.1001 < Gi < 0.4604	-0.0565 < Ci < 0.4808	-0.3058 < Ei < 0.2335	-0.1504 < Pi < 0.3875
4	0.4604 < Gi < 1.0518	-0.4666 < Ci < -0.0565	-0.8933 < Ei < -0.3058	0.3875 < Pi < 0.9980
5	1.0518 < Gi < 1.8175	-0.8313 < Ci < -0.4666	-1.4769 < Ei < -0.8933	0.9980 < Pi < 1.8182

3.4.2.4. Mean Subindicators per Hexagon

To enable the subsequent cluster analysis at an area level and identify area level patterns, the visual walkability subindicators were aggregated to a hexagonal grid covering the city of Leicester. Hexagonal units were utilised rather than census geographies such as the output

area to provide complete spatial partitioning without gaps or overlaps and without having inconsistent and unusual shapes, while also being consistent temporally as the census geographies could also be updated more frequently (Uber Technologies Inc, 2018). For this study, the H3 hierarchical hexagonal system developed by Uber Technologies Inc (2018) was used to generate the hexagonal grid over Leicester.

The hexagonal grids were generated at resolution 9, which resulted in 774 hexagon cells with a mean area of 0.105 km² and average edge length of 0.2 km per each hexagon cell. For each hexagon, the points failing within its boundaries were identified and the mean value of each visual walkability subindicator calculated among those points. This resulted in four mean subindicator values per hexagon representing its aggregate visual walkability conditions. Figures in Appendices B showcase the mean subindicator values per hexagon for psychological greenery, visual crowdedness, outdoor enclosure, and visual pavement respectively. Additionally, after computing the IVW index values in Section 3.5, the mean IVW per hexagon was calculated to visualise the overall visual walkability variation across the hexagons, presented in Figure 4.13 within Section 4.1.

3.5. Developing the IVW Index

To formulate the overall Integrated Visual Walkability (IVW) index, the four categorised walkability subindicators – psychological greenery, visual crowdedness, outdoor enclosure, and visual pavement, were aggregated following the approach used by Zhou *et al.* (2019). The IVW was calculated by summing the four categorised subindicators and then multiplying by 5, as shown in the equation below.

$$IVW = (Gi_{Level} + Ci_{Level} + Ei_{Level} + Pi_{Level}) \times 5$$

This aggregates the categorised subindicator levels into a composite IVW index on a scale of 20 to 100, where higher values indicate streetscapes with better visual walkability conditions. The equal weights and scoring align with the methodology formulated by Zhou *et al.* (2019) to generate a summated index capturing the overall pedestrian-friendliness of visual streetscape elements.

3.6. Cluster Analysis

Cluster analysis refers to unsupervised machine learning techniques that group data points based on similarity, without the use of predefined labels or classes (Ghosh and Kumar, 2013). This reveals inherent patterns in the data distribution and relationships between features. Points assigned to the same cluster are more similar to each other than points in different clusters. Clustering can help uncover latent structures and profiles within complex multidimensional data.

As an alternative to aggregating the visual walkability subindicators into a composite IVW index, clustering techniques were applied on the subindicators aggregated at the hexagon level. This explores whether hexagons naturally cluster based on similarities in the mean subindicator values, revealing groups of areas exhibiting common visual walkability characteristics. Two key clustering algorithms were utilised – K-Means clustering and Fuzzy C-Means clustering. The clustering techniques were applied on the transformed subindicators that were aggregated to a hexagonal level rather than the categorised data utilised for the IVW index, as nuanced spatial information would be lost while clustering categorical data.

3.6.1. K-Means Clustering Algorithm

The K-Means clustering technique, proposed by MacQueen (1967), performs crisp clustering by partitioning data points into k clusters by minimising the within-cluster sum of squares (WCSS) between points and their assigned cluster centroid. The steps for the K-Means clustering algorithm are:

1. Initialise k random cluster centroid
2. Assign each data point to the nearest centroid based on distance
3. Recompute the cluster centroid as the mean of assigned points
4. Repeat step 2-3 until the centroids stop moving

The result is a crisp cluster where each point is assigned to exactly one of the k clusters. The optimal k is often determined through the elbow method and silhouette analysis.

The elbow method, proposed by Thorndike (1953), analyses the percentage of variance explained as the number of clusters (k) increases. This is measured by the WCSS, which quantifies the variance within each cluster. As k increases, WCSS will rapidly decrease up to

an elbow point, then flatten out as additional clusters have diminishing returns in reducing WCSS. The optimal k is selected at this elbow as the variance would have sufficiently reduced. It is identified by plotting WCSS against k values and visually inspecting the elbow point where the curve bends. This elbow k represents the best trade-off between distortion and complexity.

The silhouette analysis introduced by Rousseeuw (1987) provides another quantitative measure of clustering validity by analysing the silhouette coefficient of each data point. The silhouette coefficient for a point measure how close it is to other points in its cluster versus points in other clusters. It ranges from -1 to 1, with higher values indicating the point is well-matched to its assigned cluster and poorly matched to other clusters. The optimal k is chosen by maximising the average silhouette coefficient across all data points, and a higher silhouette coefficient indicates clusters with strong cohesion and clear separation.

3.6.2. Fuzzy C-Means Clustering Algorithm

Fuzzy C-Means (FCM) is a soft clustering technique introduced by Bezdek (1981) that allows the data points to have partial membership across multiple clusters, contrasting crisp clustering methods like K-Means that assign points exclusively to one cluster. FCM aims to partition a dataset into an optimal number of fuzzy clusters by minimising an objective function that quantifies the total variance within clusters. The membership degrees indicate the degree to which points belong to each cluster. Cluster centroids represent the mean of points weighted by their degree of membership. A fuzzifier parameter controls the level of cluster overlap, and a value of 2 was used for this study. FCM provides more nuanced clustering than K-Means, uncovering subtle patterns in complex data.

The algorithm initialises random cluster centroid and membership degrees, then iteratively updates the memberships based on distances between points and centroids, and recomputes the centroids as the membership-weighted mean of points. This repeats until the centroids stabilise. The optimal number of clusters can be determined using the elbow method and the silhouette analysis mentioned before.

To focus the analysis on core cluster associations, hexagons with low membership degrees less than 0.5 in all clusters were filtered out. A threshold of 0.5 was chosen because clusters below this can be considered weak assignments for those hexagons. Examining the remaining

hexagons enables a clearer perspective on the primary clusters with strong visual walkability profiles.

3.6.3. Cluster Analysis with Points of Interest (POI) Diversity Data

In addition to the clustering done with the visual walkability characteristics, cluster analysis was also done after incorporating amenity diversity data to capture the accessibility dimension of walkability. While visual elements directly relate to visual walkability and pedestrian experience, amenity mix indicates the broader urban vibrancy and 15-minute city characteristics of neighbourhoods as discussed in section 2.4.

To quantify amenity diversity or Points of Interest (POI) diversity, an index was formulated using Shannon's diversity index (Shannon, 1948). This metric originated in information theory to measure entropy but has been widely adopted in ecology and urban planning to represent the variety and balance of types within a system (Zachary and Dobson, 2021). Shannon's index is calculated as:

$$H = - \sum_{i=1}^s p_i \ln(p_i)$$

Here, p_i represents the proportion of elements belonging to the i^{th} type out of the total elements in a system; \ln is natural logarithm, and s is the total number of types. It measures both richness (number of types) and evenness (distribution of types). In this study, it was applied to OpenStreetMap amenity data obtained for various categories such as points of interest, points of worship, transportation, and other services (OpenStreetMap, 2023). A table containing the different types of amenities used to calculate the POI diversity index is provided in Appendix C-1, while a map showing the amenities is displayed in Appendix C-2.

For each hexagon, the Shannon index H was computed based on the distribution of amenity types within it. This quantified the diversity and vibrancy of each neighbourhood's amenity access. The raw index values were standardised using z-score and transformed with inverse hyperbolic sine, as highlighted in the distribution plot in Figure 3.11. Figure 3.12 maps the POI diversity index across Leicester at a hexagonal level. Incorporating this POI diversity index when clustering provided additional context about amenity mix and accessibility complementary to the visual walkability subindicators. While the visual metrics capture

granular on-the ground elements affecting pedestrian walking experience, the POI diversity represents broader neighbourhood functionality motivating walking.

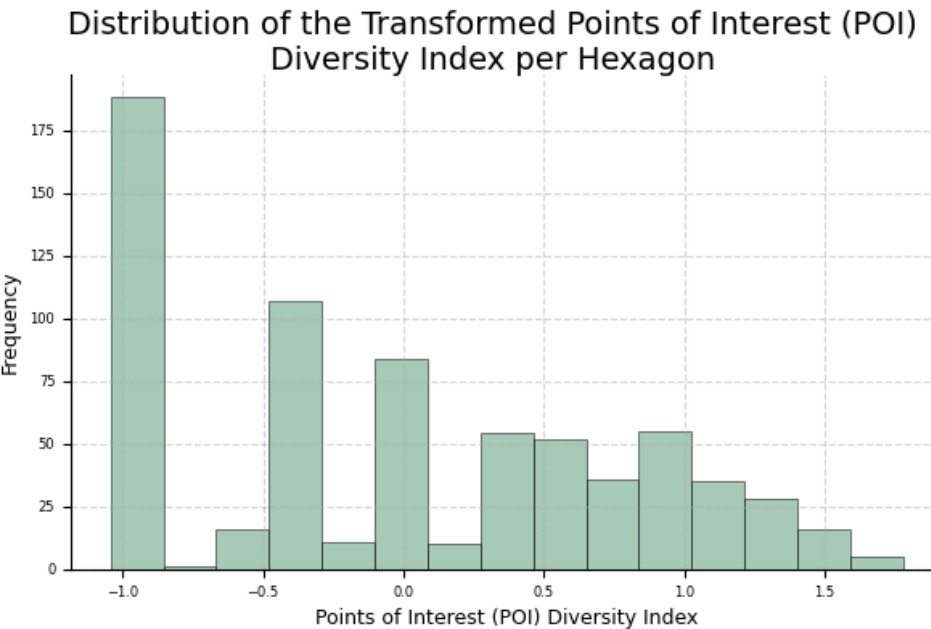


Figure 3.11: Histogram of the POI Diversity Index.

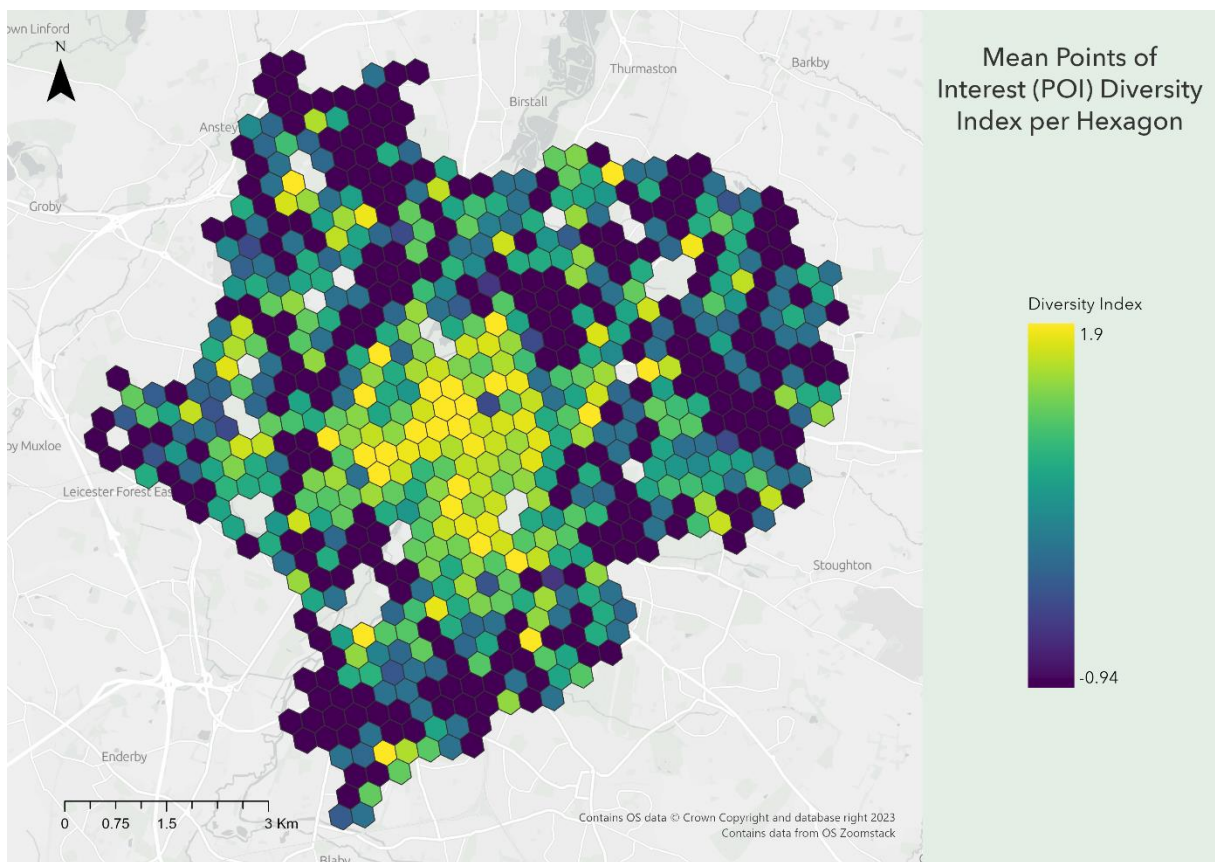


Figure 3.12: Map showing the Mean POI Diversity Index per hexagon (Map scale: 1:60000).

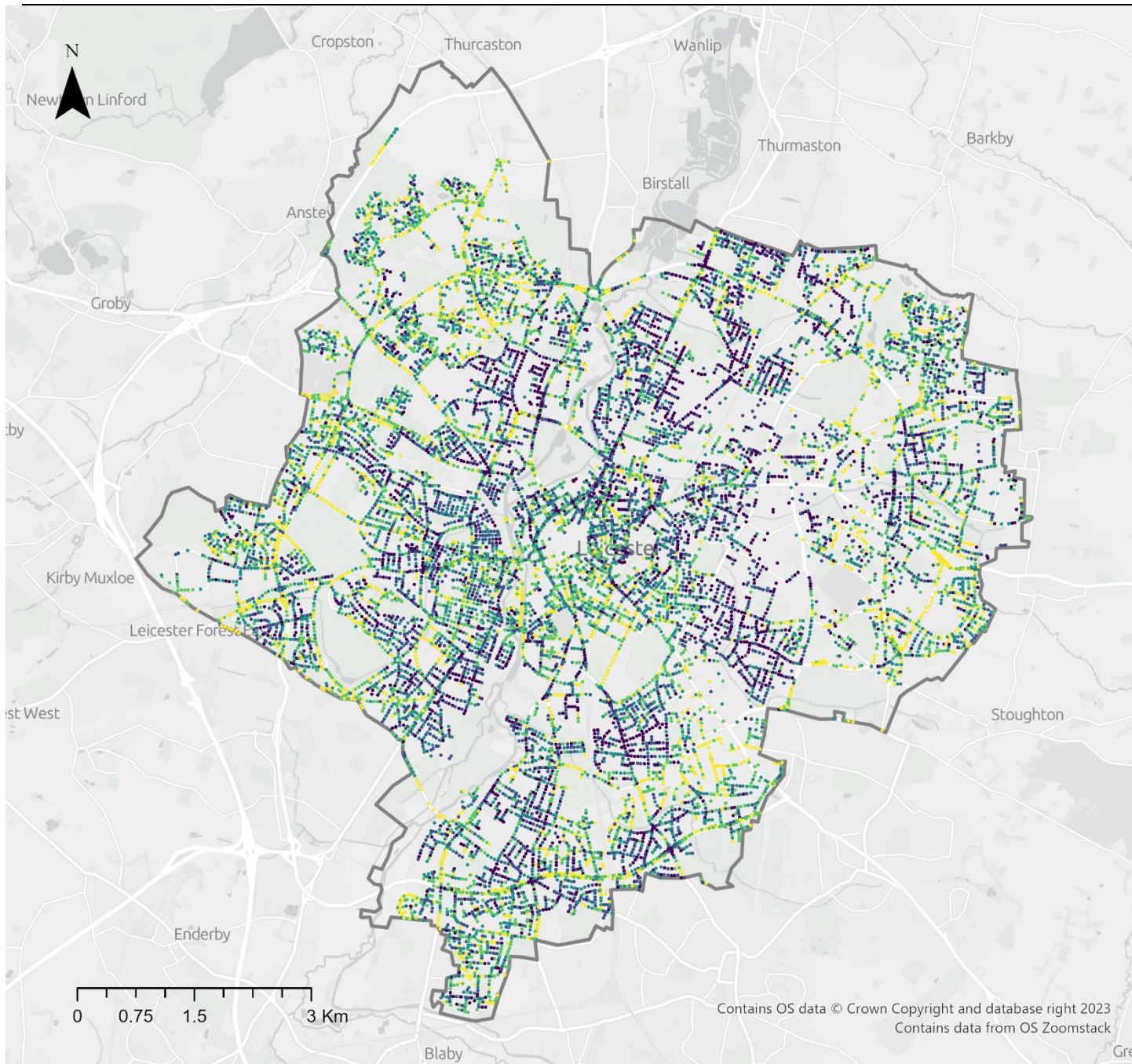
Chapter 4. Results and Analysis

The following chapter presents the results formulated from the implementation of the adapted Integrated Visual Walkability (IVW) framework for Leicester and the subsequent clustering analysis. Section 4.1 presents the overall IVW index for Leicester, along with the indices for the subindicators including Psychological Greenery (Gi), Visual Crowdedness (Ci), Outdoor Enclosure (Ei), and Visual Pavement (Pi). Results highlighting the Mean IVW at a hexagonal level are also presented in this section. Section 4.2 shows results from the clustering analysis performed with the walkability subindicators, spread into two subsections each for K-Means and Fuzzy C-Means (FCM). Similarly, in section 4.3, the results from the clustering analysis of the walkability subindicators and the Points of Interest (POI) diversity index are presented within two subsections for the K-Means and the Fuzzy C-Means clustering techniques. A dashboard built using R Shiny that showcases the results and allows for easier interpretation of them is available at <https://adhbsyed.shinyapps.io/walkabilitydashboard/>.

4.1. Visual Walkability Profile of Leicester

The following map (Figure 4.1.) highlights the spatial pattern of the IVW index in Leicester. Each point on the map shows its respective IVW score calculated from the SVI utilising the methodology detailed in section 3.6. The IVW score for the different points along the road network of Leicester ranges from a low score of 20 and goes up to a perfect score of 100 for only 102 points. The distribution of the IVW index is highlighted in Figure 4.2. A reasonably normal distribution of the IVW index can be observed both within the map and within the histogram.

Spatially, streets with higher visual walkability tend to be around the city centre area and in and around the city's outskirts, with streets with lesser visual walkability sandwiched between them. Some of the roads with notably good visual walkability tend to be around Beaumont Leys, Braunstone, Knighton, Spencefield Lane and the University of Leicester. Streets with particularly low visual walkability can be observed around Aylestone, Belgrave, Evington, and Newfoundpool. High visual walkability could also be observed in streets along and around the river Soar, particularly along the Western Boulevard on Bede Island in central Leicester.



Integrated Visual Walkability (IVW) Index for Leicester

Higher IVW Score indicates better Visual Walkability.

IVW

- 20 - 40
- 41 - 50
- 51 - 60
- 61 - 75
- 76 - 100

Boundary

Figure 4.1: Integrated Visual Walkability Index for Leicester (Map Scale: 1:65000).

Distribution of the Integrated Visual Walkability (IVW) Index

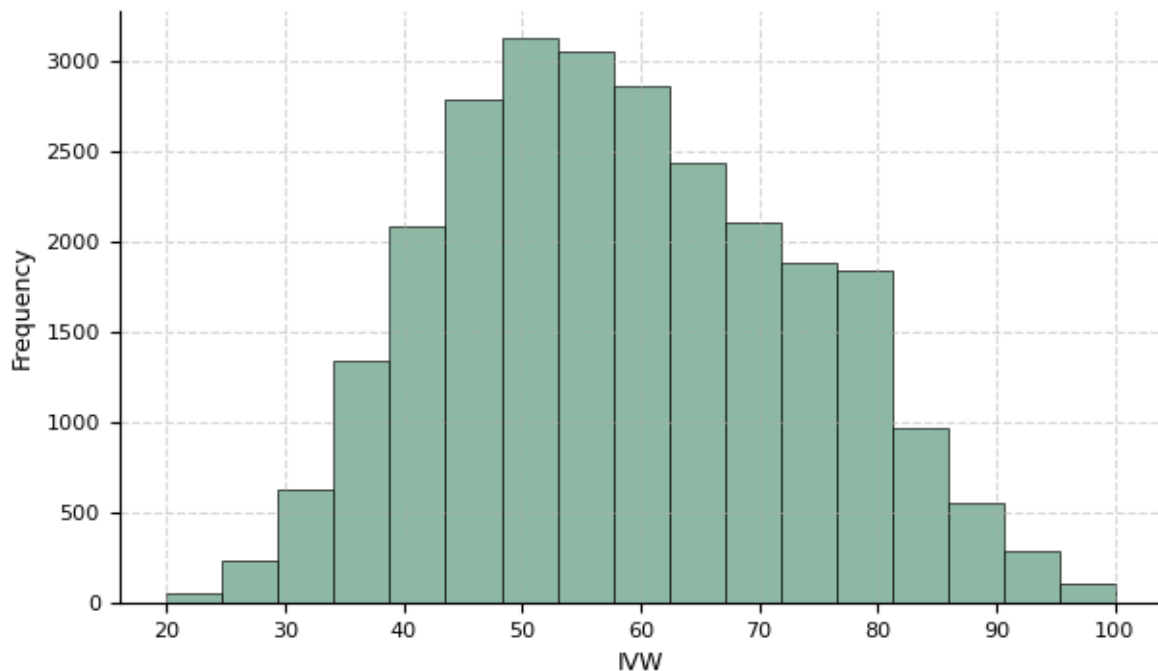
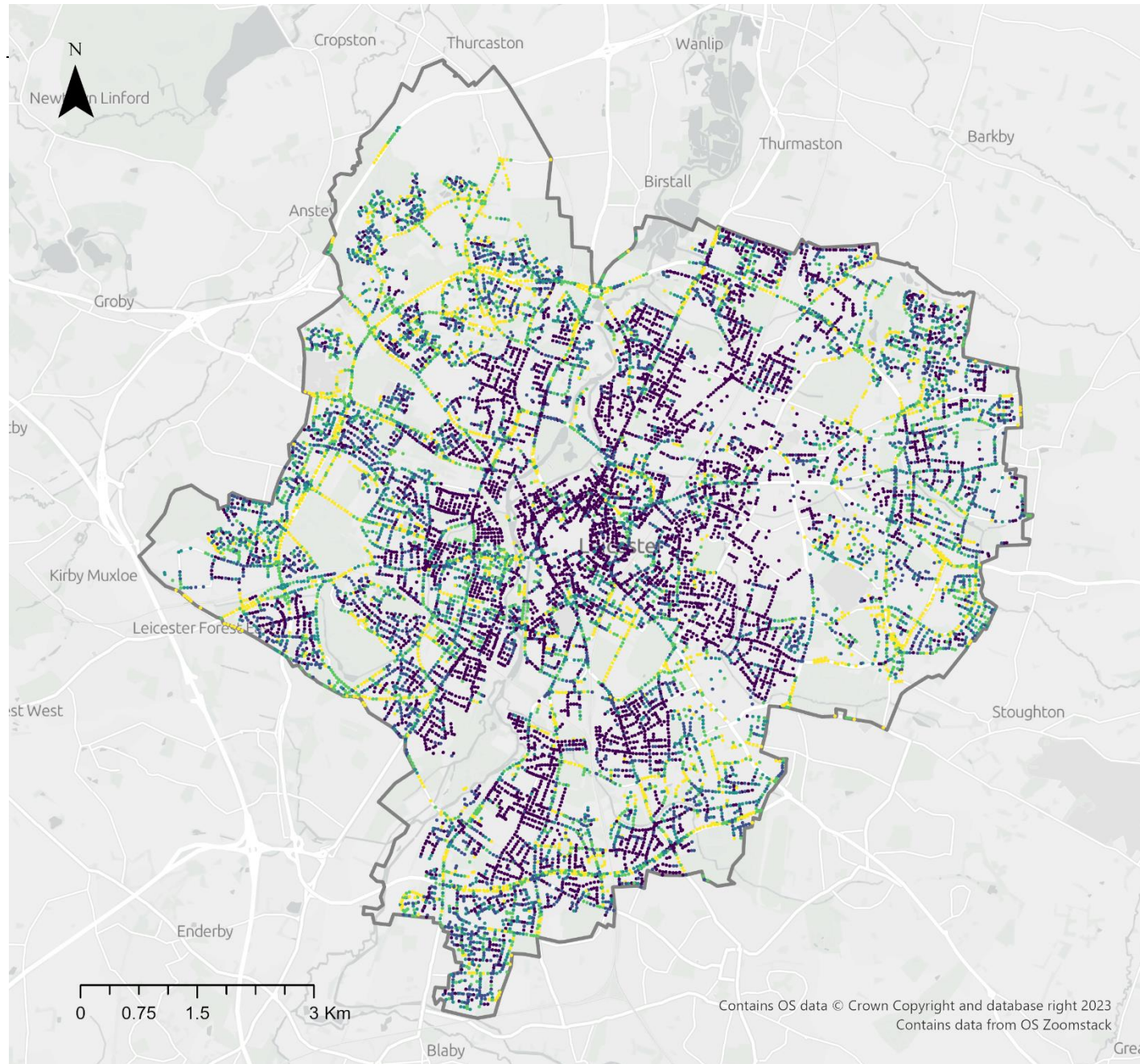


Figure 4.2: Histogram showing the distribution of the Integrated Visual Walkability Index.

The results observed in this study reinforce the findings of Zhou *et al.* (2019), which showed high visual walkability streets in close proximity to lower walkability streets. This implies that disparities arise from subtle differences between the specific walkability subindicators, rather than overall urban form. While neighbouring streets likely share similarities in their general built environment, minor variations in particular visual elements distinguish a highly walkable street from a less walkable one nearby. One street may have slightly more greenery, better enclosure, or less crowdedness than another, making it more visually appealing for walking, even though their broader urban morphology is comparable.

These nuanced distinctions suggest that visual walkability is characterized by complex interactions between fine-grained streetscape attributes. Achieving universally high visual walkability requires addressing the precise factors creating localised perceptual frictions for pedestrians, beyond general built environment patterns. The multidimensional perspectives revealed through this research can aid targeted improvements by uncovering key subindicator relationships differentiating walkable and less walkable areas.

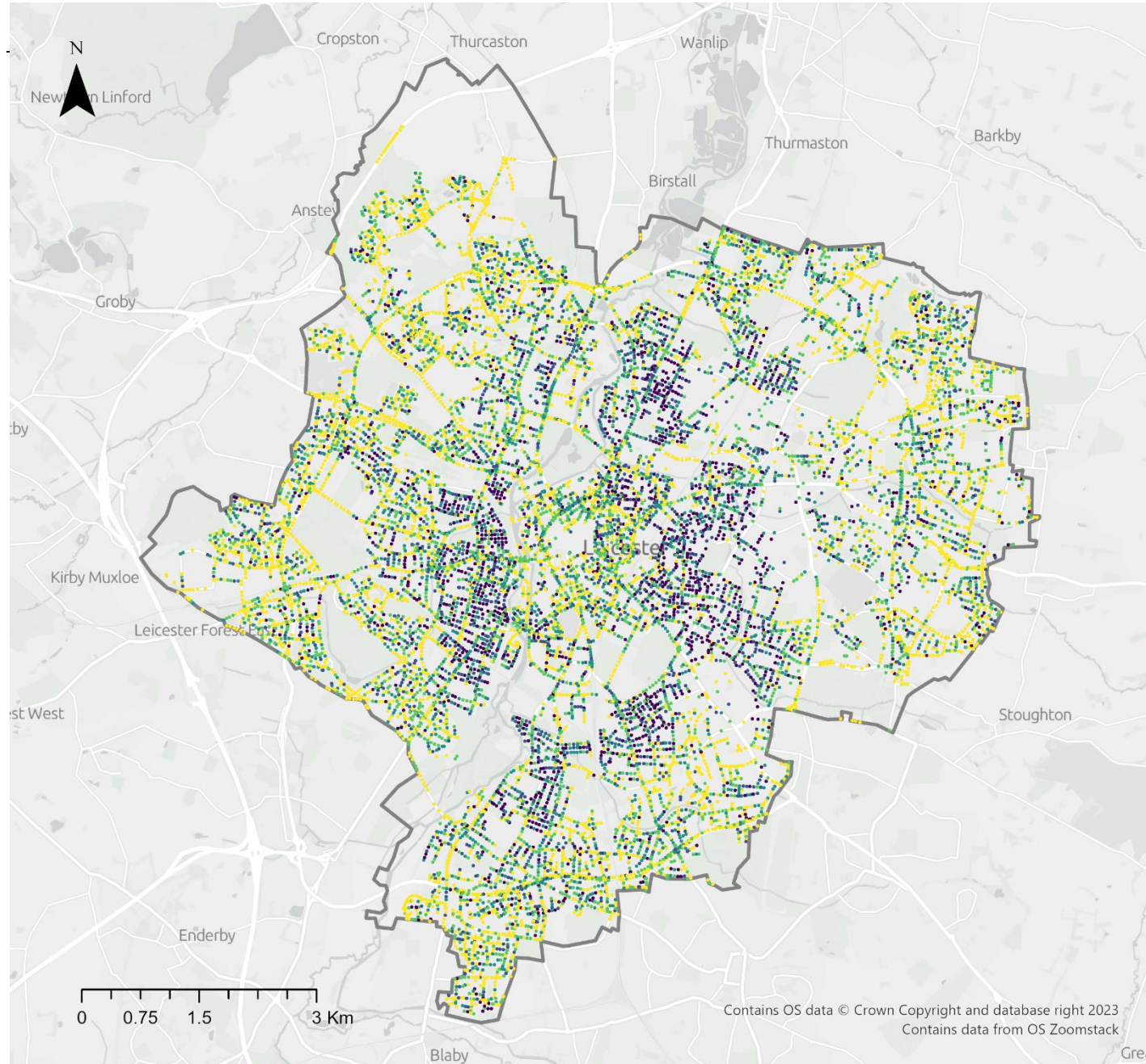


Greenery Index (Gi) for Leicester

Higher Gi Score indicates
more greenery along the
roads of Leicester

- Gi
- 1
 - 2
 - 3
 - 4
 - 5
- Boundary

Figure 4.3: Greenery Index for Leicester (Map Scale: 1:65000).



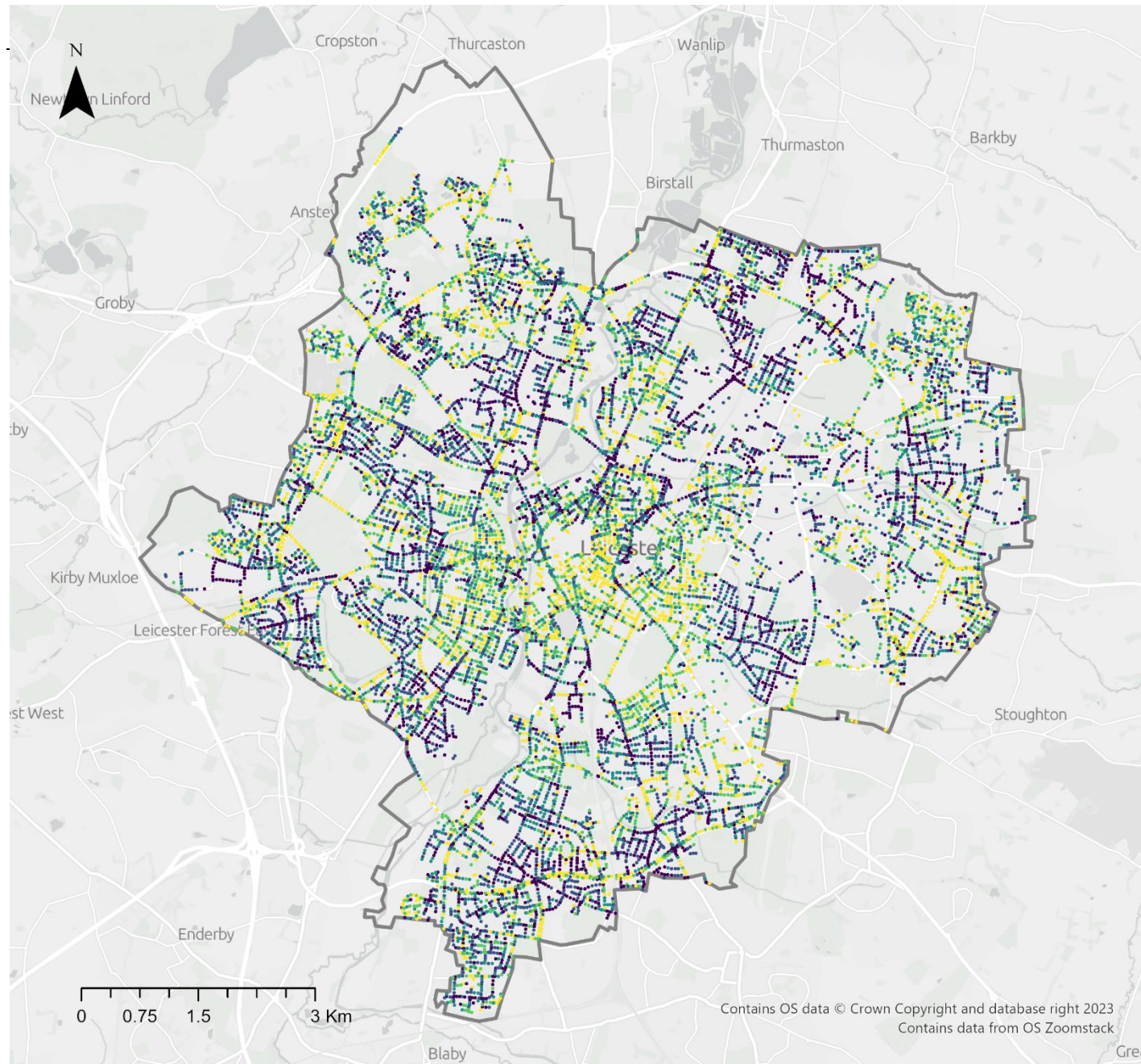
Visual Crowdedness Index (Ci) for Leicester

Higher Ci Score indicates less visual crowdedness along the roads of Leicester

Ci
1
2
3
4
5

Boundary

Figure 4.4: Visual Crowdedness Index for Leicester (Map Scale: 1:65000).

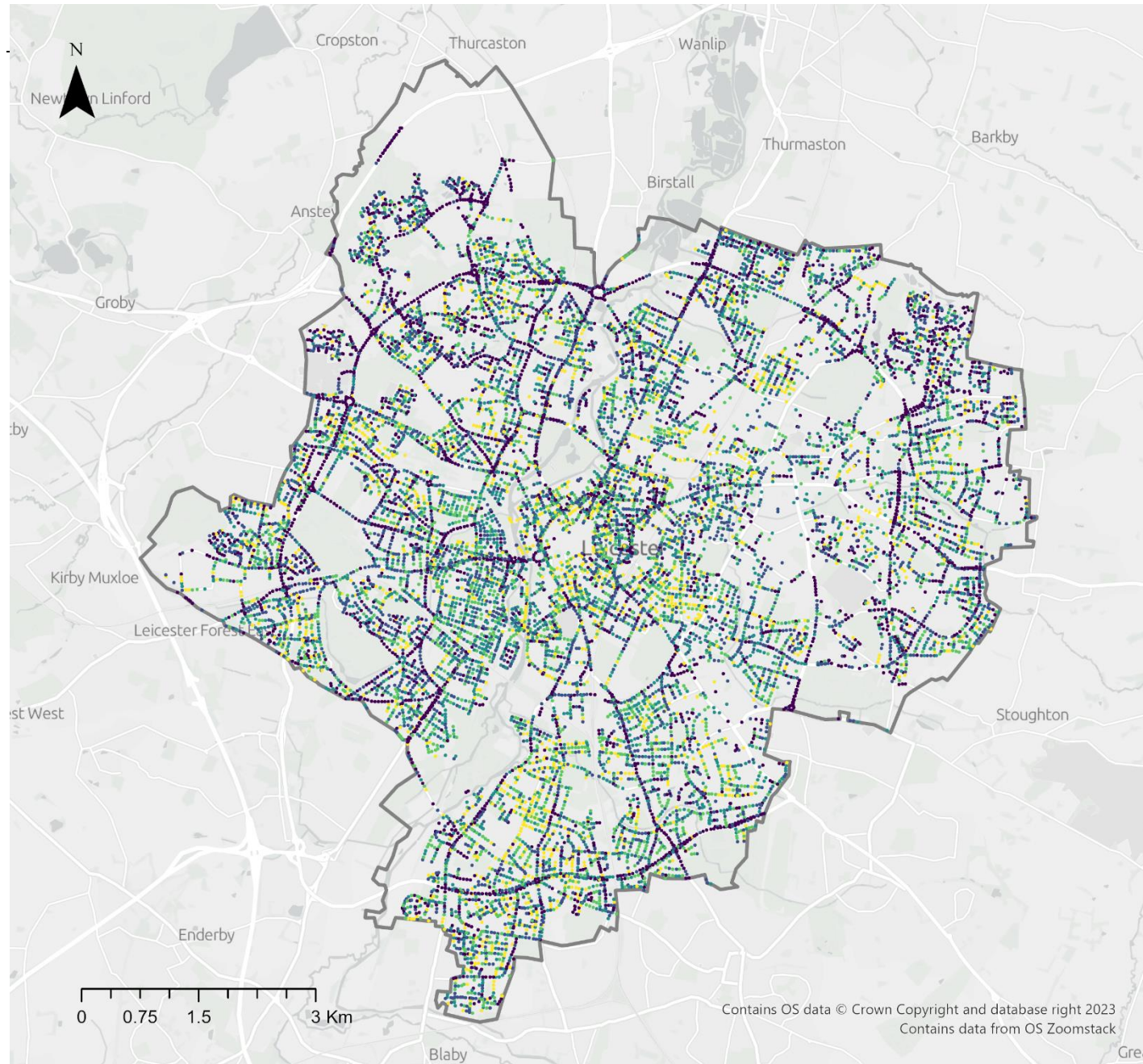


Outdoor Enclosure Index (Ei) for Leicester

Higher Ei Score indicates better outdoor enclosure along the roads of Leicester

- Ei
- 1
 - 2
 - 3
 - 4
 - 5
- Boundary

Figure 4.5: Outdoor Enclosure Index for Leicester (Map Scale: 1:65000).



Visual Pavement Index (Pi) for Leicester

Higher Pi Score indicates a better ratio of pavement to road along the streets of Leicester

- Pi
- 1
 - 2
 - 3
 - 4
 - 5
- Boundary

Figure 4.6: Visual Pavement Index for Leicester (Map Scale: 1:65000).

Examining the spatial distribution of the four visual walkability subindicators individually reveals more nuanced patterns with the overall index. Each subindicator displays distinct geographical variations across Leicester. As Figure 4.3 illustrates, streets with abundant greenery per the Psychological Greenery Index tend to be located on the outskirts of the city. The urban centre generally has less vegetation, with some exceptions like the greener streets surrounding Victoria Park, the University of Leicester campus, and Bede Island. Some of the streets in the outskirts with higher levels of Gi include Spencefield Lane and Shirley Road in Knighton. Higher levels of greenery can also be observed along the ring road encircling Leicester, the A563. The greenery index illustrates that greenery is not distributed evenly across the urban landscape of Leicester. Instead, it mostly clusters on the peripheries of the city while most of the interior urban streets experience a relative lack of vegetation and greenery, which can result in subpar pedestrian walking experience along some of the central streets.

The visual crowdedness index also varies across Leicester, although higher levels of crowding are more confined when compared to the greenery index. As Figure 4.4 illustrates, most of the streets in Leicester exhibit low to moderate levels of visual crowdedness, with some pockets of higher crowding appearing between the less crowded city centre and the outskirts of the city. The most overcrowded areas emerge in residential neighbourhoods bordering the city centre, such as Evington, Westcotes, and Clarendon Park. The increased visual crowdedness in these central neighbourhoods stems from the on-street parking congestion. With more cars parked along the curbs, these streets appear more chaotic and cluttered from a pedestrian viewpoint. Besides these pockets of crowdedness in the interior neighbourhood, the broader urban landscape of Leicester is characterised by low levels of visual crowdedness. This suggests that crowdedness and the visual encroachment of physical obstacles into the walking path tend to be localised issues rather than citywide ones. This subindicator clearly highlights the prevalence of high visual crowdedness in specific parts of the city, likely related to parking availability and street layouts in those areas.

The degree of the outdoor enclosure subindicator also shows distinct geographical variation across Leicester. As illustrated in Figure 4.5, streets in the city centre exhibit high levels of outdoor enclosure, especially along the University of Leicester campus and University Road. Outdoor enclosure levels also rate higher along the outer edge of the city, like in Spencefield

Lane. This relates to the proportion and configuration of vertical structures framing street views – areas with an optimal amount of buildings and trees delineating the visual field have higher outdoor enclosure levels. The university area and outskirts possess well-defined outdoor spaces shaped by surrounding vertical elements that provide comfortable visual boundaries. However, some of the residential neighbourhoods between the outskirts and the centre lack these vertical features to properly enclose the street views, leading to diminished pedestrian comfort. Ideal enclosure relies on vertical elements that are appropriately balanced – not too scarce nor overly abundant. This subindicator thus identifies streets that could benefit from thoughtful urban design using vertical structures like street trees to improve visual walkability.

The visual pavement index displays some distinct spatial patterns across Leicester, as shown in Figure 4.6. Many of the major roads and the ring road encircling the city exhibit low visual pavement levels. Their wide road widths dominate the visual field from a pedestrian viewpoint, minimising the visible pavement area. However, most streets within the city centre and urban residential neighbourhoods display favourable pavement ratios, with ample sidewalks comprising more visual space, except for some unexpected areas near the University of Leicester and scattered across the city, which surprisingly show lower visual pavement levels. This likely results from inaccurate segmentation of road versus pavement pixels by the SegFormer-B5 model. Overall, streets with wider sidewalks and narrower roads create improved visual pavement ratios and more pedestrian-friendly environments, but the major roads prioritise road width over walkability as they are vehicle-focused rather than pedestrian-focused. While model limitations affect the visual pavement subindicator, the index still highlights areas where unbalanced road-to-pavement proportions may discourage walking or negatively impact pedestrian comfort.

The distributions of the four subindicators highlighted in Figure 4.7 reveal how each subindicator may influence the overall IVW index. As seen in the bar plots, the psychological greenery index skews right, with most points rating low in greenery, while few points ranking highly. The visual crowdedness subindicator shows the opposite left-skewed distribution, with most points along the streets experiencing minor crowding. Outdoor enclosure exhibits a more normal distribution, with points relatively evenly distributed across all enclosure levels.

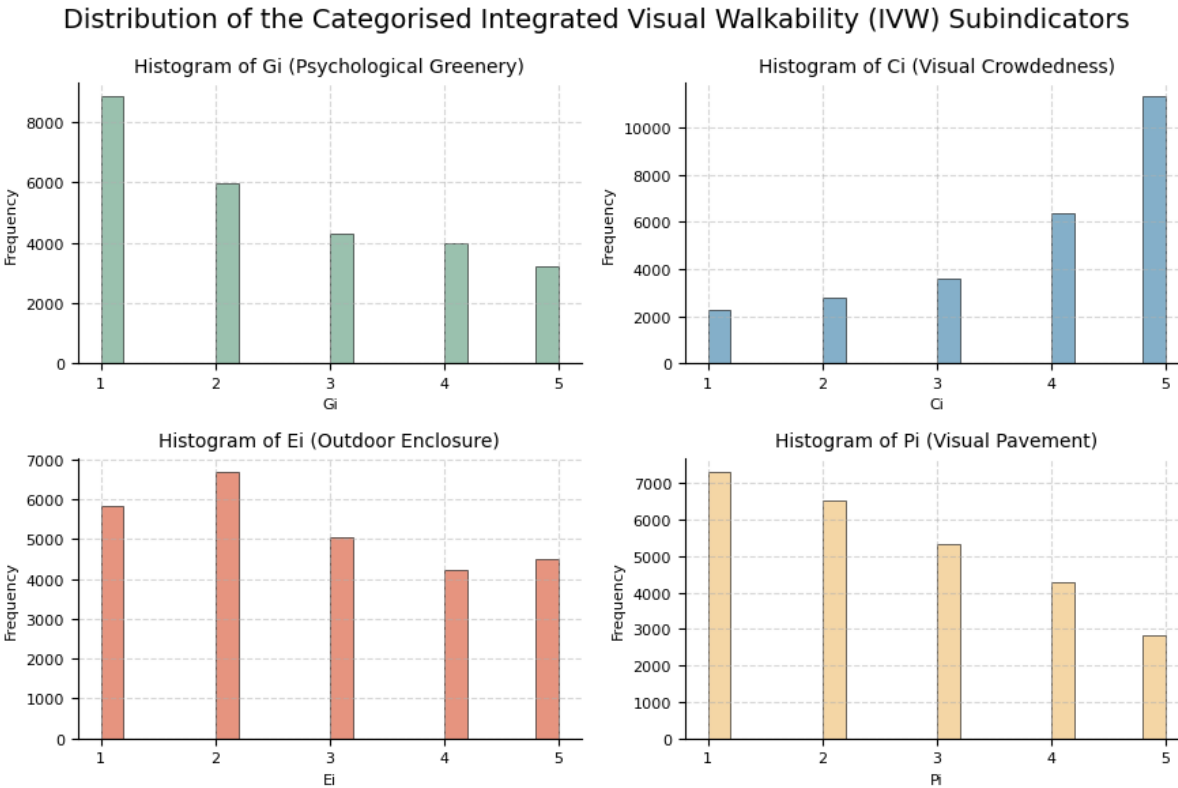


Figure 4.7: The distribution of the categorised IVW Subindicators.

Finally, the visual pavement mirrors greenery in a right-skewed distribution, with low pavement levels predominating. Since the overall IVW index averages these four subindicators, their uneven distribution shapes the final composite result. The skewness toward low greenery and pavement depresses visual walkability for many streets, but the abundance of uncrowded streets counterbalances this effect, while the normal enclosure distribution exerts moderate influence. Thus, insufficient greenery and low pavement-to-road ratio emerge as chief factors limiting visual walkability in Leicester, while ample uncrowded space mitigates the impact. Targeting improvements to greenery and pavement width on streets would likely enhance overall visual walkability the most. However, the limitations of the segmentation model in the context of the visual pavement subindicator must be factored in, which will be discussed further in Chapter 5.1.

Samples of SVI taken randomly at varying IVW levels visually validate the quantitative findings and showcase a gradual overall decline in visual walkability. Streets with the highest IVW score of 100 (Figure 4.8) and 85 (Figure 4.9) clearly demonstrate optimal conditions, with abundant



Figure 4.8: Street View Imagery with an IVW score of 100. Contains Google Street View data © Google © 2023.



Figure 4.9: Street View Imagery with an IVW score of 85. Contains Google Street View data © Google © 2023.



Figure 4.10: Street View Imagery with an IVW score of 65. Contains Google Street View data © Google © 2023.

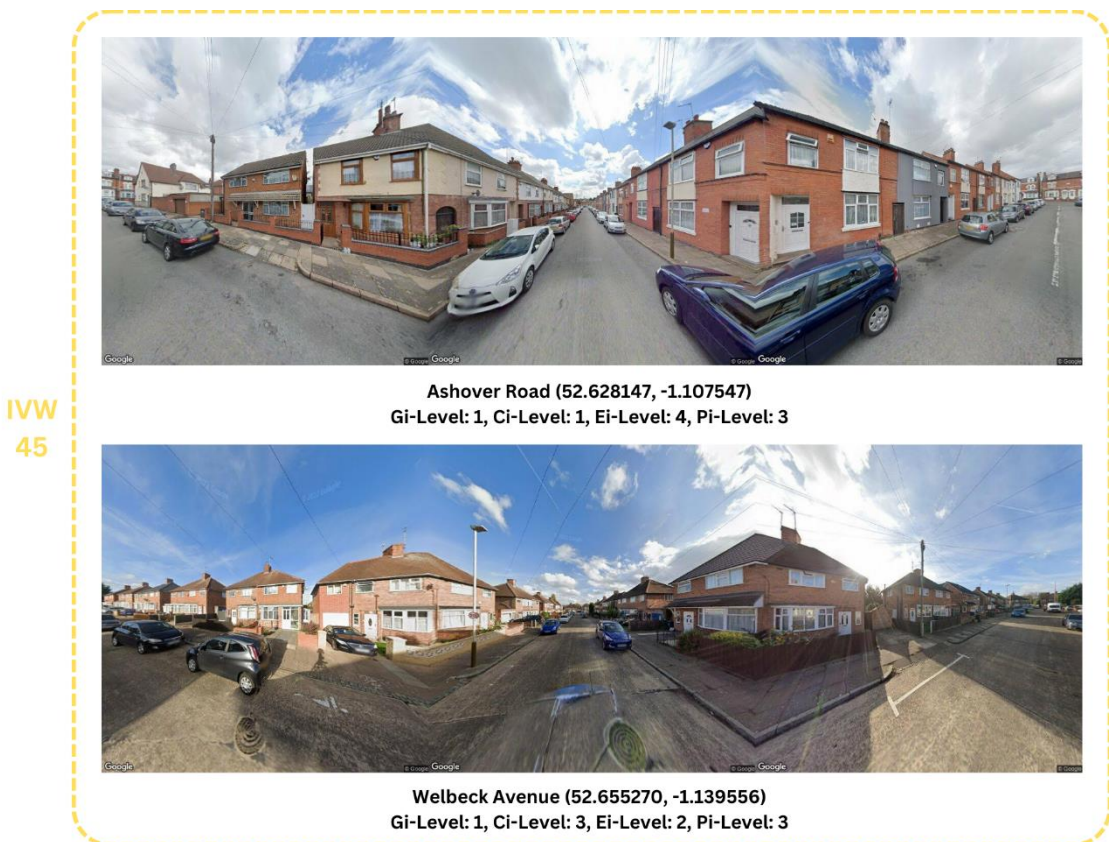


Figure 4.11: Street View Imagery with an IVW score of 45. Contains Google Street View data © Google © 2023.



Figure 4.12: Street View Imagery with an IVW score of 25. Contains Google Street View data © Google © 2023.

greenery, minimal crowding, good enclosure, and reasonable pavement-to-road ratios. As the IVW score decreases, deficiencies become apparent in some subindicators within the SVI, illustrating the composite effect on overall visual walkability. Lower IVW scores of 65 (Figure 4.10) exhibit shortcomings in greenery and pavement, while the lowest scores (Figure 4.11, Figure 4.12) display inadequacies across most of the four subindicators. The selected SVI examples mirror the quantified IVW levels, with perceptions of overall visual walkability incrementally diminishing. The SVI provides qualitative visual reinforcement that improving the key limiting subindicators would enhance the overall visual walkability in Leicester.

The spatial distribution of mean IVW scores aggregated at the hexagon level is mapped in Figure 4.13. The visualisation of walkability patterns across hexagonal units reinforces the localised variations revealed through the IVW analysis, providing a summarised overview of Leicester's visual walkability. Similarly, maps depicting the four subindicators at a hexagonal level can be found in Appendix B.

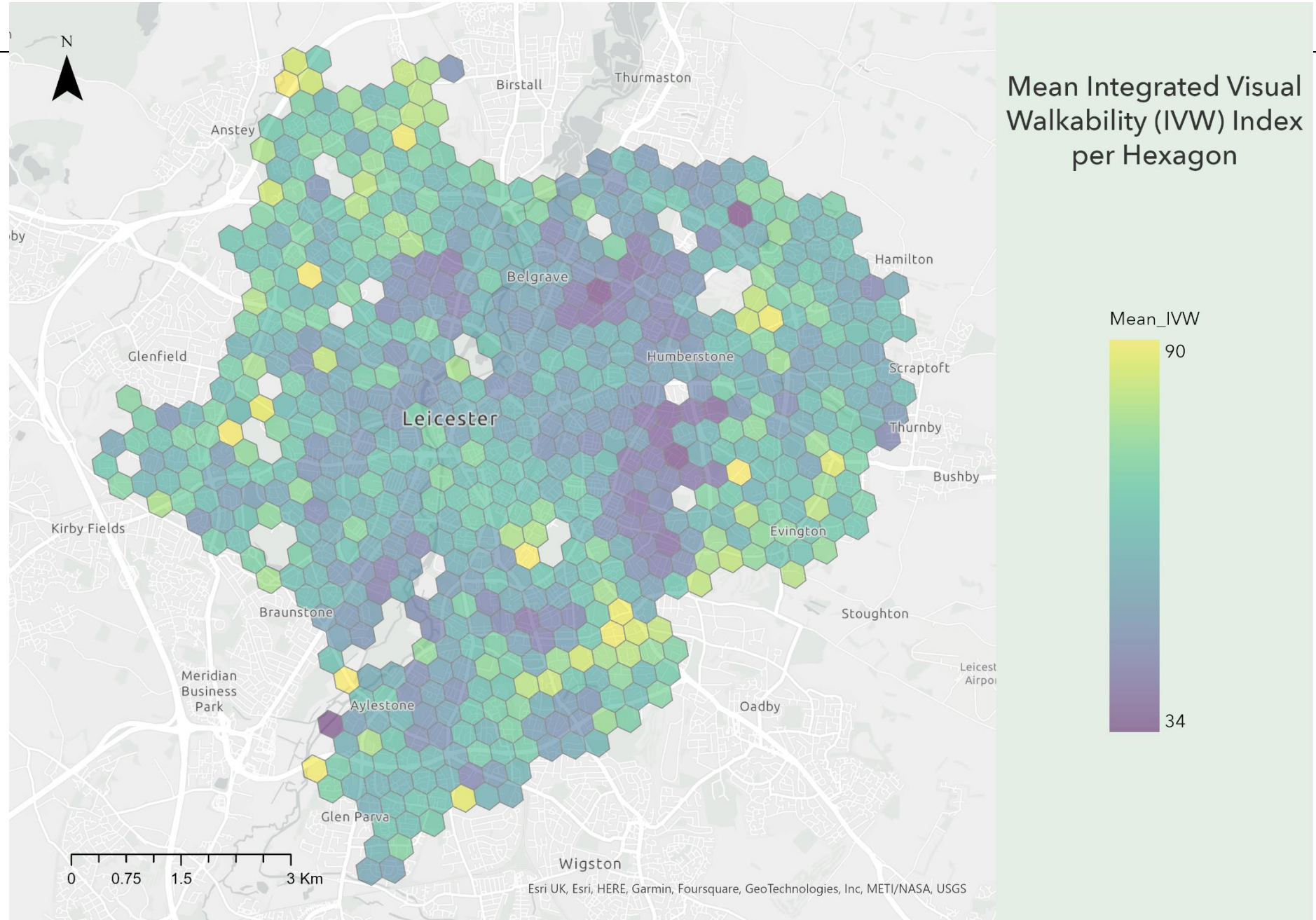


Figure 4.13: Mean Integrated Visual Index per Hexagon (Map Scale: 1:60000).

4.2. Cluster Analysis of the Visual Walkability Subindicators

As an alternative to aggregating the visual walkability subindicators into a composite IVW index, clustering techniques were applied to uncover patterns among the subindicators at the hexagonal level, as detailed in section 3.6. For each hexagon, the four subindicators were aggregated by taking the mean value within that unit. Clustering explores whether hexagons naturally cluster based on similarities in the mean subindicator values, revealing groups of areas with common visual walkability characteristics. Prior to clustering, a pair plot (Figure 4.14) was created to visualise the relationships between each pair of mean subindicators, enabling analysis of the correlations between the subindicators across the hexagonal units.

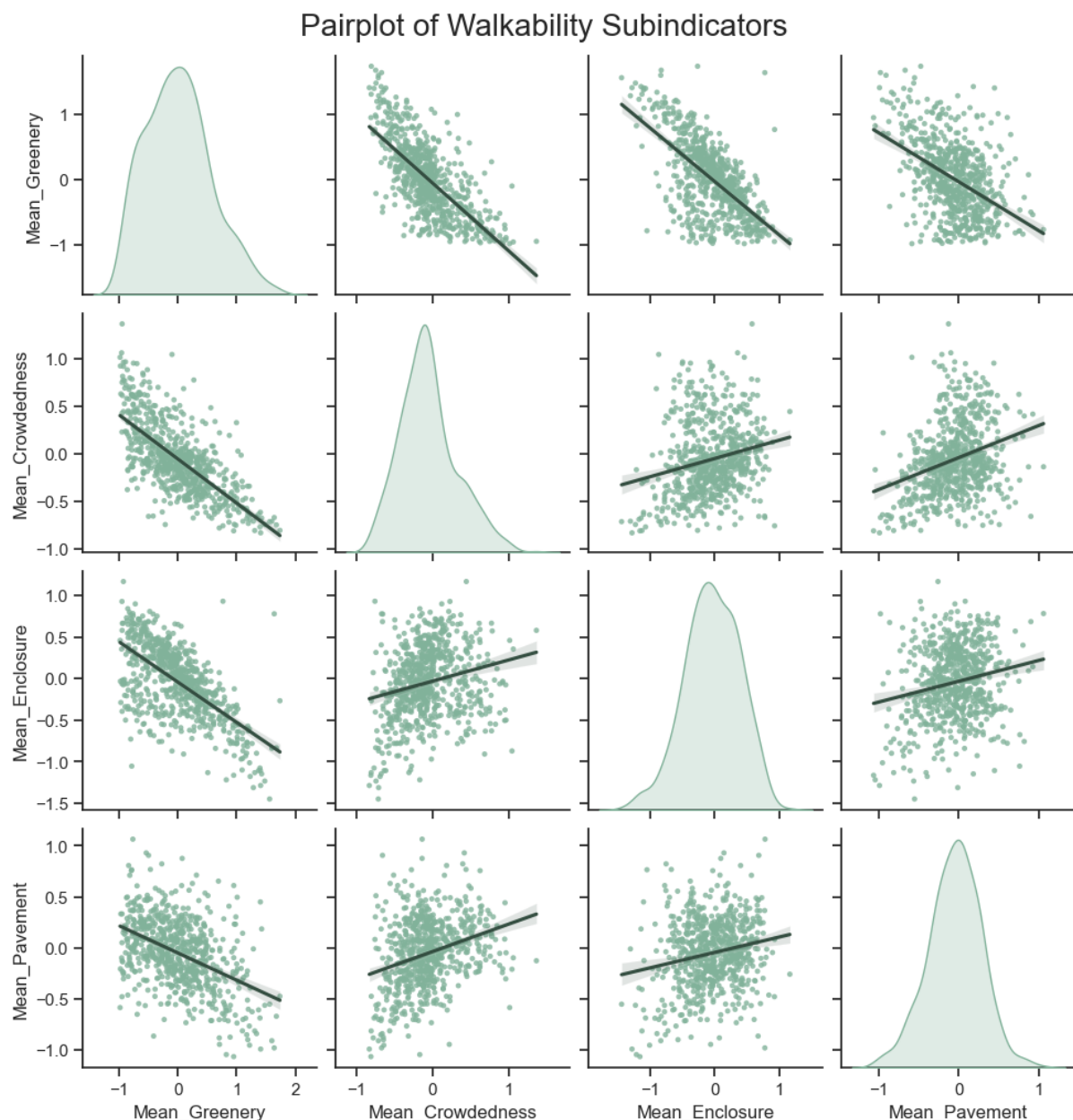


Figure 4.14: Pair plot visualising relationships between the visual walkability subindicators.

As mentioned in section 3.6, the clustering is done with the transformed and standardised subindicators data rather than the subsequent categorised version used to develop the IVW index. Thus, when interpreting the results, higher values of ‘Mean Greenery’ and ‘Mean Pavement’ indicate better scores for the psychological greenery and visual pavement subindicators. However, for the outdoor enclosure and visual crowdedness subindicators, the opposite applies – lower ‘Mean Enclosure’ and ‘Mean Crowdedness’ values indicate better scores on those subindicators. Hence, the directionality of the relationship between the subindicators must be considered when examining the clusters. Clustering on continuous standardised data characterises groups based on precise relative positioning across the full measurement scales. This retains nuanced information about correlations and distributions. Clustering the categorical values would have discarded the granular relationships between the subindicators. The standardised continuous values better reveal subtle visual walkability patterns between subindicators across the urban landscape of Leicester. Two clustering techniques were utilised on the subindicators: K-Means and Fuzzy C-Means.

Examining the pair plot in Figure 4.14 in detail reveals some notable correlations between the subindicators. Mean Greenery exhibits strong negative correlation with Mean Crowdedness, Mean Enclosure, and Mean Pavement. In contrast, Mean Crowdedness shows positive correlation with Mean Enclosure and Mean Pavement, though the correlation is weaker. Between Mean Enclosure and Mean Pavement, moderate positive correlation emerges. However, the relationships between crowdedness, enclosure, and pavement are not as strongly correlated as those with greenery. Overall, the pronounced negative association between greenery and the other subindicators is the most definitive pattern in the pair plot.

4.2.1. K-Means Clustering

To determine the optimal number of clusters (k), the elbow method and silhouette method were utilised as highlighted in section 3.6.1. Based on the elbow plot showing the within clusters sum of squares (WCSS) for different k values (Figure 4.15), $k = 4$ was selected as the elbow point, even though there was no very clear bend. This was further validated through the silhouette scores, which showed $k = 4$ provided the most meaningful maximum silhouette coefficient, indicating optimal cohesion and separation (Figure 4.16). While $k = 3$ resulted in a similar silhouette coefficient and $k = 2$ gave the maximum silhouette coefficient, the number of clusters would have been too few to capture meaningful visual walkability patterns across the urban landscape. Thus, $k = 4$ was chosen as the optimal number of clusters for K-Means.

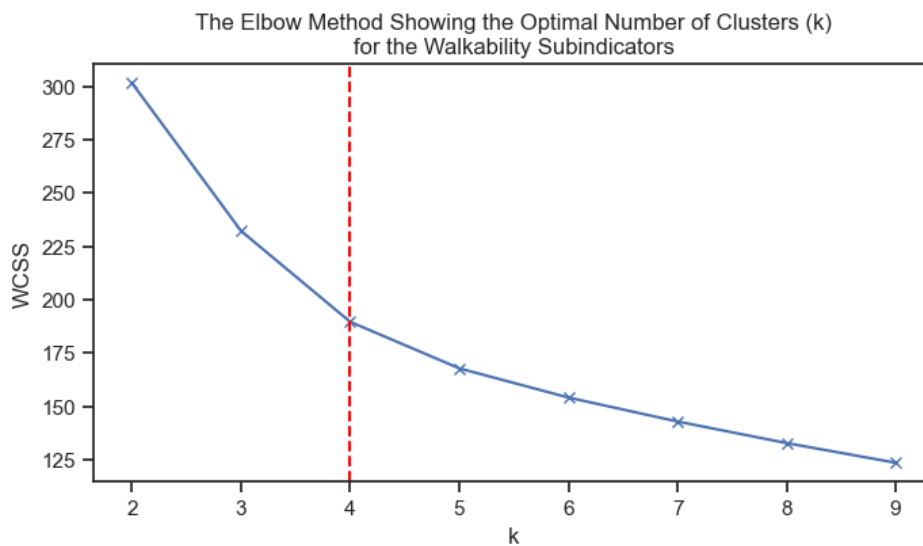


Figure 4.15: Elbow plot showing the optimal number of clusters for the walkability subindicators.

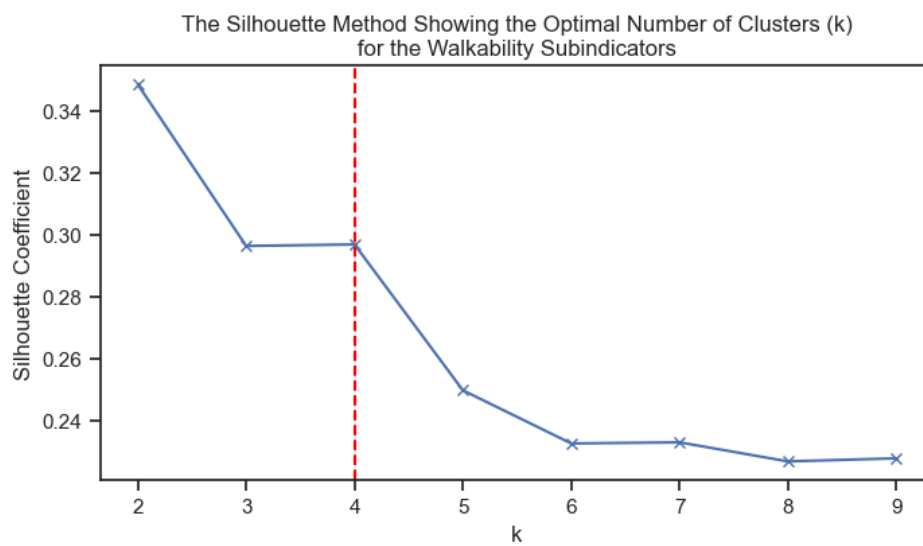


Figure 4.16: Silhouette plot showing the optimal number of clusters for the walkability subindicators.

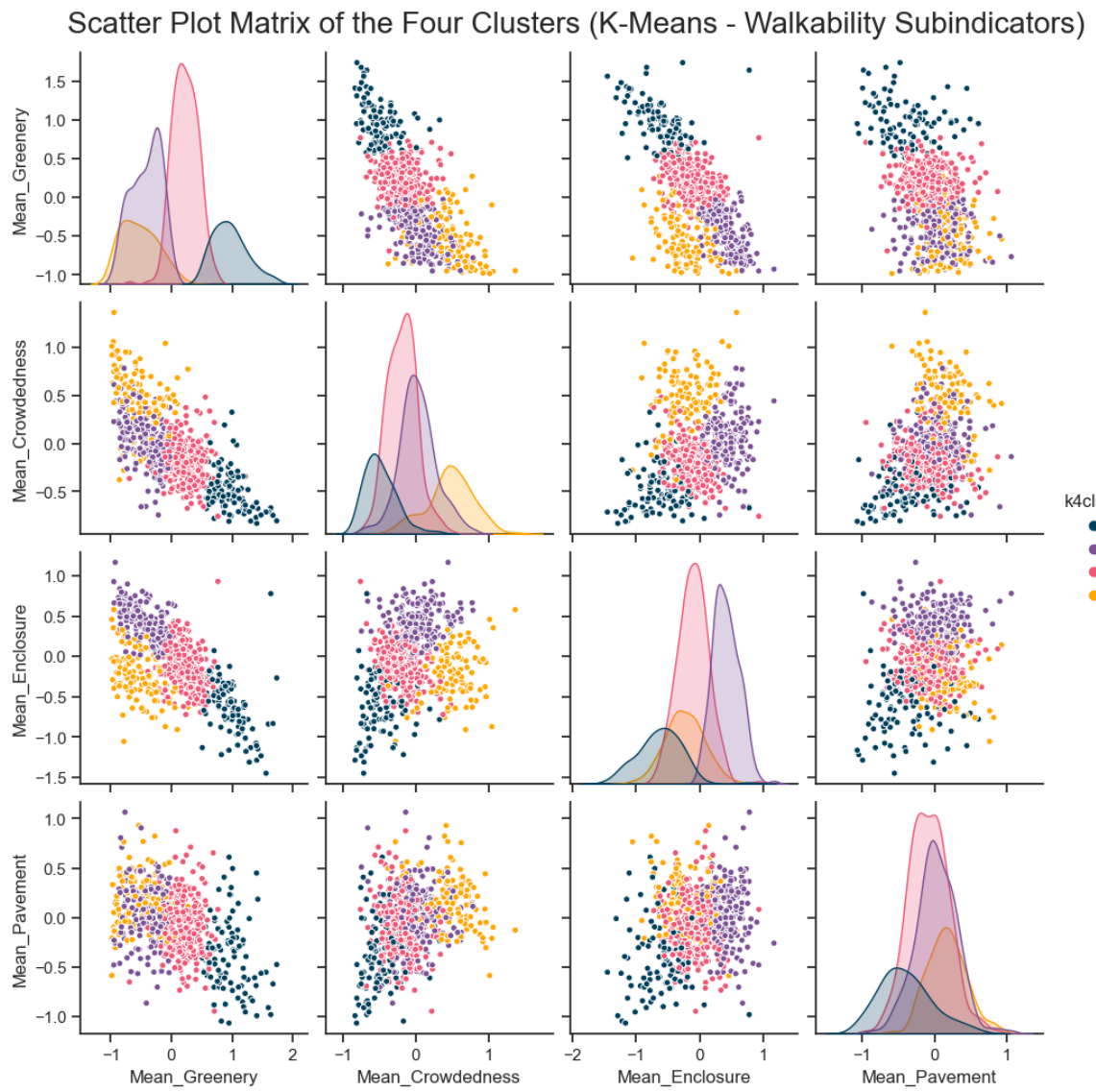


Figure 4.17: Pair plot showing the four clusters of the walkability subindicators data obtained via K-Means.

With 4 clusters, the model revealed groupings of hexagons exhibiting distinct visual walkability profiles. The pair plot in Figure 4.17 visualises the relationships between the walkability subindicators within each cluster. Initial examination shows some differences between clusters – Clusters B and C appear relatively tight and unimodal while Cluster A and D have higher variance. This means that the points within Cluster B and C are very similar to the cluster centroid for the respective subindicator, while the wider spreads in Cluster A and D indicate more variability within the cluster. The Mean Enclosure and Mean Pavement subindicators also possess numerous outliers across the clusters. The Mean Pavement subindicator in particular exhibits significant overlap between the four clusters. These patterns provide context on the cluster characteristics before delving into the subsequent geographic and statistical analysis.



Figure 4.18: Heatmap showing the K-Means cluster averages for the visual walkability subindicators.

After examining the cluster heatmap (Figure 4.18) showing the centre means for the subindicators across clusters along with the spatial distribution map (Figure 4.19), the following interpretations can be made regarding the visual walkability profiles of each K-Means cluster.

Cluster A:

Cluster A exhibits the lowest visual crowdedness and outdoor enclosure with the highest psychological greenery, but also the lowest visual pavement. It appears concentrated along major roads on the outskirts as well as some central areas near the University of Leicester incorrectly grouped due to model errors. This cluster likely represents major transportation corridors with ample vegetation but with insufficient pedestrian infrastructure limiting accessibility.

Cluster B:

Cluster B displays the second highest visual crowdedness potentially due to dense on-street parking, along with the highest outdoor enclosure. It has the second lowest psychological

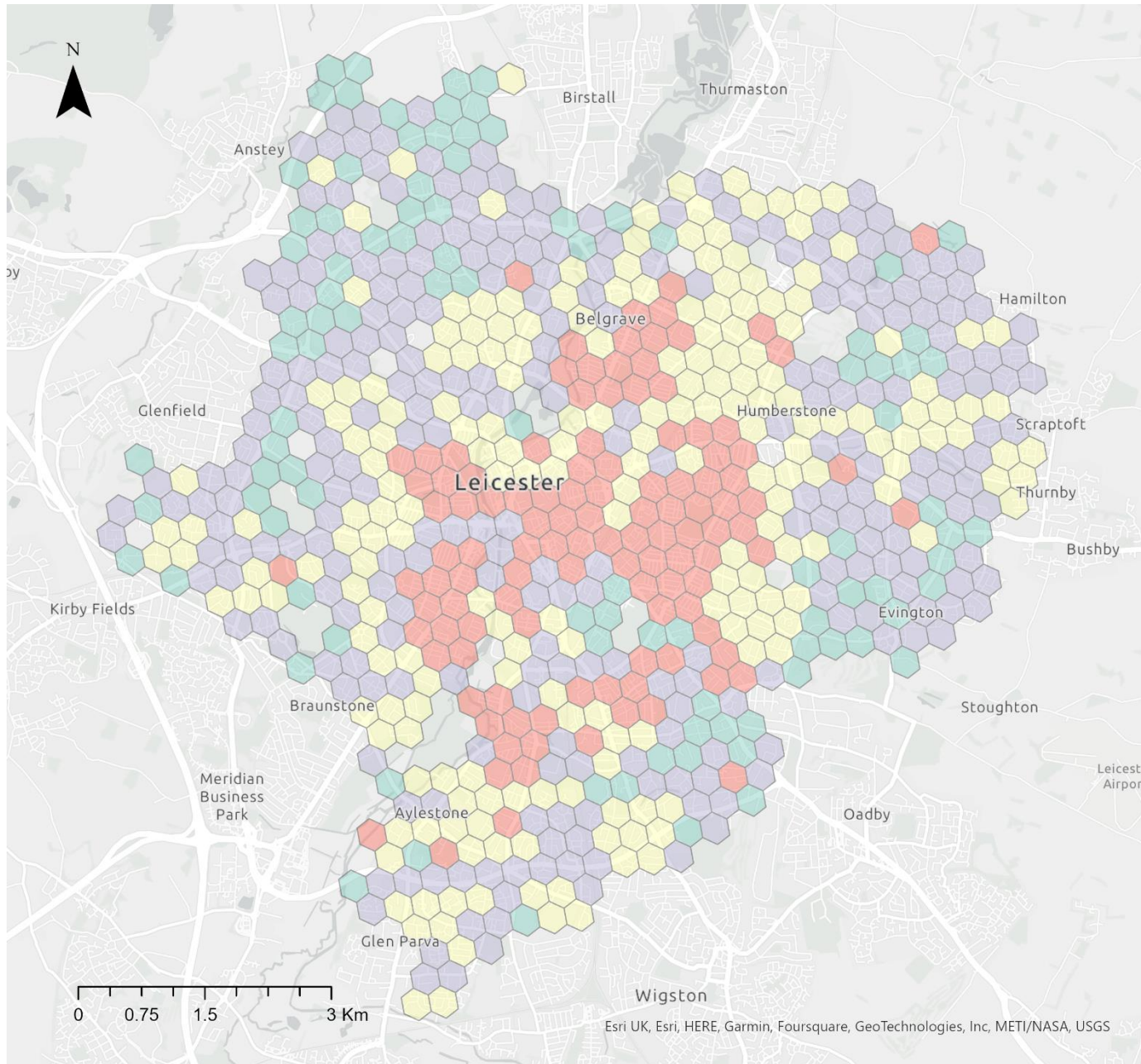
greenery but has reasonably higher pavement to road ratios. This suburban cluster contains streets with decent walkability but lacking much visual appeal and green elements. Residential areas make up this cluster.

Cluster C:

With moderate means for all subindicators, Cluster C emerges as a relatively well-balanced cluster in terms of visual walkability. It does not stand out as exceptional in any one element but has reasonably positive conditions for all subindicators. Cluster C streets are dispersed across central neighbourhoods and outskirts, characterised by semi-high visual walkability.

Cluster D:

Cluster D contains the most visually crowded streets with low outdoor enclosure and minimal psychological greenery but ample pavement. Concentrated in the urban core and around the city centre, this cluster represents the busy commercial and residential areas that suffer from lack of vegetation but have well-developed pedestrian infrastructure. The high activity and lack of green elements hampers the visual walkability in these areas.



Visual Walkability Clusters (K-Means)

Clusters derived from the Visual Walkability Subindicators in Leicester

Cluster

- A
- B
- C
- D

Figure 4.19: Map of Leicester showing the visual walkability clusters from K-Means (Map Scale: 1: 60000).

4.2.2. Fuzzy C-Means Clustering

As highlighted in section 3.6.2, Fuzzy C-Means clustering was applied as a soft clustering technique to uncover patterns among the visual walkability subindicators, in contrast to the crisp clustering of K-Means. A fuzzifier value of 2 was utilised without tuning, as this provides a reasonable level of fuzziness to balance cluster overlap and distinction for the visual walkability data. After clustering, data points were assigned to their maximum membership cluster. With the FCM approach established, the optimal number of clusters was selected using the elbow and silhouette analysis described further.

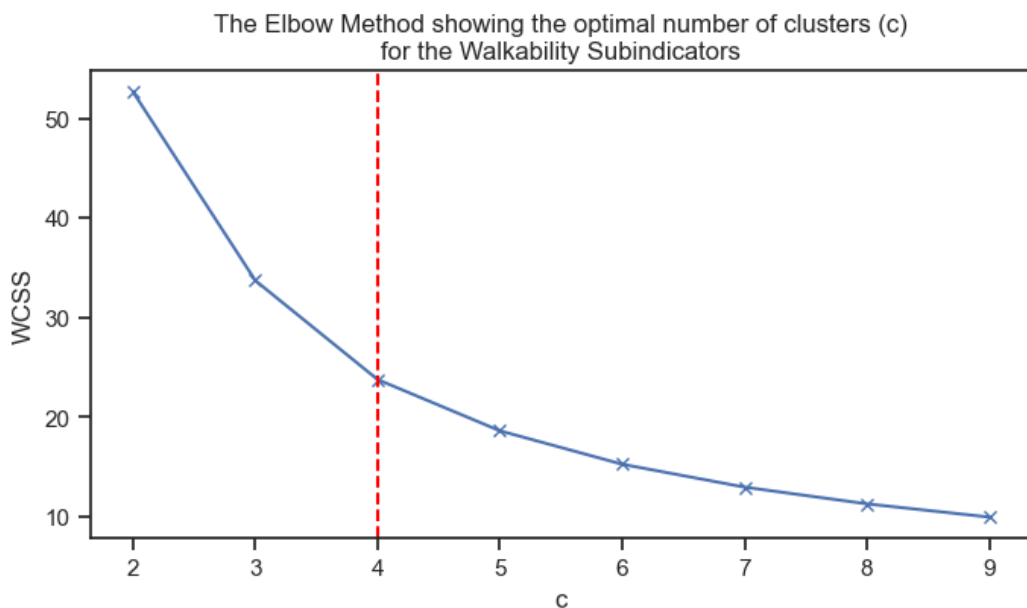


Figure 4.20: Elbow plot showing the optimal number of FCM clusters for the visual walkability subindicators.

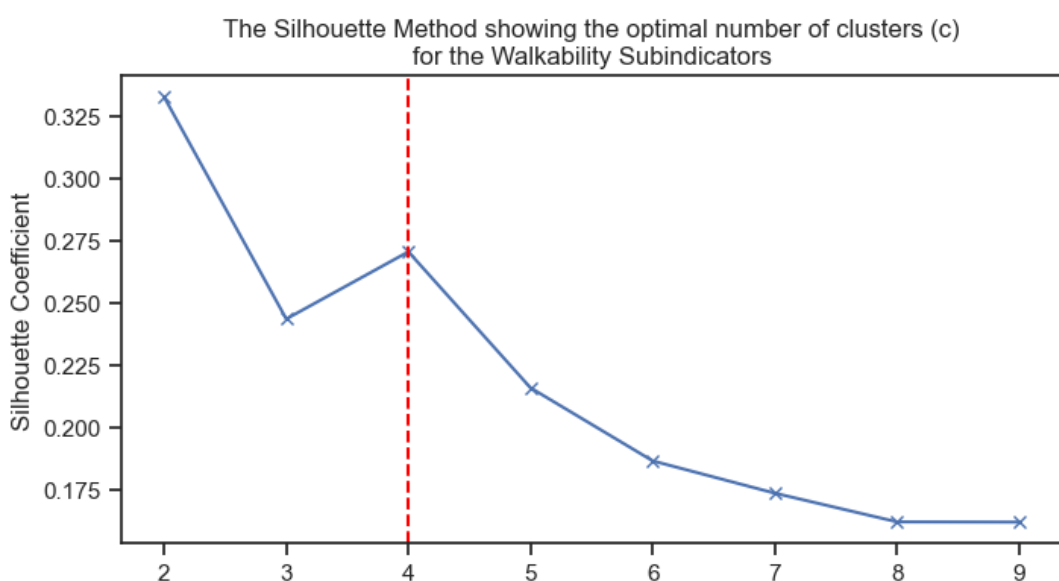


Figure 4.21: Silhouette plot showing the optimal number of FCM clusters for the visual walkability subindicators.

The elbow method indicated an optimal number of clusters (c) of 4 for FCM based on the within cluster sum of squares plot (Figure 4.20), though there was no distinct elbow point. While $c = 3$ was another possibility, it would provide too few clusters to capture meaningful visual walkability patterns. The choice of $c = 4$ was further validated by the silhouette scores (Figure 4.21). While $c = 2$ gave the maximum silhouette coefficient, this would have affected the interpretability. For $c = 4$, a high silhouette coefficient was obtained at 0.2704, and provided a better balance between maximising cohesion and separation. There was a notable drop in the silhouette score after $c = 4$ as well. Therefore, $c = 4$ was selected as the optimal number of soft clusters for FCM to uncover nuanced visual walkability patterns.

Scatter Plot Matrix of the Four Clusters (Fuzzy C-Means - Walkability Subindicators)

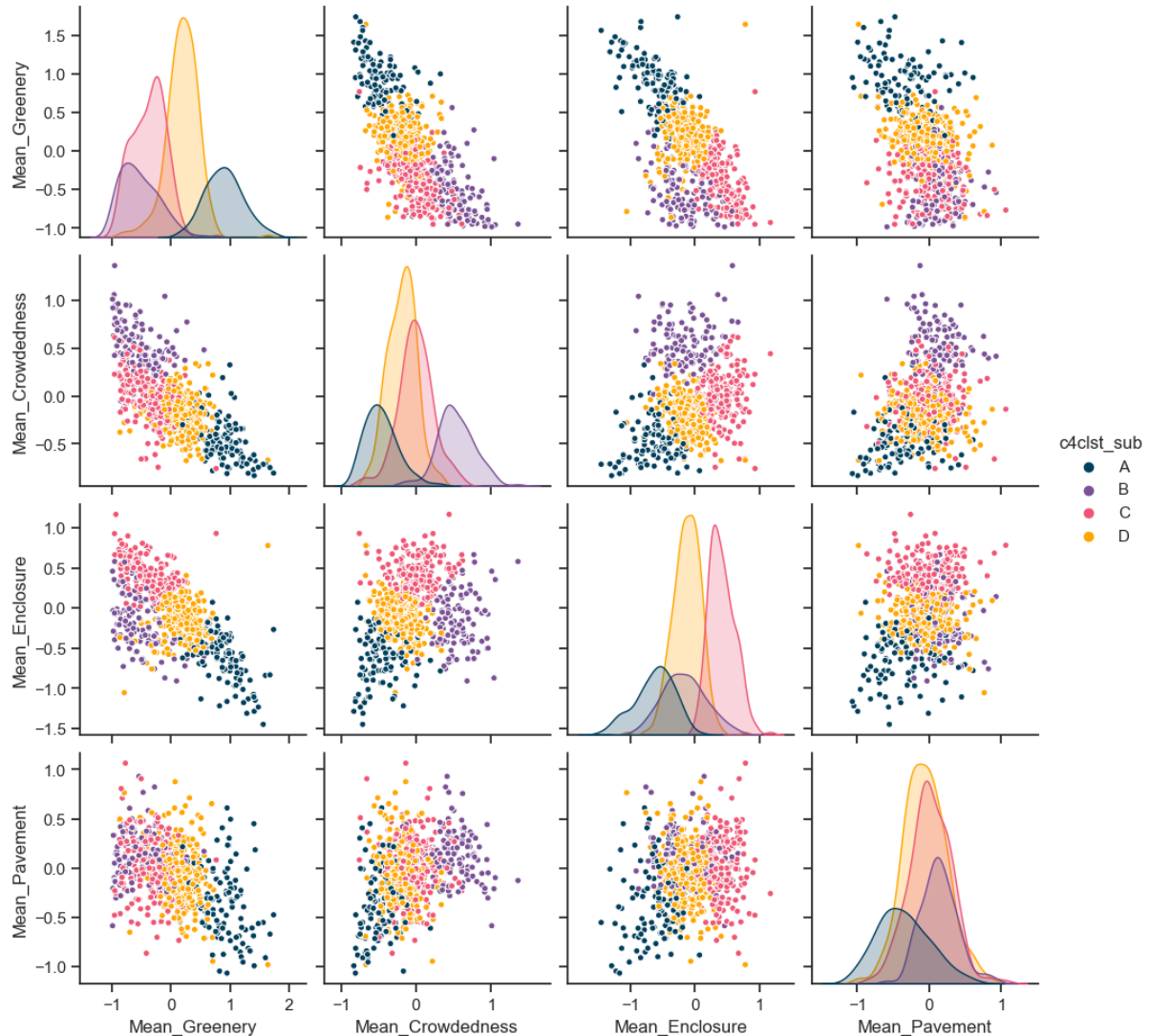


Figure 4.22: Pair plot showing the four clusters of the walkability subindicators data obtained via FCM.

The pair plot in Figure 4.22 provides visualisation of the relationships between the visual walkability subindicators within each fuzzy cluster. Examination of the 4 soft clusters reveals distinct yet overlapping walkability profiles with notable similarities to the hard K-Means clusters. Most distinctly, Clusters C and D exhibit tight, unimodal distributions akin to K-Means Clusters B and C, while Clusters A and B display higher variance similar to K-Means Clusters A and D, though to a lesser degree. This indicates Clusters C and D have low variability around sub-indicator centroids, while Clusters A and B show greater internal variance. Again, significant overlap can be noticed between clusters for the Mean Pavement subindicator. Numerous outliers can also be seen outside the cluster boundaries, particularly for Mean Enclosure and Mean Pavement. These patterns both reinforce and diverge from the K-Means clusters, highlighting the distinct insights surfaced through soft clustering.

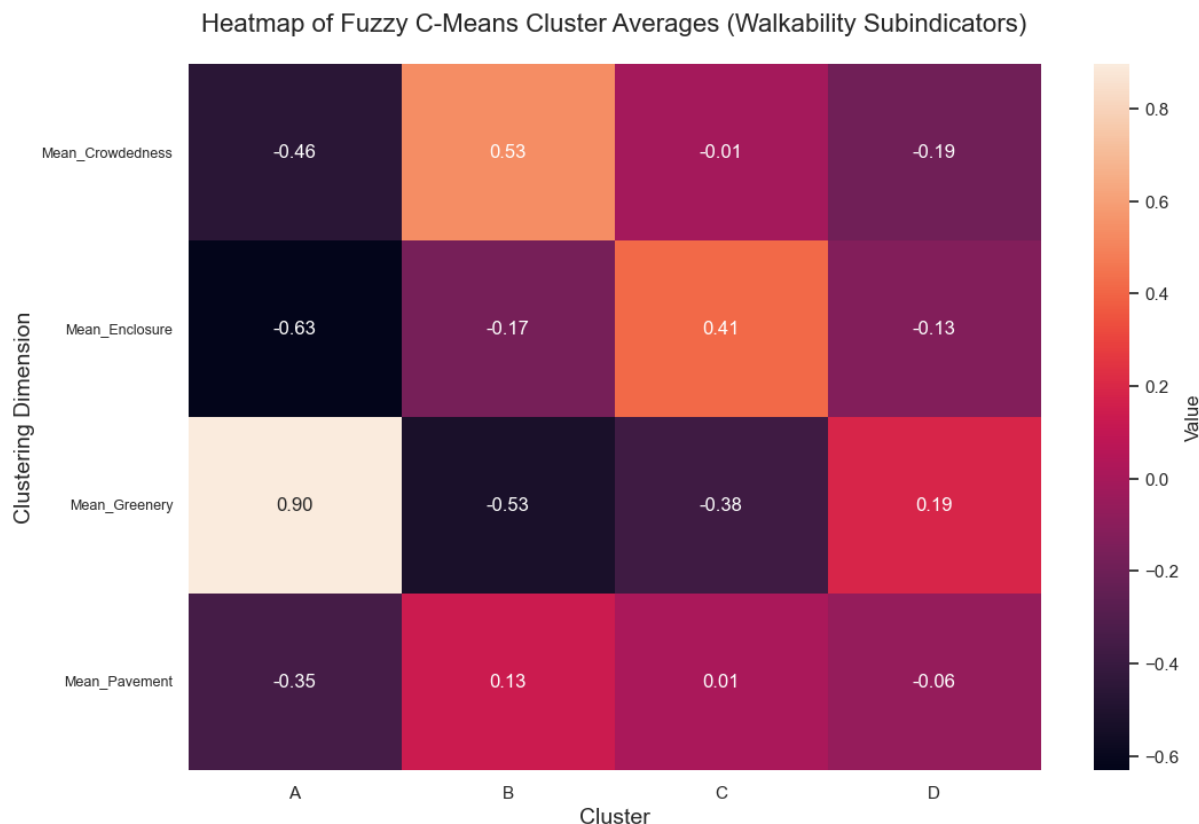


Figure 4.23: Heatmap showing the FCM cluster averages for the visual walkability subindicators.

After examining the FCM cluster heatmap (Figure 4.23) and the spatial distribution map (Figure 4.24), the following interpretations can be made regarding the visual walkability profiles.

Cluster A:

Cluster A exhibits the lowest visual crowdedness and outdoor enclosure with the highest psychological greenery, but also the lowest visual pavement. It appears concentrated along major outer roads and some central areas near University of Leicester that were likely incorrectly grouped due to model limitations. This cluster likely represents major transportation corridors with ample roadside vegetation, but with insufficient pedestrian infrastructure. It mirrors K-Means Cluster A.

Cluster B:

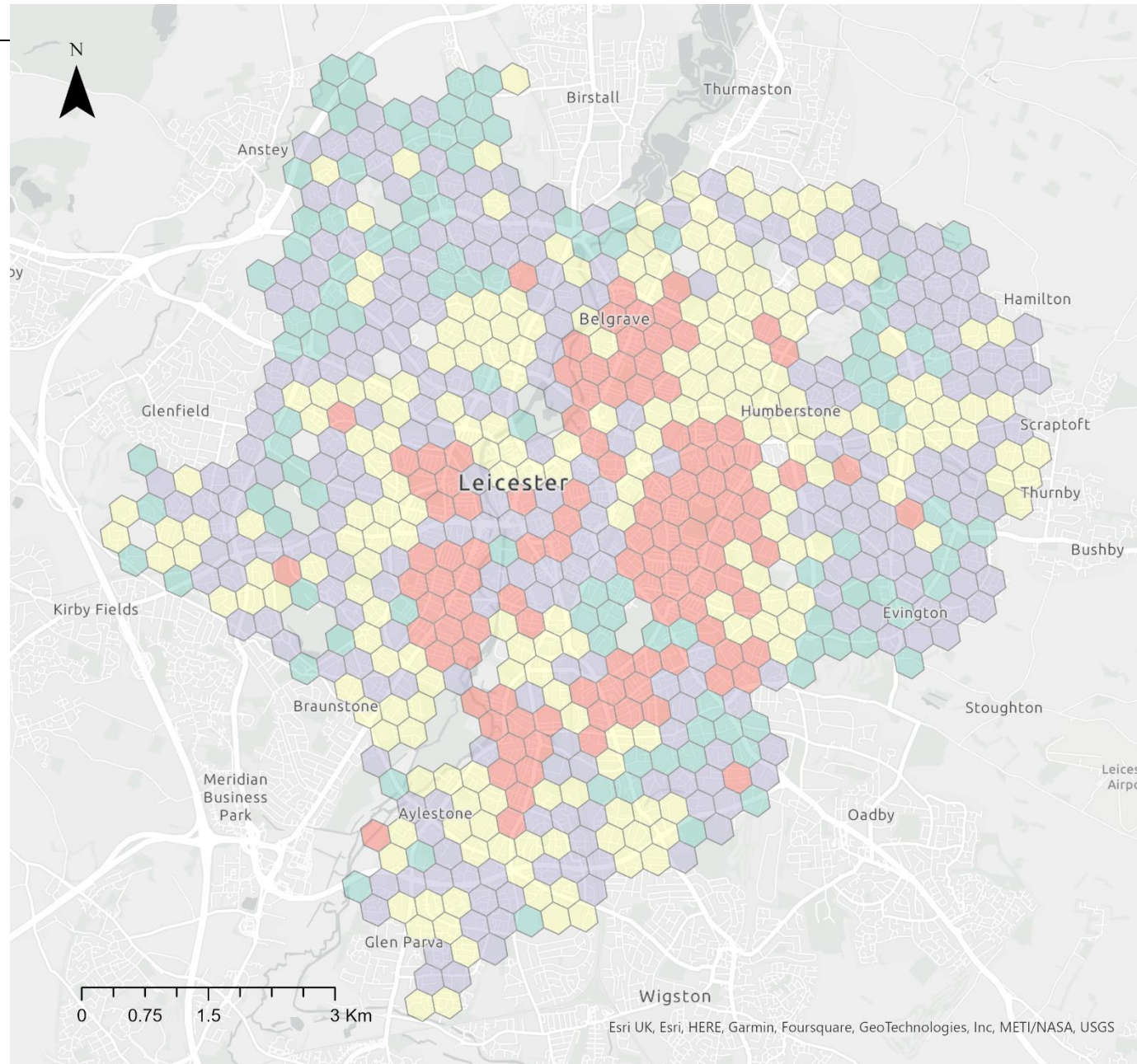
Cluster B contains the most crowded streets with medium outdoor enclosure, the lowest psychological greenery but the highest visual pavement. It represents the busy city centre and urban residential areas that suffer from lack of green elements but possess well-developed pedestrian infrastructure. The high visual crowdedness likely arises from the crowds within the city centre and from the dense on-street parking in the surrounding residential areas.

Cluster C:

Cluster C consists of moderately crowded streets with the highest outdoor enclosure, low psychological greenery but also relatively high visual pavement. It captures urban residential areas and neighbourhoods that, besides having good pedestrian infrastructure, lack visual appeal and vegetation. The crowdedness is less pronounced than Cluster B, potentially attributed to less on-street parking congestion.

Cluster D:

Cluster D displays moderately low visual crowdedness and outdoor enclosure with medium levels of psychological greenery and visual pavement. It emerges as a relatively balanced cluster characterised by semi-decent visual walkability that is dispersed throughout the city.



Visual Walkability Clusters (Fuzzy C-Means)

Clusters derived from the Visual Walkability Subindicators in Leicester

Cluster

- A
- B
- C
- D

Figure 4.24: Map of Leicester showing the visual walkability clusters from FCM (Map Scale: 1: 60000).

4.2.2.1. Filtering Weak Membership Clusters

As highlighted in section 3.6.2, clusters with low membership degrees less than 0.5 were excluded to focus the analysis on clusters with strong membership degrees. A threshold of 0.5 was chosen because clusters below this can be considered weak associations for those data points. Removing these low membership clusters aids in filtering out outliers and clarifies the visualisation and interpretation of clusters with firm visual walkability patterns. After filtering, the size of substantial clusters decreased a fair amount as shown in the bar plot comparison (Figure 4.25). Examination of the final resulting clusters reveal better statistical relationships with the subindicators with lesser noise from the weaker outlier assignments.

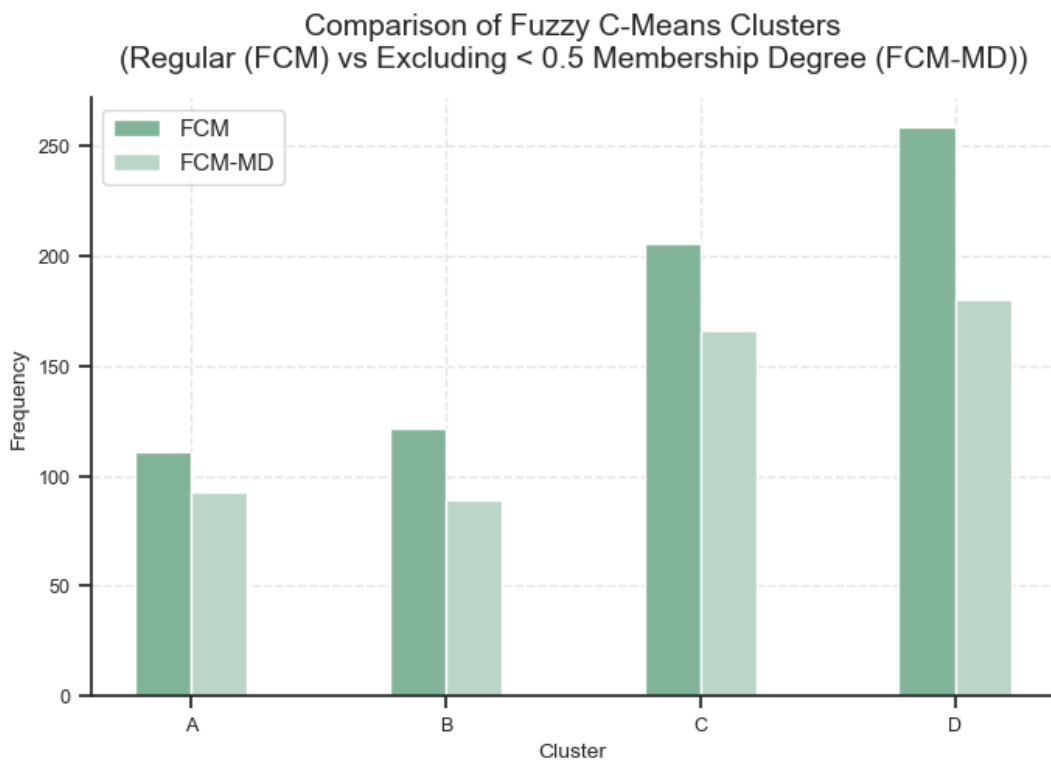


Figure 4.25: Bar plot comparing the size of FCM clusters before and after filtering.

Examining Figure 4.25 and Table 4.1, a notable reduction in clusters sizes after discarding low membership hexagons below 0.5 degrees can be noticed. Cluster A saw its count decrease from 109 to 91 (-16.1%), Cluster B from 115 to 88 (-23.47%), Cluster C from 216 to 168 (-22.22%), and Cluster D from 258 to 188 (-27.13%). In total, 18, 27, 48, and 70 hexagons were filtered out of Clusters A, B, C, and D respectively, with Cluster D exhibiting the largest drop. Filtering thereby enables the accentuation of the core hexagons with firmer cluster associations due to the removal of the weaker outlier assignments. Focusing only on these highly associated groupings omits noise from the weakly affiliated hexagons. This enables

clearer and more accurate interpretations of visual walkability, especially when examining the spatial distribution of the remaining clusters.

Table 4.1: Cluster counts before and after removing hexagons with membership degrees below 0.5.

Cluster	Number of Hexagons Before Filtering	Number of Hexagons After Filtering	Difference in Percent (%)
A	109	91	16.51
B	115	88	23.47
C	216	168	22.22
D	258	188	27.13

Scatter Plot Matrix of the Four Clusters (Fuzzy C-Means - Walkability Subindicators) After Excluding Clusters with Membership Degree Less Than 0.5)

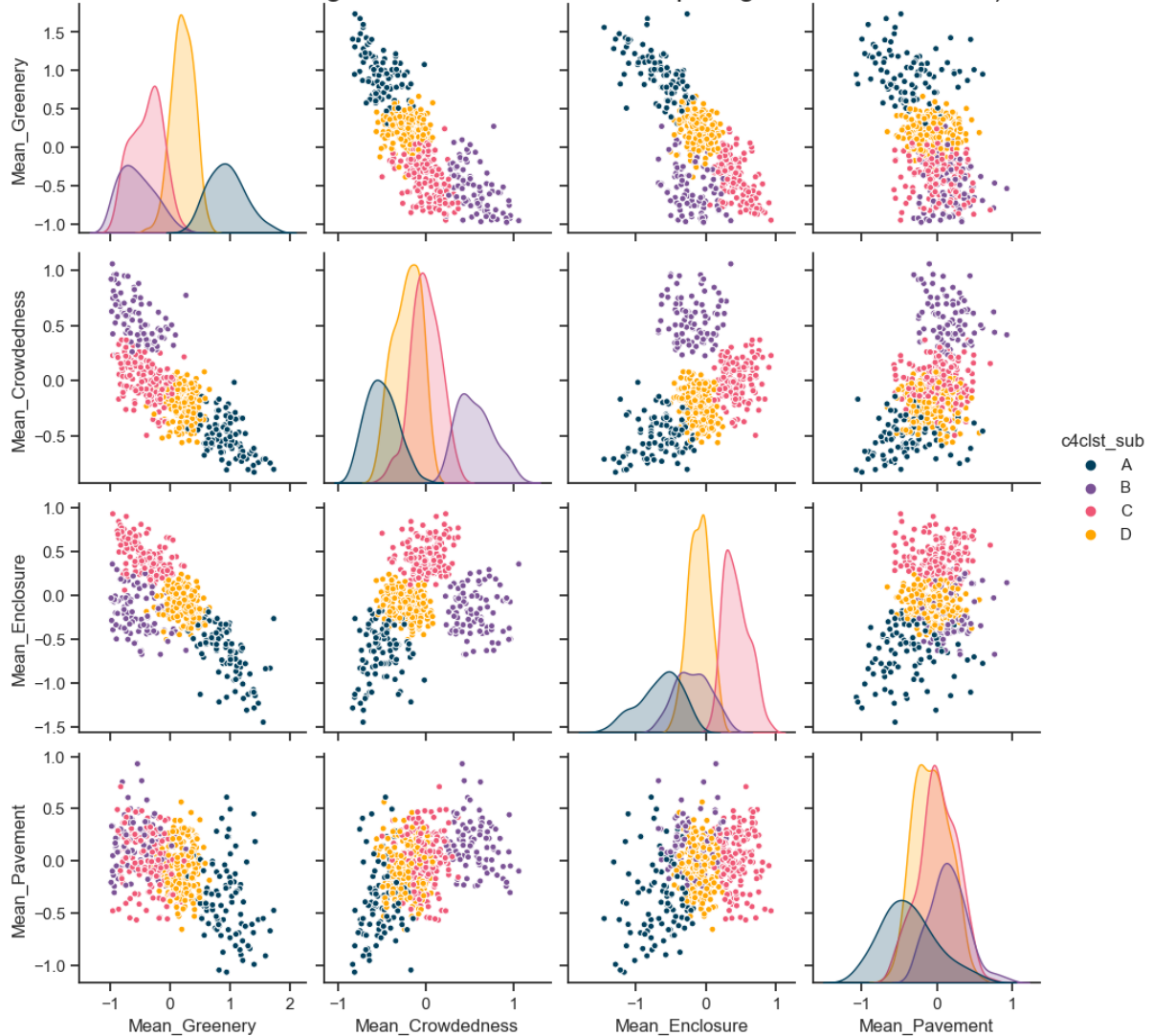


Figure 4.26: Pair plot showing the four clusters of the walkability subindicators data obtained via FCM after filtering.

Examination of the pair plot (Figure 4.26) and the spatial distribution map (Figure 4.27) after filtering provides further perspective. Geographically, the filtered low membership hexagons appear concentrated in central areas and regions between the city centre and outskirts, suggesting weaker cluster association in those zones. Comparing the pre- and post- filtering pair plots reveal a notable reduction in points situated distant from cluster centres and boundaries for all four subindicators, although points in Mean Pavement are still fairly spread out. The distribution is fairly similar but notably better for Mean Crowdedness because it's a bit narrower. Distribution has improved slightly for Mean Pavement as well; however, significant overlap persists between all clusters on this subindicator, indicating ongoing model limitations. Overall, filtering clarifies the subindicator relationships by reducing noise from weak assignments. Cluster separation also exhibits marginal improvement, though Mean Pavement has persistent overlapping. The geographic distribution suggests most clusters capture meaningful visual walkability patterns.

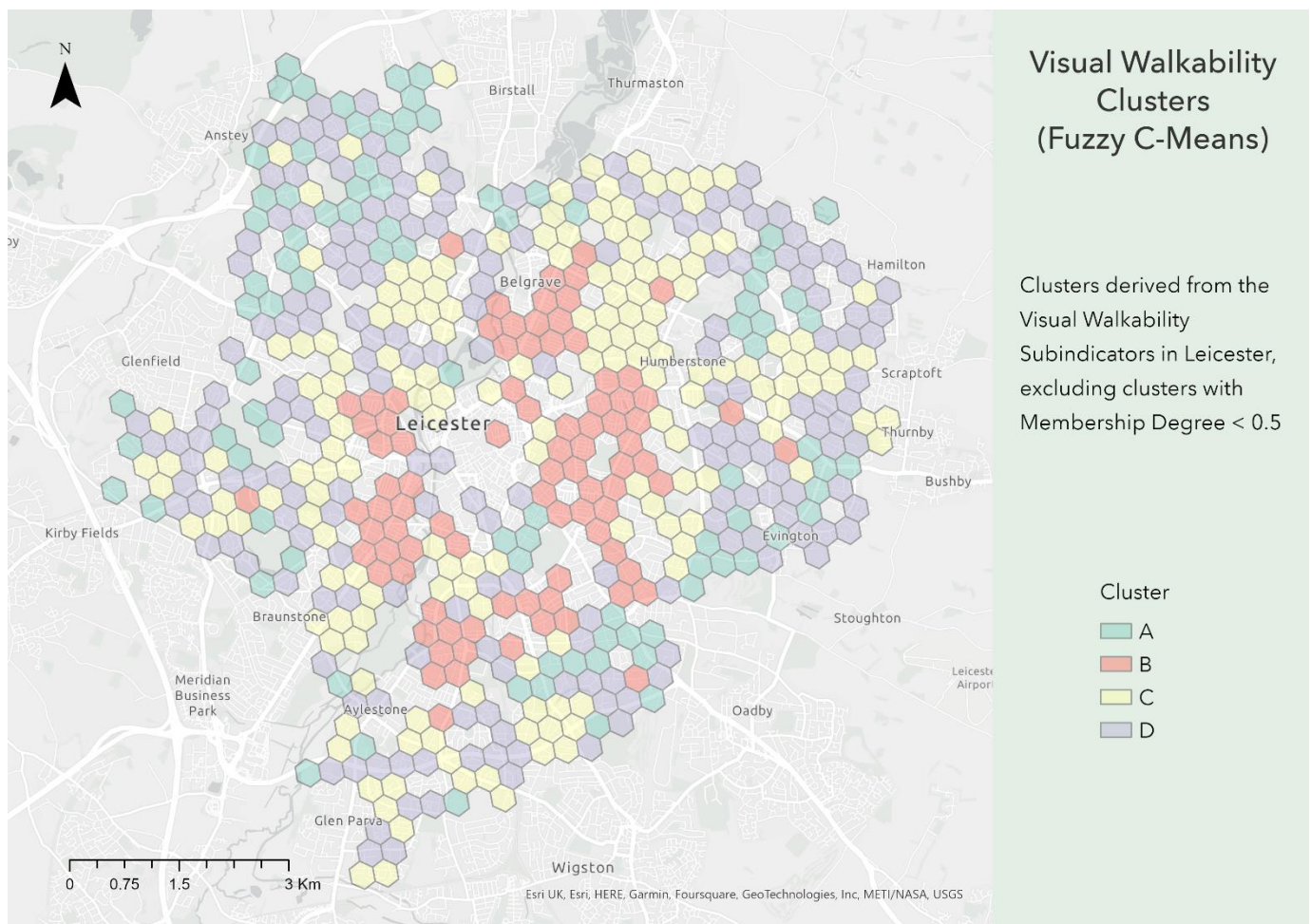


Figure 4.27: Map of Leicester showing the visual walkability clusters from FCM after filtering (Map Scale: 1: 60000).

An alluvial diagram, created using the RAWGraphs tool (Mauri *et al.*, 2017), is used to visualise how the K-Means clusters transitioned into the FCM clusters in Figure 4.28. The vertical axis displays the clusters, with K-Means clusters on the left and FCM clusters on the right. The ribbons illustrate the magnitude of flow between clusters across the two models. It can be observed that Cluster A mostly remained intact from K-Means to FCM. Cluster B predominantly flowed into Cluster C for FCM, while Cluster C primarily transitioned into Cluster D. Lastly, Cluster D largely converted into Cluster B under FCM. The alluvial plot effectively communicates the cluster mapping between the two methods.

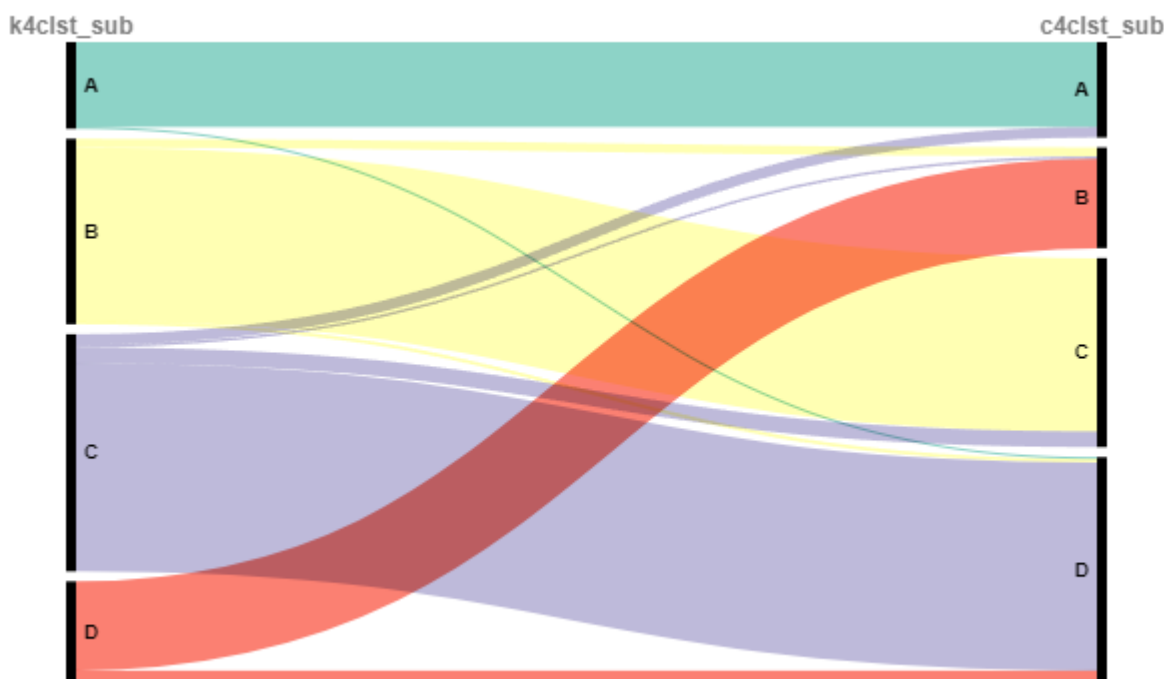


Figure 4.28: Alluvial diagram representing the flow of cluster assignment of the hexagons between the two clustering techniques.

4.3. Cluster Analysis with the POI Diversity Data

As highlighted in section 3.6.3, cluster analysis was also performed incorporating the POI diversity index to identify relationships between visual walkability and accessibility-related walkability. The POI diversity index, calculated using Shannon's entropy formula, quantified the amenity mix and urban vibrancy of each hexagon based on the variety and distribution of amenity types within it. Cluster analysis on both visual and POI indicators examined potential correlations and distinct patterns between the two walkability dimensions.

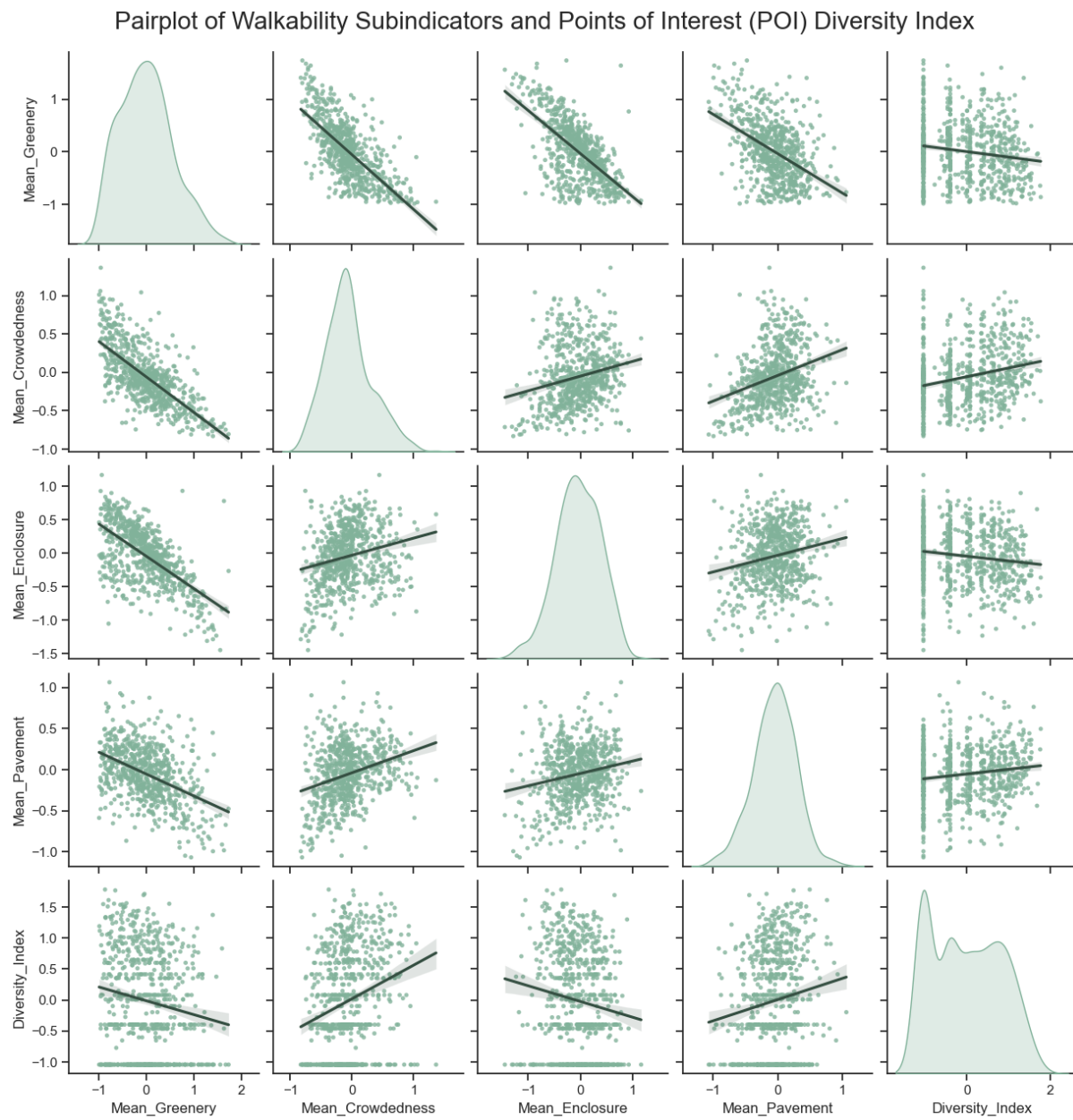


Figure 4.29: Pair plot visualising relationships between the visual walkability subindicators and the POI diversity index.

Examination of the pair plot incorporating the POI diversity (Figure 4.29) revealed some notable trends. As the POI diversity index increased, psychological greenery exhibited a downward trend, while visual crowdedness increased. Outdoor enclosure displayed a downward trajectory as well, indicating improved enclosure with greater POI diversity. Lastly, visual pavement had an upward trend with increasing amenity mix, though the relationship is not starkly pronounced.

4.3.1. K-Means Clustering

Determining the optimal number of clusters for K-Means clustering followed similar analysis as clustering with only the visual walkability subindicators. The elbow method suggested $k = 4$ as a reasonable elbow point, though there was no distinct bend (Figure 4.30). Silhouette analysis indicated $k = 4$ provided the maximum meaningful silhouette score, while $k = 2$ was the highest value and $k = 3$ resulted in the second highest score (Figure 4.31). However, $k = 4$ was selected as the other values would yield too few meaningful clusters given the multidimensional data.

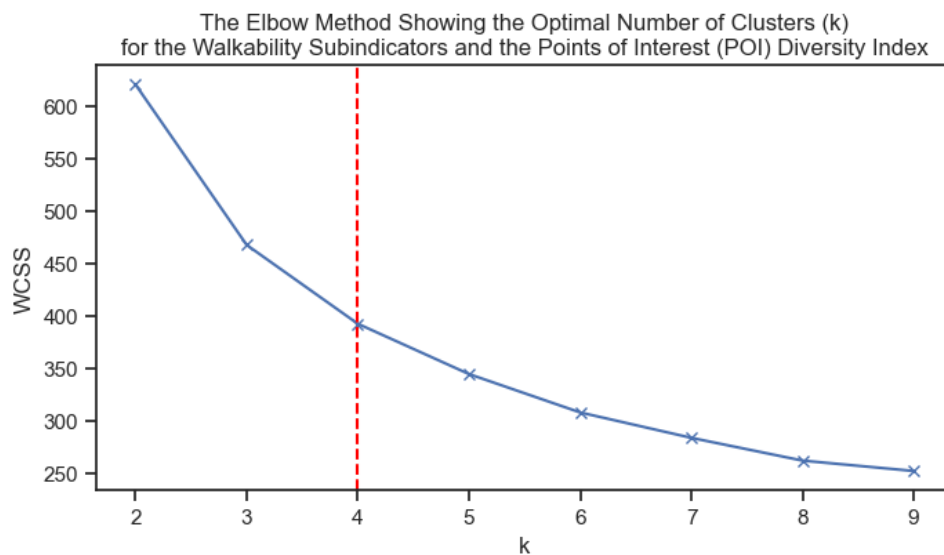


Figure 4.30: Elbow plot showing the optimal number of clusters for the walkability subindicators and the POI diversity.

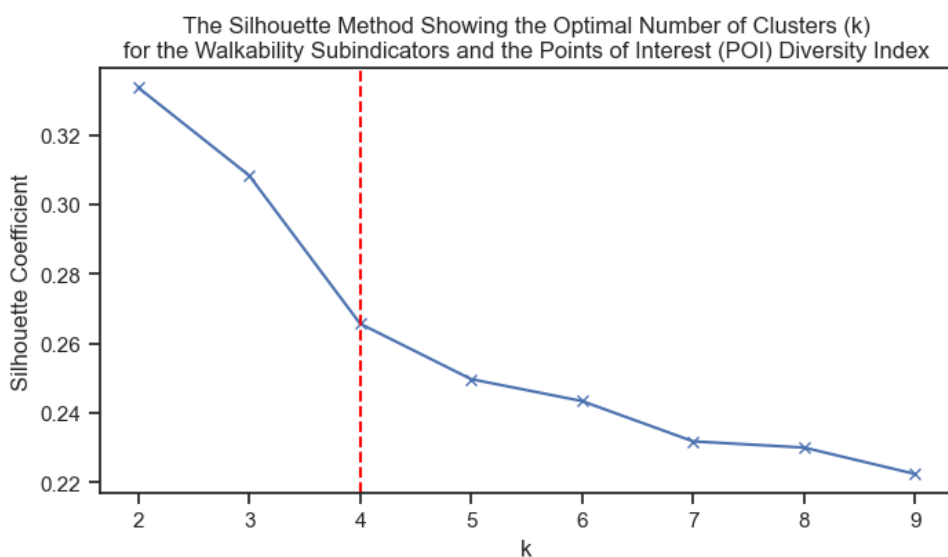


Figure 4.31: Silhouette plot showing the optimal number of clusters for the walkability subindicators and POI diversity data.

Examination of the cluster pair plot (Figure 4.32) revealed clear groupings formed based on the relationships between POI diversity and psychological greenery, visual crowdedness, and outdoor enclosure. However, the visual pavement subindicator again did not cluster as cleanly. Compared to the earlier visual-only clusters, distributions appear tighter for all variables except POI diversity index, which was skewed towards lower values owing to many hexagons having minimal amenity diversity. Significant overlap persisted between clusters, potentially more than the prior walkability clustering. The plot suggests amenity diversity strongly shaped the cluster patterns in conjunction with the visual elements.

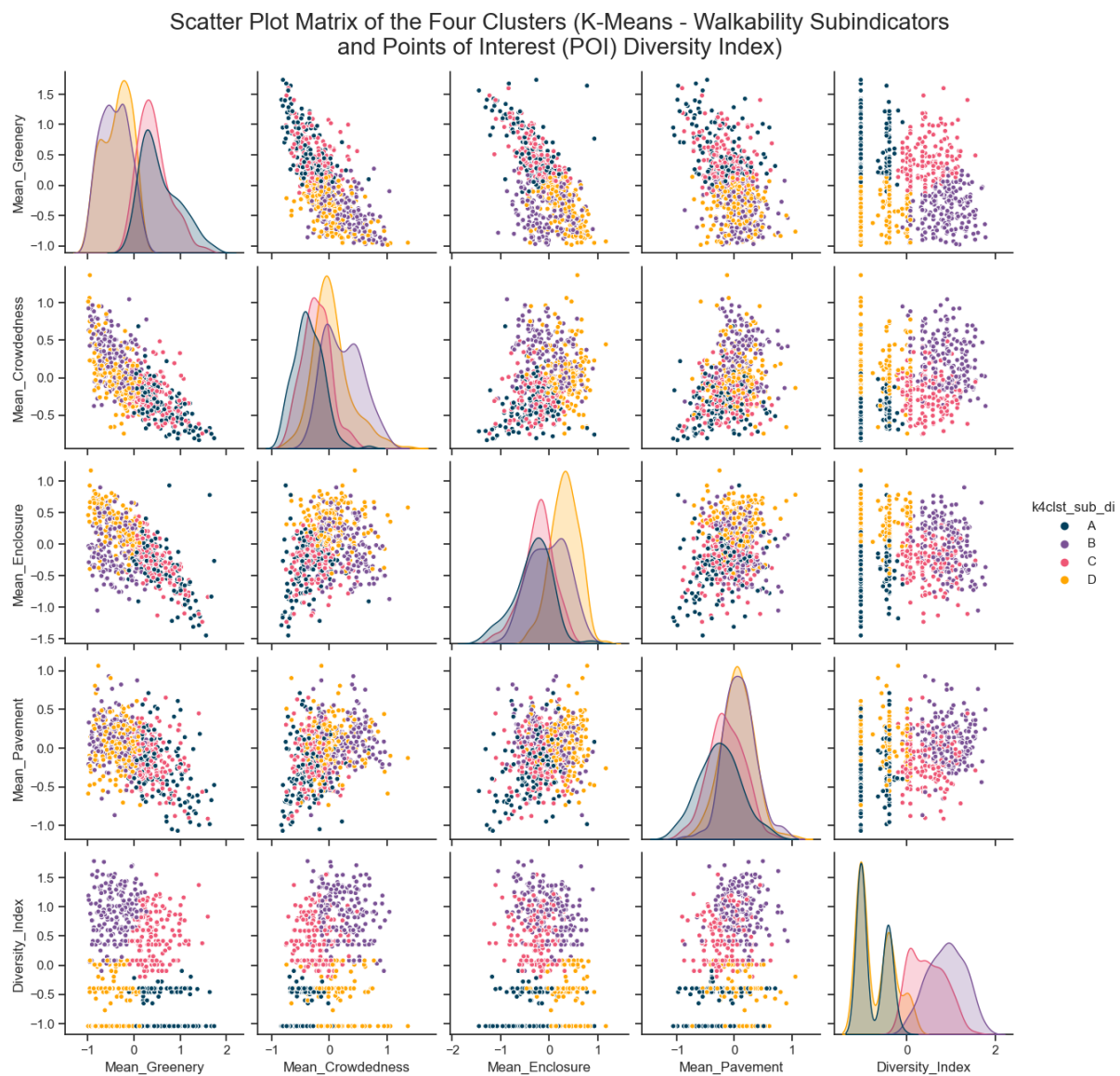


Figure 4.32: Pair plot showing the four clusters of the walkability subindicators and POI diversity data obtained via K-Means.

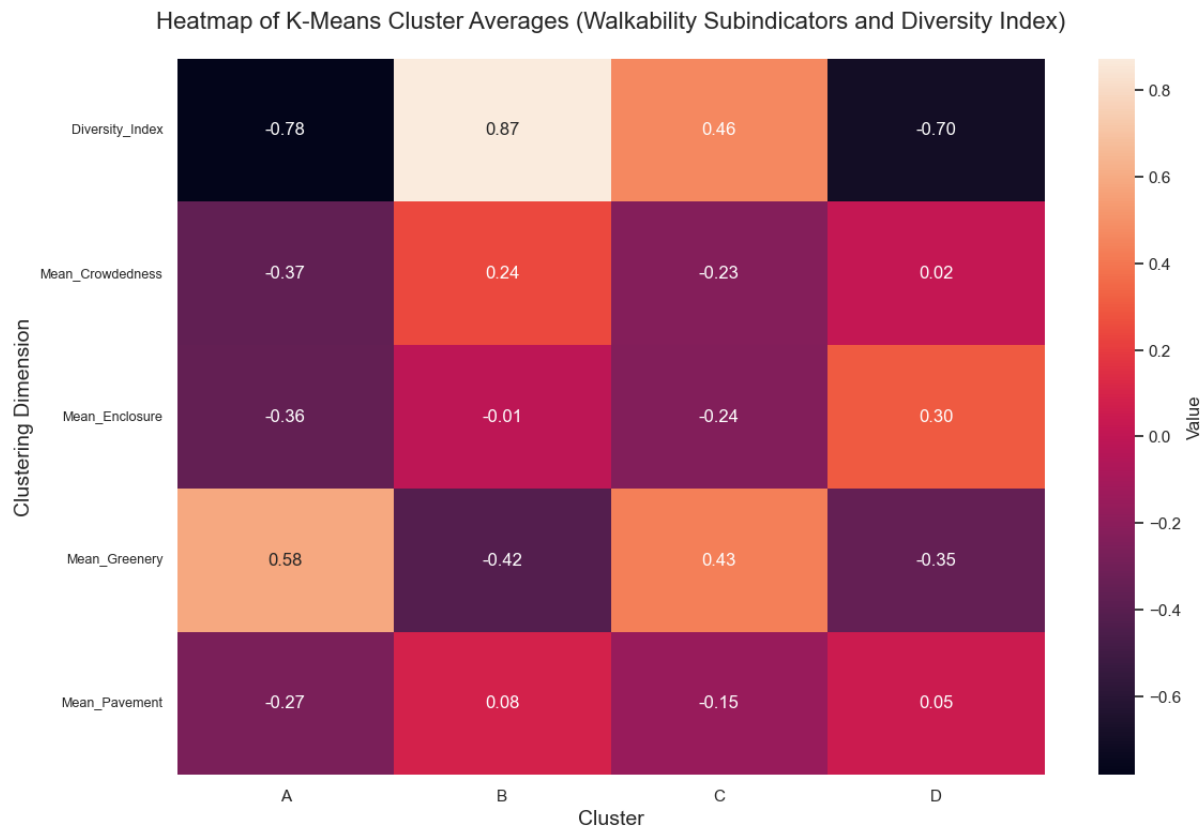


Figure 4.33: Heatmap showing the K-Means cluster averages for the walkability subindicators and POI diversity.

After examining the K-Means cluster heatmap (Figure 4.33) and the spatial distribution map (Figure 4.34), the following interpretations can be made regarding the walkability profiles.

Cluster A:

This cluster possesses the lowest POI diversity and visual crowdedness with high psychological greenery but insufficient visual pavement. Concentrated along major outer roads, it likely represents corridors with vegetation but inadequate pedestrian infrastructure and amenity access.

Cluster B:

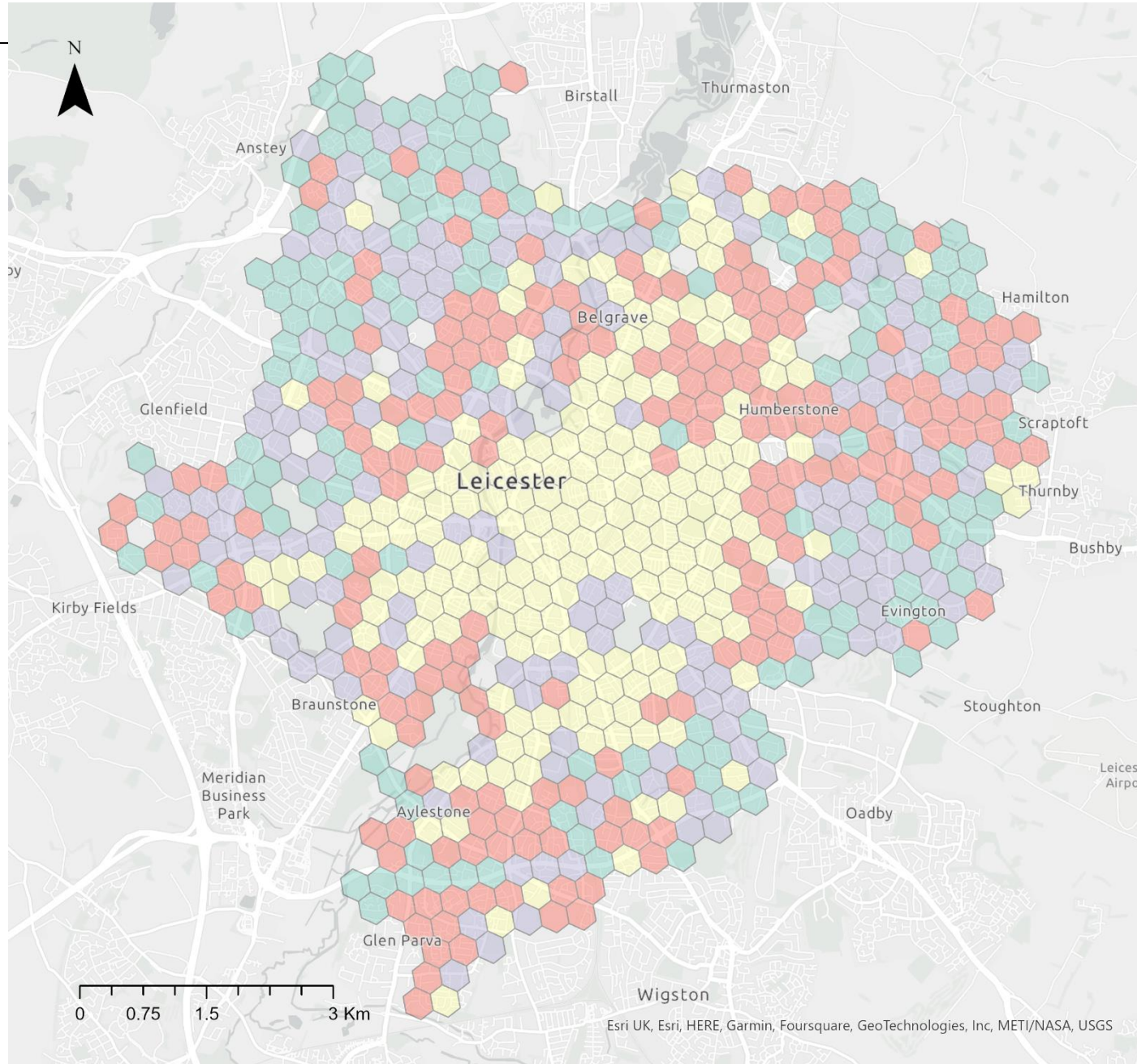
This cluster exhibits the highest POI diversity index and visual crowdedness with low greenery but ample pavement. Capturing the city centre and commercial areas and also the urban residential areas around it, it comprises busy streets with many nearby amenities but lacking visual appeal and green space.

Cluster C:

Cluster C displays the second highest POI diversity and lowest visual crowdedness with moderately high greenery and pavement. Dispersed throughout central neighbourhoods, it encapsulates the most visually walkable areas with good amenity mix.

Cluster D:

This cluster possesses low POI diversity like Cluster A but with high enclosure, low greenery, and medium pavement. Occurring in suburban residential areas, it represents neighbourhoods with poor amenity access and walkability.



Walkability Clusters (K-Means)

Clusters derived from the Visual Walkability Subindicators and the Points of Interest (POI) Diversity Index in Leicester

Cluster

- A
- B
- C
- D

Figure 4.34: Map of Leicester showing the walkability clusters from K-Means (Map Scale: 1: 60000).

4.3.2. Fuzzy C-Means Clustering

FCM clustering was applied next to enable soft cluster assignments. The elbow method indicated an optimal number of clusters $c = 4$, similar to the K-Means outcome (Figure 4.35). Silhouette analysis also showed $c = 4$ the maximum silhouette score that would give meaningful clusters, though $c = 2$ and $c = 3$ resulted in higher coefficients (Figure 3.36). Examining the cluster pair plot (Figure 4.37), tight distributions emerged with less variance between clusters. Relationships between POI diversity and other subindicators were well-defined, except for the ongoing limitations with visual pavement.

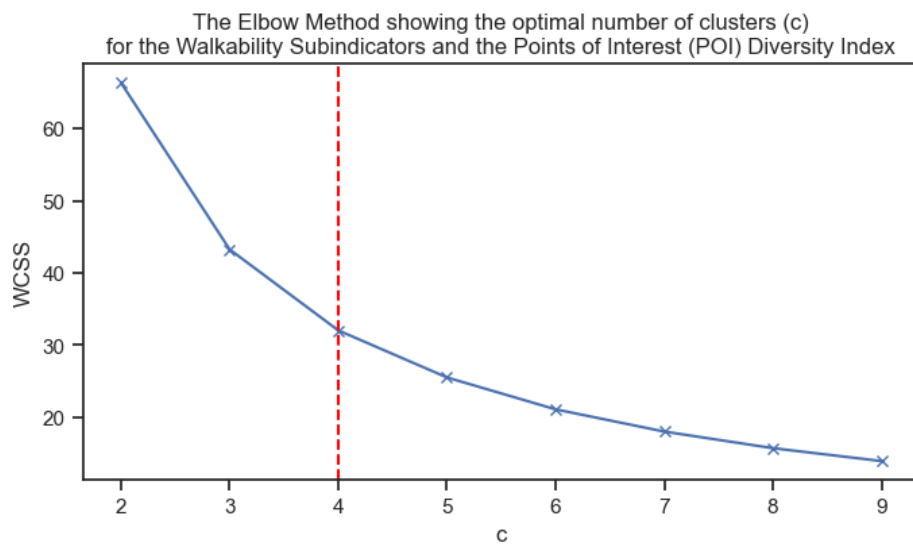


Figure 4.35: Elbow plot showing the optimal number of FCM clusters for the walkability subindicators and the POI diversity.

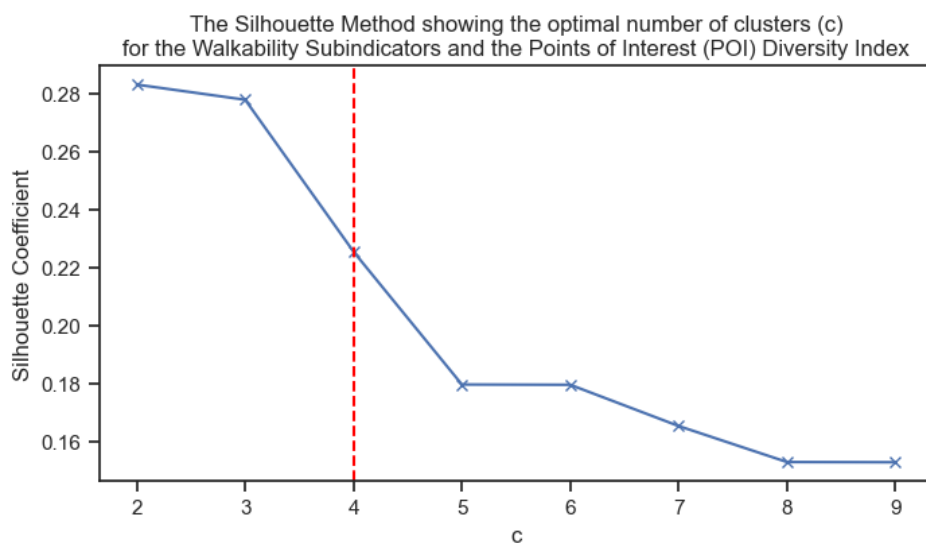


Figure 4.36: Silhouette plot showing the optimal number of FCM clusters for walkability subindicators and POI diversity.

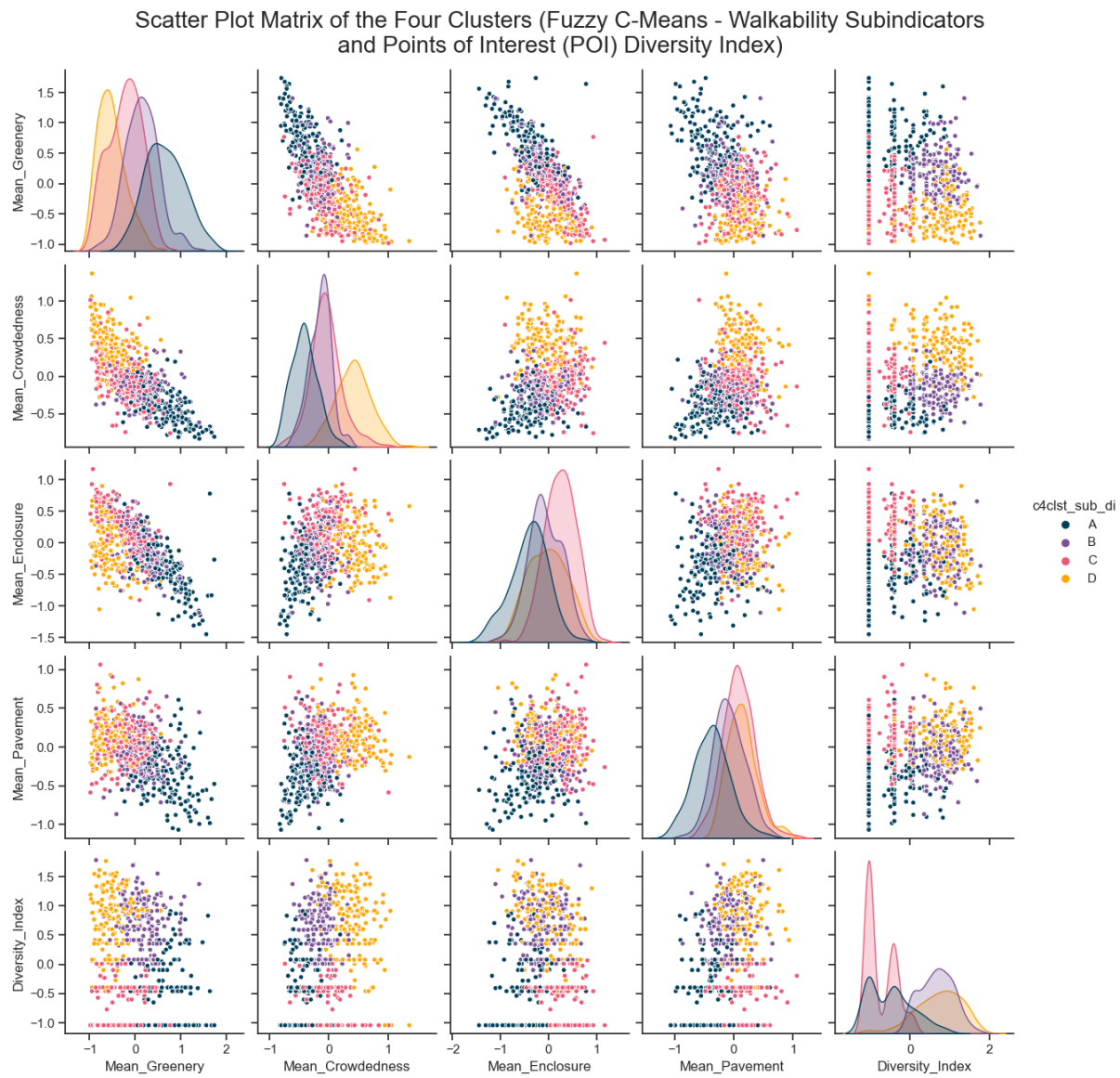


Figure 4.37: Pair plot showing the four clusters of the walkability subindicators and POI diversity data obtained via FCM.

After examining the FCM cluster heatmap (Figure 4.38) and the spatial distribution map (Figure 4.39), the following interpretations can be made regarding the walkability profiles.

Cluster A:

Cluster A possesses the second lowest POI diversity with low visual crowdedness, enclosure and pavement, but high greenery. Concentrated along major outer roads, it represents green yet inaccessible and pedestrian-unfriendly corridors.

Cluster B:

Cluster B exhibits the second highest POI diversity and lowest visual crowdedness and enclosure, with moderately high greenery and pavement. Occurring throughout central neighbourhoods and outskirts, it encapsulates the most visually walkable and vibrant areas.

Cluster C:

Cluster C displays low POI diversity with high visual crowdedness and enclosure, but lower greenery and pavement quality. Present in suburban residential areas, it comprises neighbourhoods with poor amenity access and walkability.

Cluster D:

Cluster D contains the highest POI diversity index with extreme visual crowdedness, medium enclosure, minimal greenery but ample pavement. As the urban city centre and residential neighbourhoods, it is walkable in infrastructure but crowded and lacking green visual appeal.

Heatmap of Fuzzy C-Means Cluster Averages (Walkability Subindicators and Diversity Index)

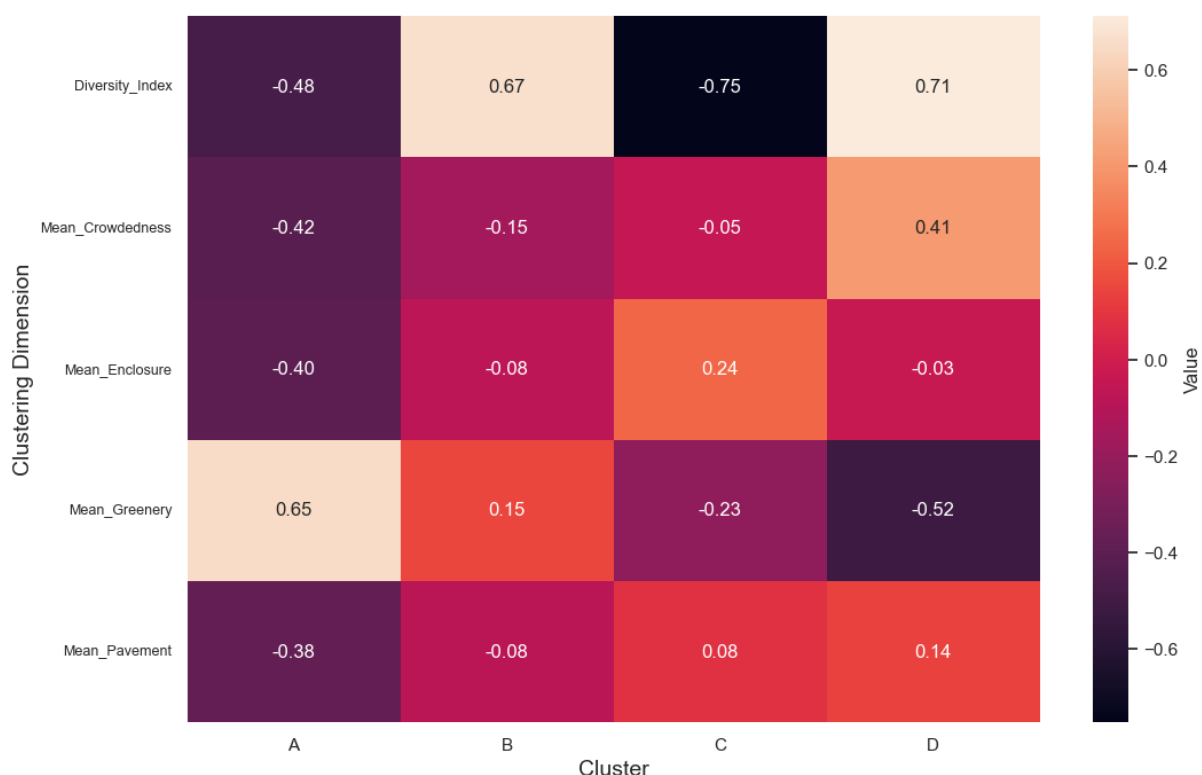


Figure 4.38: Heatmap showing the FCM cluster averages for the walkability subindicators and POI diversity.

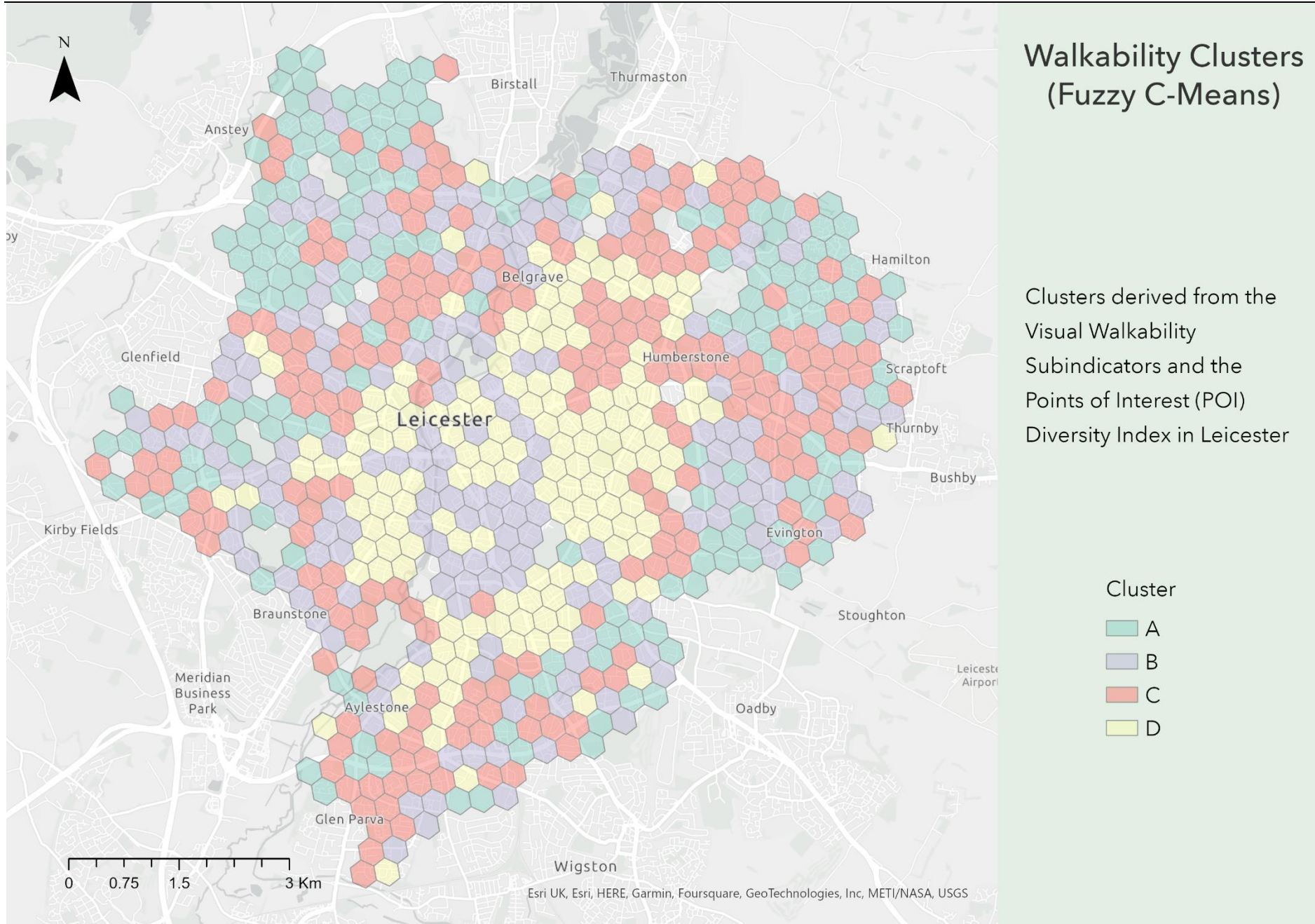


Figure 4.39: Map of Leicester showing the walkability clusters from FCM (Map Scale: 1: 60000).

4.3.2.1. Filtering Weak Membership Clusters

Filtering out hexagons with membership degrees below 0.5 resulted in approximately half of the data being excluded, as shown in the bar plot (Figure 4.40). Specifically, Cluster A lost 45% of its hexagons, Cluster B lost 58.75%, Cluster C lost 42.38%, and Cluster D lost 37.74%, as shown in Table 4.2. This indicates that many hexagons have low membership values, likely due to some limitation in the data structure, and most likely due to the poor performance with the visual pavement subindicator. A threshold of 0.5 does not seem unreasonably stringent. Hence, the distribution of membership degrees suggests there are underlying issues causing a sizable portion of hexagons to not associate strongly with any cluster.

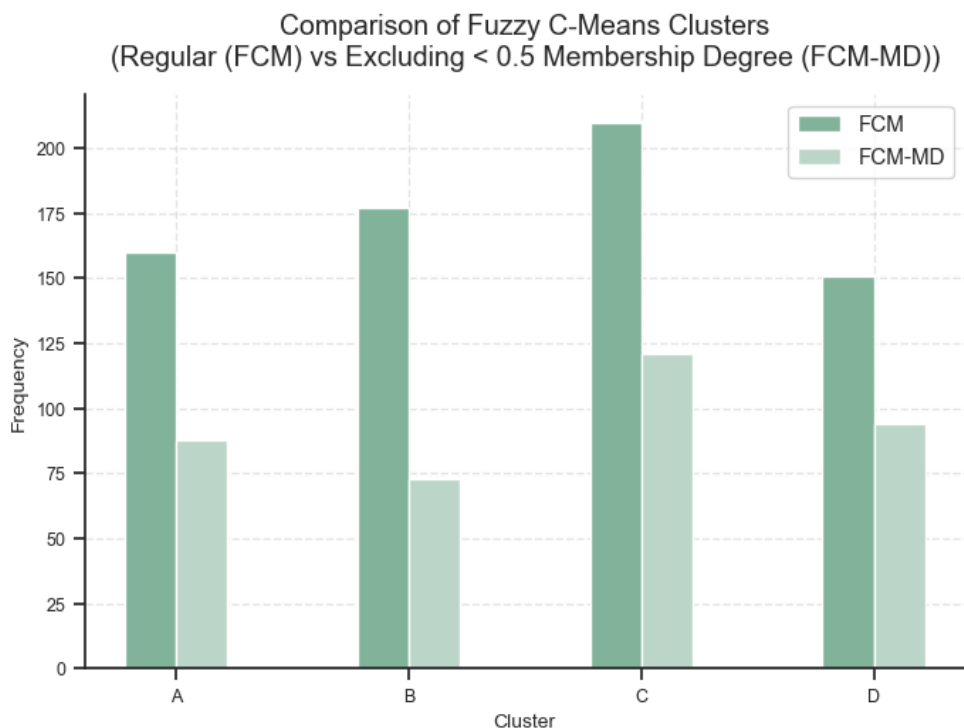


Figure 4.40: Bar plot comparing the size of FCM clusters before and after filtering.

Table 4.2: FCM Cluster counts before and after removing hexagons with membership degrees below 0.5.

Cluster	Number of Hexagons Before Filtering	Number of Hexagons After Filtering	Difference in Percent (%)
A	160	88	45.00
B	177	73	58.75
C	210	121	42.38
D	151	94	37.74

Scatter Plot Matrix of the Four Clusters (Fuzzy C-Means - Walkability Subindicators and Points of Interest (POI) Diversity Index) After Excluding Clusters with Membership Degree Less Than 0.5

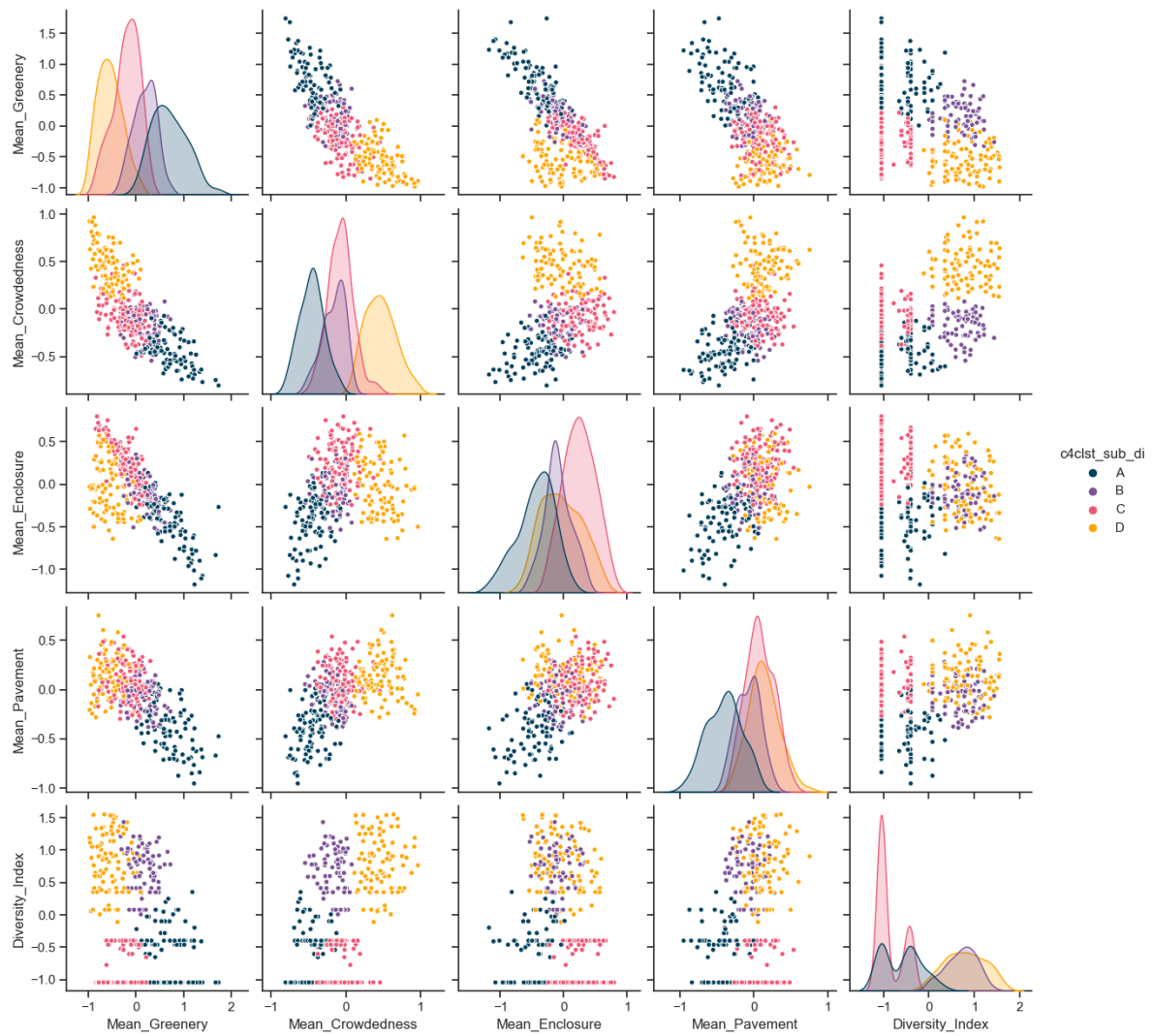


Figure 4.41: Pair plot showing the four clusters of the walkability subindicators and POI data obtained via FCM after filtering.

Examination of the pair plot (Figure 4.41) reveals tighter cluster distributions and fewer outliers after filtering, with well-defined relationships between POI diversity and other subindicators. However, considering the substantial data exclusion, these patterns may not represent the full dataset adequately. The geographic distribution (Figure 4.42) shows large filtered areas, notably in the city centre and outskirts. With such significant spatial omission, the filtered clusters and relationships likely skew perspectives on broader walkability patterns, despite appearing improved in isolation.

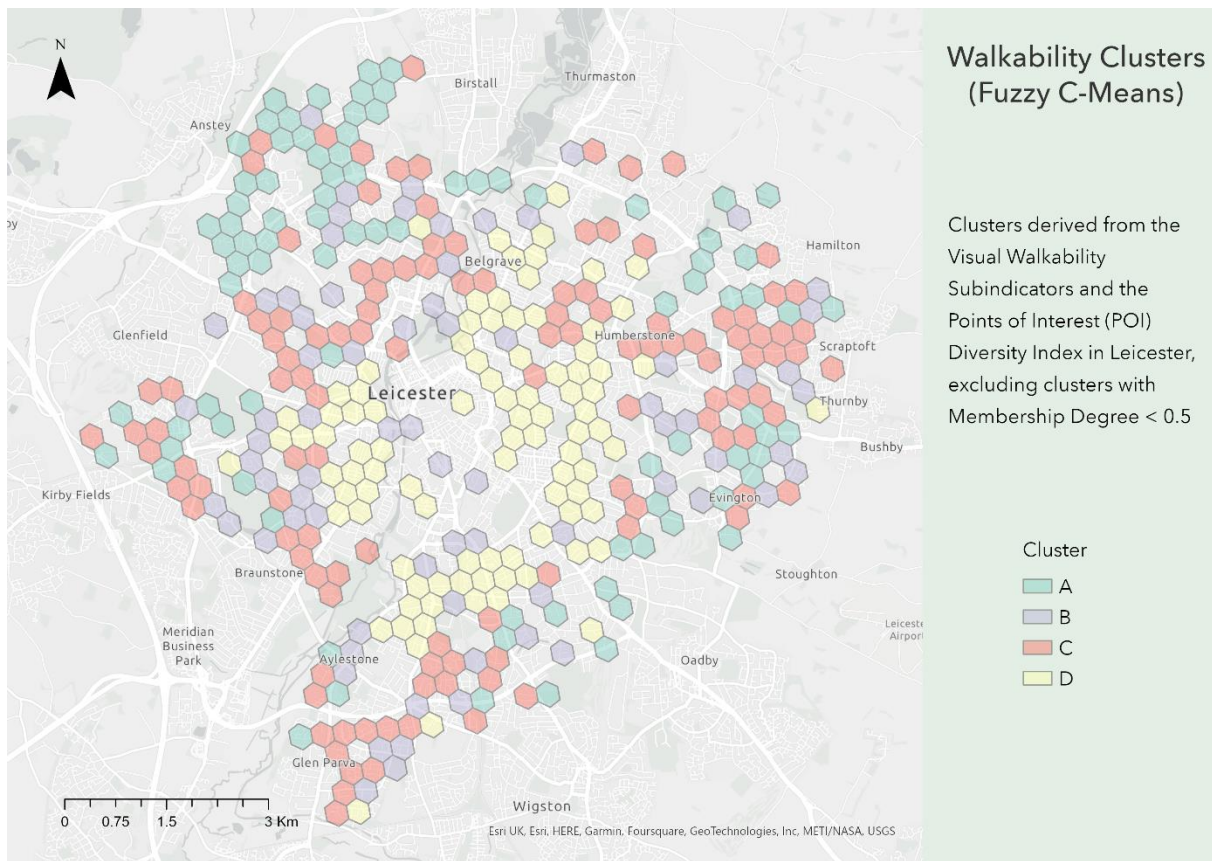


Figure 4.42: Map of Leicester showing the walkability clusters from FCM after filtering (Map Scale: 1: 60000).

The alluvial plot (Figure 4.43) visualises the mapping between the K-Means and Fuzzy C-Means clusters for the hexagons. It illustrates that Cluster A remained largely intact between the crisp and soft clustering solutions. Cluster B from K-Means predominantly transitioned into Cluster D under FCM. Cluster C primarily converted into Cluster B with the shift to fuzzy clustering. Lastly, a majority of Cluster D became Cluster C. While some clusters were preserved, the algorithms diverged significantly in their treatment of others, particularly Cluster B. The alluvial diagram effectively communicates these mapping relationships and cluster transitions between K-Means and Fuzzy C-Means incorporating POI diversity.

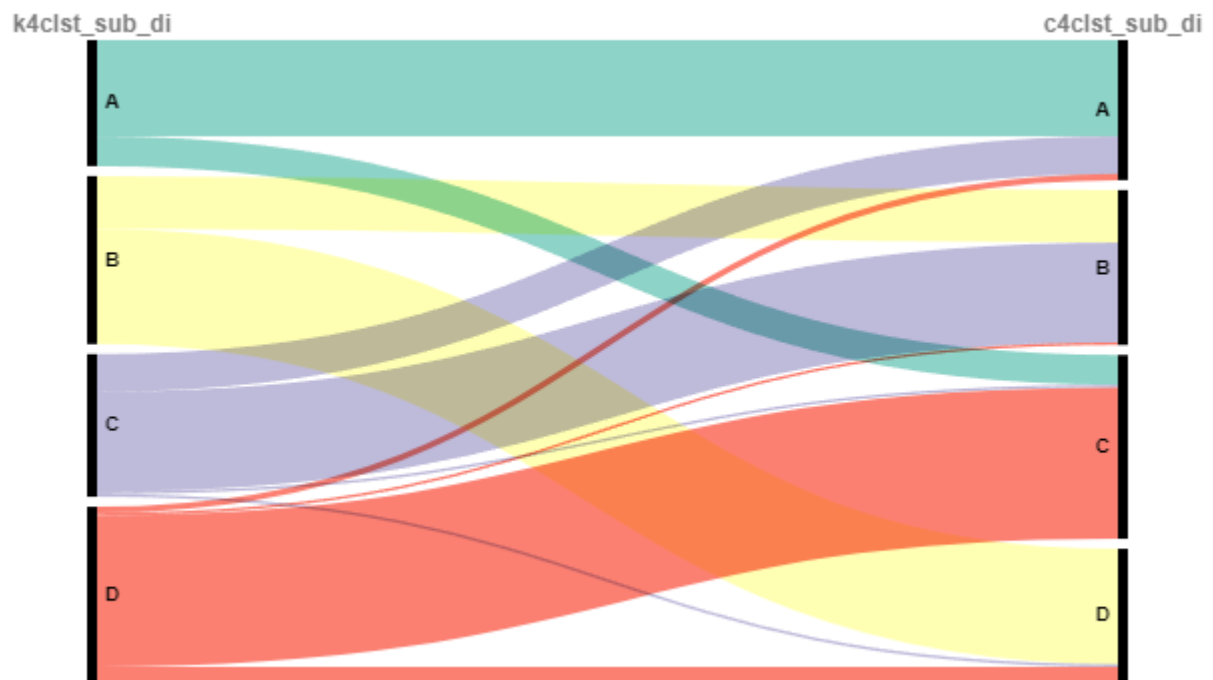


Figure 4.43: Alluvial diagram representing the flow of cluster assignment of the hexagons between the two clustering technique for the walkability subindicators and POI diversity.

Maps showing all four cluster analysis results are shown below in Figures 44-47 for easier visual comparison.

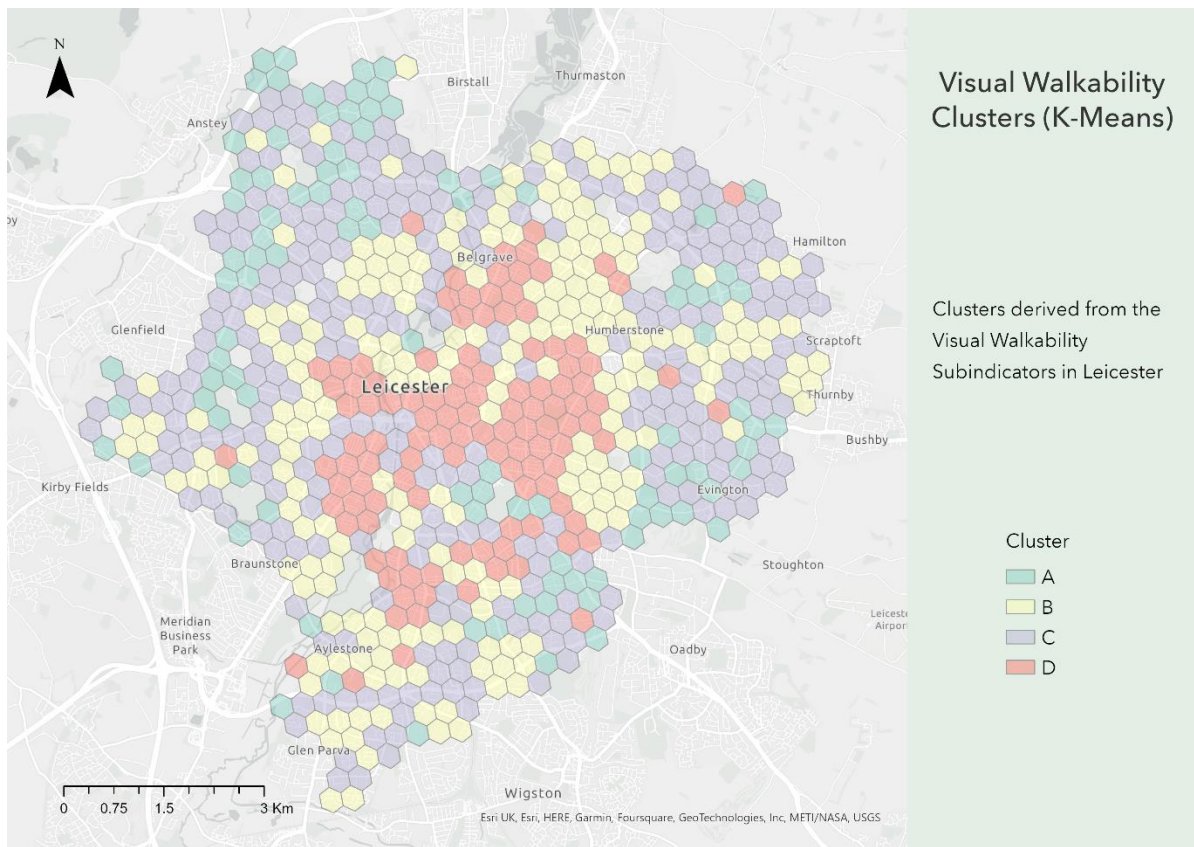


Figure 4.44: Map of Leicester showing the visual walkability clusters from K-Means (Map Scale: 1: 60000).

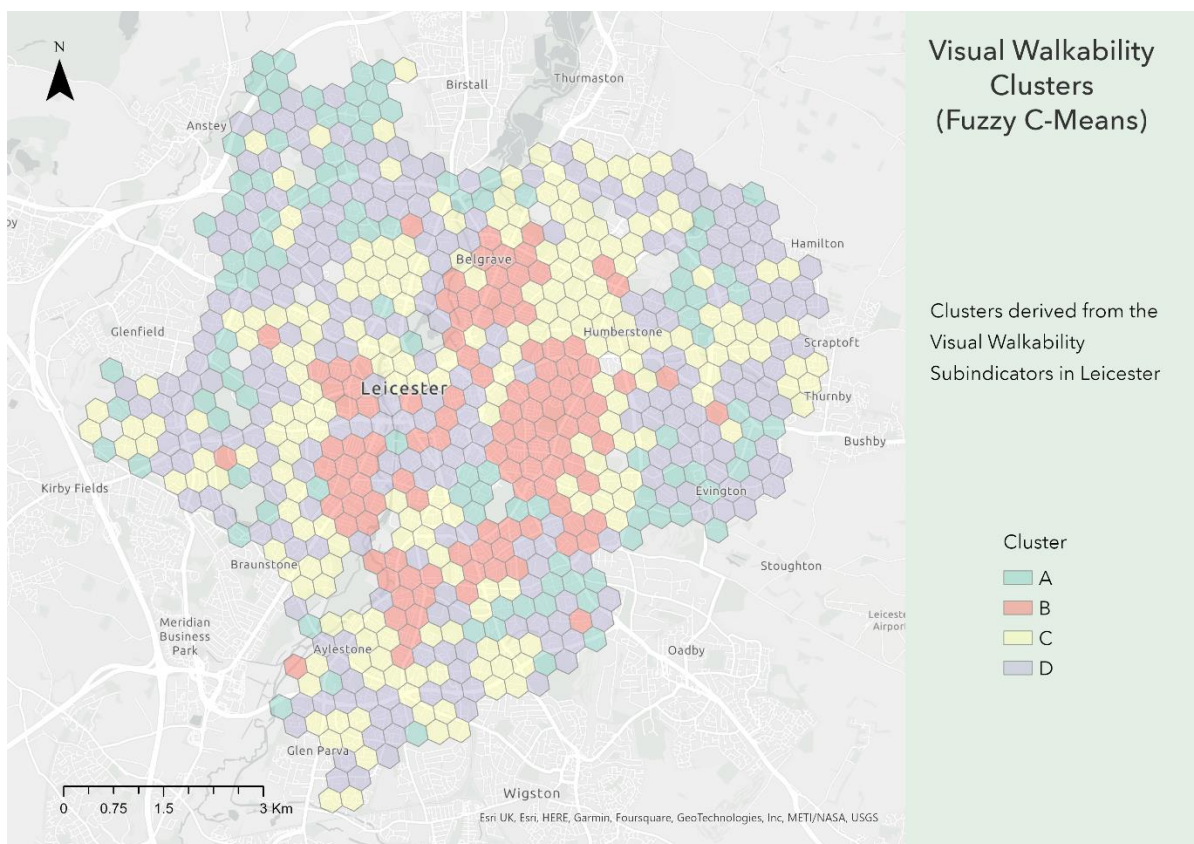


Figure 4.45: Map of Leicester showing the visual walkability clusters from FCM (Map Scale: 1: 60000).

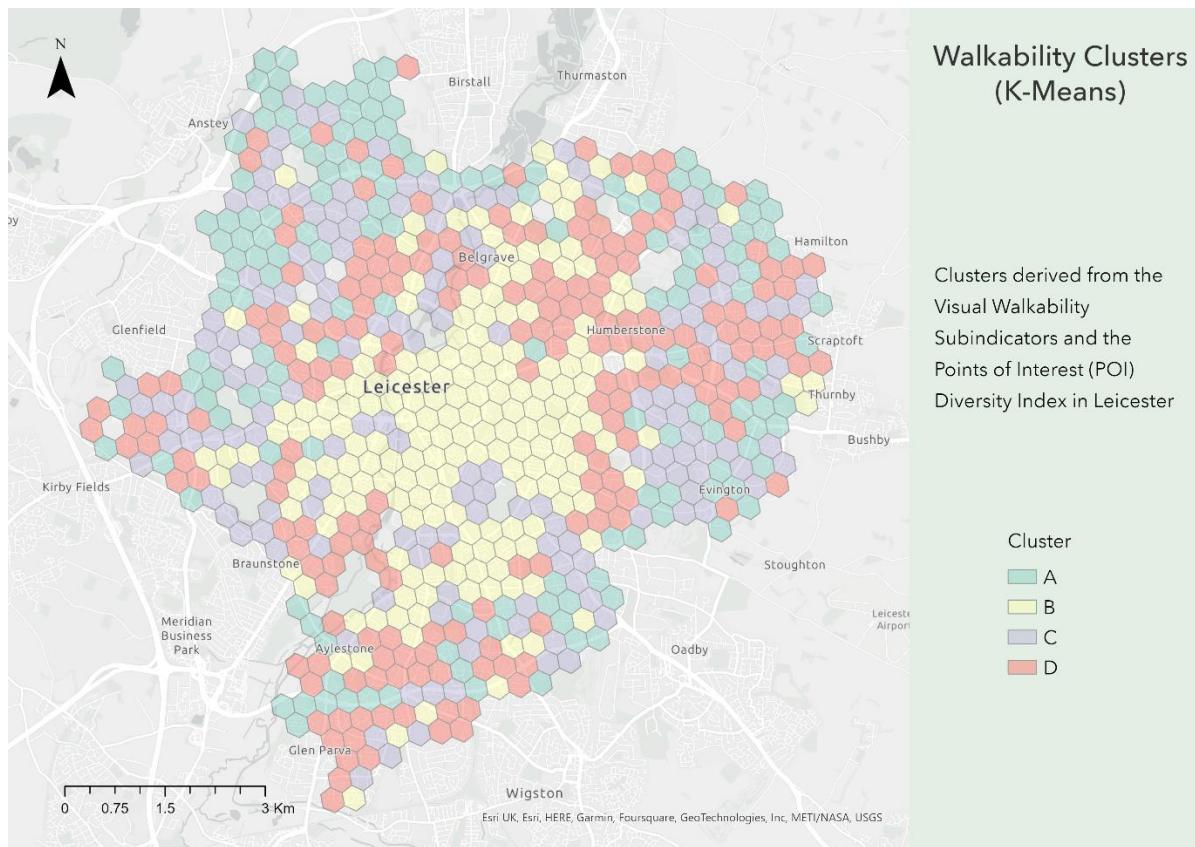


Figure 4.46: Map of Leicester showing the walkability clusters from K-Means (Map Scale: 1: 60000).

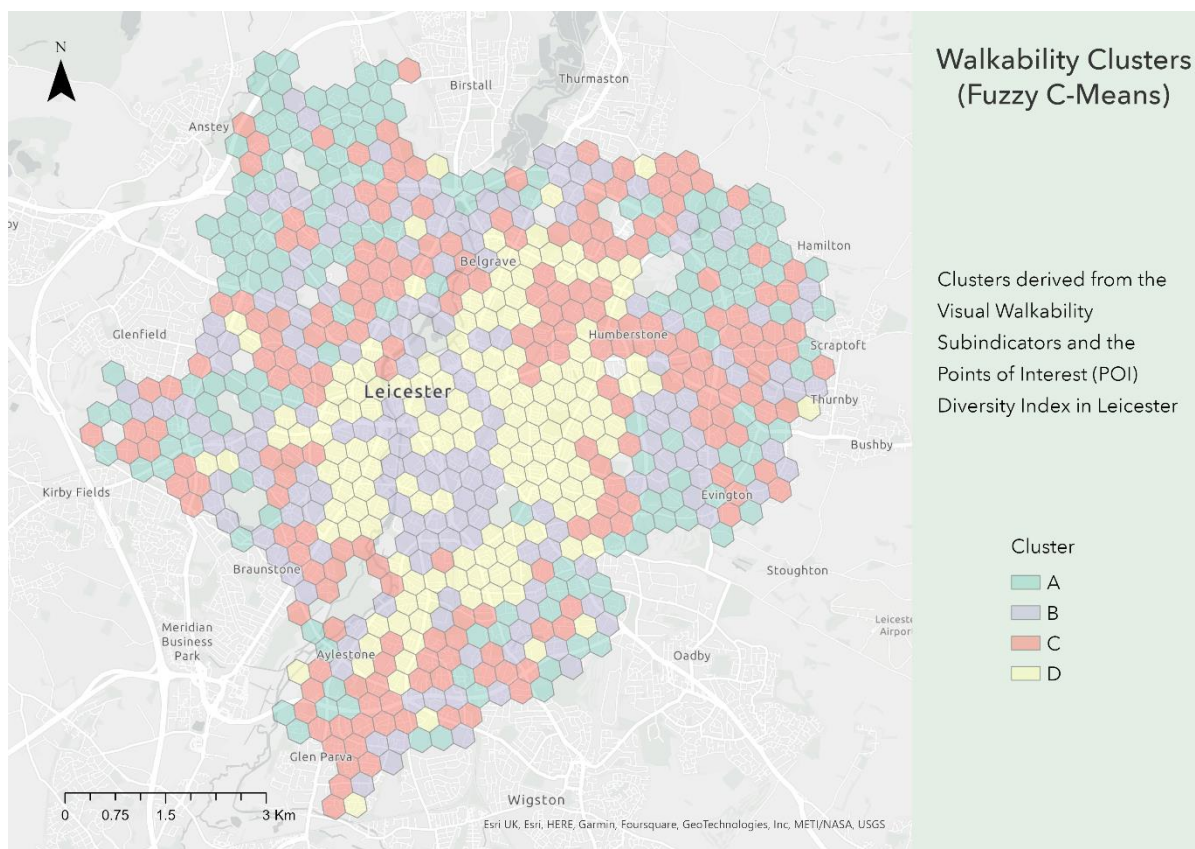


Figure 4.47: Map of Leicester showing the walkability clusters from FCM (Map Scale: 1: 60000).

Chapter 5. Discussion

This chapter will firstly discuss the model limitations and the inaccuracies effecting the visual pavement subindicator. Following this, the results pertaining to the IVW index will be discussed before moving on to the results of the cluster analysis with the visual walkability subindicators. The cluster analysis after incorporating POI diversity data will also be discussed in the context of 15-minute city principles.

5.1. Model Limitations

A key limitation was the SegFormer model's suboptimal performance segmenting roads versus pavement which affected the visual pavement subindicator. The SegFormer-B5 model is pre-trained on the ImageNet dataset and finetuned with the Cityscapes data, which contains street scenes from European cities. However, substantial differences likely exist between the road/pavement compositions in Cityscape's imagery compared to Leicester's streets. As a result, the pre-trained model did not reliably distinguish pavement pixels from road pixels in the Leicester SVI data. This led to inaccurate visual pavement ratios for quite a few points in the street network that reduced the utility of the subindicator for properly quantifying pedestrian infrastructure proportions. Examples of inaccurately segmented SVI is provided below in Figure 5.1 and Figure 5.2.

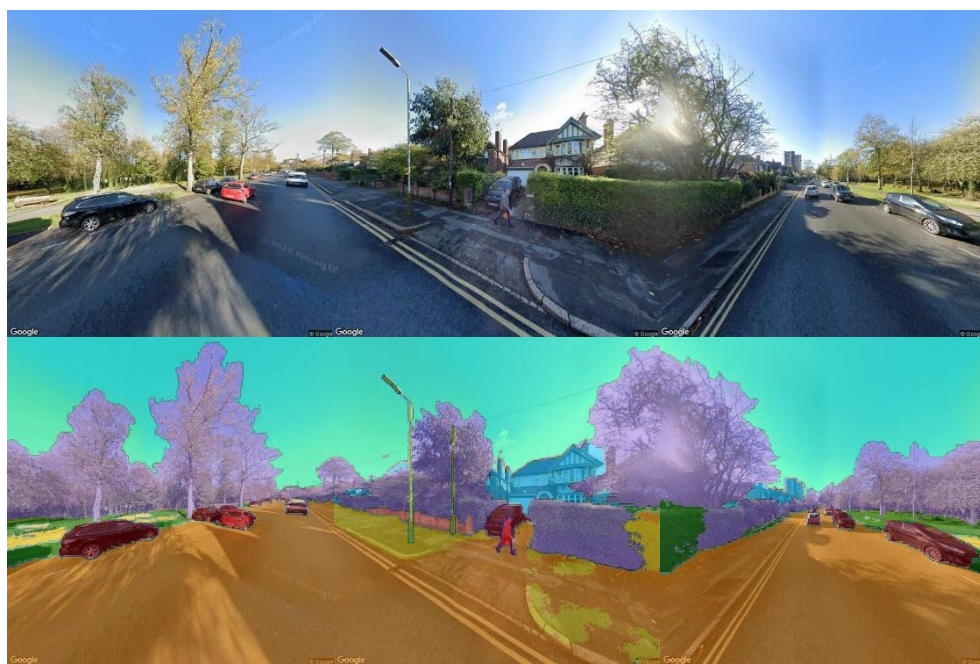


Figure 5.1: SVI with inaccurate road/pavement segmentation (IVW:70, gi:4, Ci:4, Ei:4, Pi:2), (Road: Orange, Pavement: Yellow). Contains Google Street View data © Google © 2023.

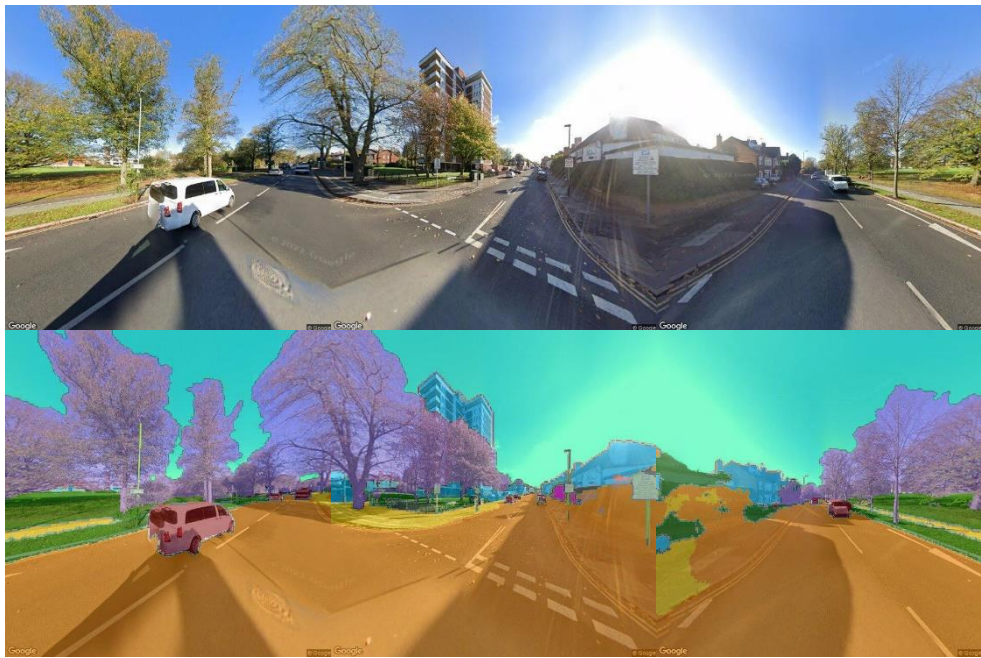


Figure 5.2: SVI with inaccurate road/pavement segmentation (IVW:65, Gi:4, Ci:4, Ei:4, Pi:1), (Road: Orange, Pavement: Yellow). Contains Google Street View data © Google © 2023.

As observed in the Figures above, it can be seen that the low visual pavement score is bringing the overall IVW score down drastically. The cluster analysis is also likely to be affected by the random inaccuracies due to this issue, which could explain why the visual pavement subindicator was clustering rather poorly. To address this, the model could be finetuned using localised Leicester imagery containing labelled examples of roads and pavements to adapt the features, albeit it would be time consuming and computationally expensive. This would enable the model to better recognise Leicester's specific road and pavement patterns. Additionally, advanced domain adaptation techniques such as Active Adversarial Domain Adaptation (Su *et al.*, 2020) could be applied to explicitly adapt the Cityscapes features to the Leicester street data distribution. Such enhancements to the training and finetuning data and model adaptations would likely significantly improve segmentation accuracy for roads and pavements, leading to more reliable quantification of pedestrian infrastructure.

5.2. IVW Framework Results

The visual walkability profile of Leicester, as assessed through the adapted IVW framework, offers a multifaceted perspective on the city's urban environment. This examination reveals a distinctive spatial distribution of visual walkability, characterised by varying levels of walkability across different areas of the city. Notably, the city centre along with the area around it and the city's periphery stand out as areas with high visual walkability. Streets in

these regions exhibit features that enhance the pedestrian experience, such as abundant greenery, well-defined outdoor spaces, and low levels of visual crowdedness. The presence of these elements contributes to a visually appealing and comfortable walking environment. In contrast, areas between the city centre and the periphery tend to have lower visual walkability. These streets often lack the same degree of greenery, experience higher levels of visual crowdedness, and have less favourable pavement-to-road ratios. These factors collectively impact the overall visual walkability, making these areas less inviting for pedestrians.

The distribution of visual walkability subindicators further complements this spatial pattern. For instance, the Psychological Greenery subindicator indicates that greenery is concentrated on the city's peripheries, creating pockets of visual appeal in these areas. Visual Crowdedness shows localised variations, with residential neighbourhoods near the city centre experiencing higher crowding due to on-street parking congestion. The Outdoor Enclosure subindicator highlights well-defined outdoor spaces in the city centre and along the outskirts, while some residential neighbourhoods lack the same level of enclosure. Visual Pavement levels also exhibit variations, with major roads often prioritising road width over pedestrian-friendliness.

These findings underscore the complexity of visual walkability in Leicester. The city's walkability is not solely determined by its overall urban form but rather by a combination of fine-grained streetscape attributes. Minor variations in greenery, enclosure, crowdedness, and pavement play a pivotal role in distinguishing highly walkable streets from less walkable ones. Enhancing visual walkability in Leicester may require targeted improvements that address the specific factors influencing local pedestrian perceptions. These could include strategies to increase greenery, reduce visual crowdedness, and improve pavement conditions in areas with lower visual walkability. Additionally, considering the limitations of the segmentation model used for the Visual Pavement subindicator is crucial, as these limitations impact the accuracy of pavement-to-road ratio assessments.

In summary, the visual walkability profile of Leicester, as revealed by the adapted IVW framework, demonstrates the importance of considering fine-grained streetscape attributes when evaluating urban walkability. The findings offer valuable insights for urban planning and

improvements aimed at creating a more pedestrian-friendly and visually appealing environment in Leicester.

5.3. Cluster Analysis Results

5.3.1. With Visual Walkability Subindicators

The unsupervised cluster analysis of the visual walkability subindicators revealed unique perspectives beyond the composite IVW index by uncovering latent groupings of hexagons exhibiting shared relationships. Both the K-Means and Fuzzy C-Means algorithms effectively segmented the urban landscape into differentiated walkability profiles that clustered geographically across the city. The four identified clusters characterised meaningful variations, such as greenery-rich transportation corridors, crowded commercial zones, and residentially enclosed neighbourhoods. A notable finding was the identification of highly localised pockets that exhibited similar visual traits despite proximity to areas with very different characteristics. This granular differentiation clarifies that while general urban morphology shapes the broader environment, subtle street-level elements create discrete pedestrian experiences even across neighbouring streets. Furthermore, the analysis distinctly surfaced the pronounced negative correlation between greenery and other visual subindicators. Despite model limitations negatively affecting the visual pavement subindicator, the unsupervised techniques enabled a multidimensional understanding of localised factors influencing walkability perceptions across Leicester's urban landscape, advancing beyond the one-dimensional IVW index.

5.3.2. With Visual Walkability Subindicators and POI Diversity Index

Incorporating the POI diversity data with the visual walkability subindicators highlighted strong inverse relationships between amenity mix and greenery, as clusters with abundant amenities corresponded with low vegetation. The use of soft FCM clustering enabled more nuanced analysis through partial membership degrees, although substantial filtering of hexagons with weak associations was subsequently required, which may have potentially skewed results. Another observation was the poor clustering of the visual pavement subindicator again across both clustering techniques, likely owing to the earlier discussed model limitations. Its inaccuracy and lack of reliability may provide explanation for the sizeable

filtering of hexagons that lacked firm cluster associations without a consistent pavement measure.

While clustering incorporating POI diversity provided perspectives into urban vibrancy and amenity-vegetation trade-offs, the unreliability of the visual pavement subindicator restricted its potential interpretability. Even so, the clustering suggested that while amenity diversity enhances urban vibrancy, it corresponds with low greenery and high crowding, indicating trade-offs between visual appeal and accessibility. This reveals a contrast between creating aesthetically walkable areas and ensuring decent amenity access within the 15-minute city principles. This highlighted the multidimensionality of walkability across two key dimensions of urban planning – aesthetic appeal versus functional access.

Chapter 6. Conclusion

This dissertation presented an application of deep learning and unsupervised learning techniques to model the visual walkability of Leicester based on street-level imagery. The adapted Integrated Visual Walkability framework quantified walkability using semantic segmentation of Google Street View images to extract perceptual features related to greenery, crowdedness, enclosure, and pavement. The results revealed localised variations in walkability, with high scoring streets situated near poorer scoring ones, reflecting the complexity of interactions between fine-grained attributes distinguishing pedestrian experiences. Insufficient greenery emerged as the walkability subindicator disproportionately limiting overall visual walkability.

Cluster analysis provided additional dimensionality beyond the composite IVW index by uncovering latent relationships and spatial groupings among the visual indicators. Both K-Means and Fuzzy C-Means effectively segmented the urban landscape into differentiated walkability profiles clustered across the city. Incorporating amenity diversity data highlighted strong correlations between vibrancy and vegetation, informing planning trade-offs. However, limitations in distinguishing pavement impacted interpretability. Nonetheless, the unsupervised learning techniques enabled a multidimensional understanding of hyperlocal factors influencing walkability.

Several promising directions can build upon this research in modelling urban walkability. Fine-tuning the semantic segmentation model using localised imagery of Leicester could enhance distinction of pavement versus roads and improve subindicator reliability. Incorporating additional street-level attributes like cleanliness, safety cues, and other visual elements could provide greater dimensionality for evaluating environmental influences. Integrating other data sources such as demographic statistics or indices of multiple deprivation (IMD) could enable uncovering inequities in access to good urban design. Applying graph neural networks to model spatial connectivity could reveal deeper topological relationships between walkability indicators clustered around the city. Such graph-based deep learning techniques may better capture the complex interactions inherent in urban spatial data compared to a-spatial clustering techniques utilised in this research. In summary, there are promising

opportunities to improve walkability assessment by focusing on the following aspects: enhancing model localisation, broadening the range of visual attributes, integrating demographic data and IMD, and harnessing the power of graph-based deep learning.

List of References

- Alfonzo, M.A. (2005) 'To Walk or Not to Walk? The Hierarchy of Walking Needs', *Environment and Behavior*, 37(6), pp. 808–836. Available at: <https://doi.org/10.1177/0013916504274016>.
- Allam, Z. et al. (2022) 'Unpacking the "15-Minute City" via 6G, IoT, and Digital Twins: Towards a New Narrative for Increasing Urban Efficiency, Resilience, and Sustainability', *Sensors*, 22(4), p. 1369. Available at: <https://doi.org/10.3390/s22041369>.
- Baran, P.K. et al. (2018) 'An exploratory study of perceived safety in a neighborhood park using immersive virtual environments', *Urban Forestry & Urban Greening*, 35, pp. 72–81. Available at: <https://doi.org/10.1016/j.ufug.2018.08.009>.
- Bezdek, J.C. (1981) *Pattern Recognition with Fuzzy Objective Function Algorithms*. Boston, MA: Springer US. Available at: <https://doi.org/10.1007/978-1-4757-0450-1>.
- Boeing, G. (2016) 'OSMnx: New Methods for Acquiring, Constructing, Analyzing, and Visualizing Complex Street Networks', *Geoff Boeing*, 7 November. Available at: <https://geoffboeing.com/publications/osmnx-complex-street-networks/> (Accessed: 7 October 2023).
- Boeing, G. (2020) 'Global Urban Street Networks GraphML'. Harvard Dataverse. Available at: <https://doi.org/10.7910/DVN/KA5HJ3>.
- Botta, F. and Gutiérrez-Roig, M. (2021) 'Modelling urban vibrancy with mobile phone and OpenStreetMap data', *PLOS ONE*, 16(6), p. e0252015. Available at: <https://doi.org/10.1371/journal.pone.0252015>.
- Cordts, M. et al. (2016) 'The Cityscapes Dataset for Semantic Urban Scene Understanding', in. *Proceedings of the IEEE Computer Society Conference on Computer Vision and Pattern Recognition*, pp. 3213–3223. Available at: <https://doi.org/10.1109/CVPR.2016.350>.
- Erath, A.L., van Eggermond, M.A.B. and Ordóñez Medina, S.A. (2016) 'Introducing the pedestrian accessibility tool (PAT): Open source GIS-based walkability analysis', *Arbeitsberichte Verkehrs- und Raumplanung*, 1186. Available at: <https://www.research-collection.ethz.ch/handle/20.500.11850/118799> (Accessed: 11 October 2023).
- Frank, L.D. et al. (2010) 'The development of a walkability index: application to the Neighborhood Quality of Life Study', *British Journal of Sports Medicine*, 44(13), pp. 924–933. Available at: <https://doi.org/10.1136/bjsm.2009.058701>.
- Ghosh, S. and Kumar, S. (2013) 'Comparative Analysis of K-Means and Fuzzy C-Means Algorithms', *International Journal of Advanced Computer Science and Applications*, 4(4). Available at: <https://doi.org/10.14569/IJACSA.2013.040406>.
- Google (2023) 'Street View Static API overview'. Available at: <https://developers.google.com/maps/documentation/streetview/overview> (Accessed: 26 September 2023).

Hao, S., Zhou, Y. and Guo, Y. (2020) 'A Brief Survey on Semantic Segmentation with Deep Learning', *Neurocomputing*, 406, pp. 302–321. Available at: <https://doi.org/10.1016/j.neucom.2019.11.118>.

Hasan, M.M., Oh, J.-S. and Kwigizile, V. (2021) 'Exploring the trend of walkability measures by applying hierarchical clustering technique', *Journal of Transport & Health*, 22, p. 101241. Available at: <https://doi.org/10.1016/j.jth.2021.101241>.

Jenks, G.F. (1967) 'The Data Model Concept in Statistical Mapping', *International Yearbook of Cartography*, 7, pp. 186–190.

Jeon, J. and Woo, A. (2023) 'Deep learning analysis of street panorama images to evaluate the streetscape walkability of neighborhoods for subsidized families in Seoul, Korea', *Landscape and Urban Planning*, 230, p. 104631. Available at: <https://doi.org/10.1016/j.landurbplan.2022.104631>.

Johnson, N.L. (1949) 'Systems of Frequency Curves Generated by Methods of Translation', *Biometrika*, 36(1/2), p. 149. Available at: <https://doi.org/10.2307/2332539>.

Kelly, C.E. et al. (2011) 'A comparison of three methods for assessing the walkability of the pedestrian environment', *Journal of Transport Geography*, 19(6), pp. 1500–1508. Available at: <https://doi.org/10.1016/j.jtrangeo.2010.08.001>.

Koo, B.W., Guhathakurta, S. and Botchwey, N. (2022) 'How are Neighborhood and Street-Level Walkability Factors Associated with Walking Behaviors? A Big Data Approach Using Street View Images', *Environment and Behavior*, 54(1), pp. 211–241. Available at: <https://doi.org/10.1177/00139165211014609>.

Lee, J., He, S.Y. and Sohn, D.W. (2017) 'Potential of converting short car trips to active trips: The role of the built environment in tour-based travel', *Journal of Transport & Health*, 7, pp. 134–148. Available at: <https://doi.org/10.1016/j.jth.2017.08.008>.

Lefebvre-Ropars, G. and Morency, C. (2018) 'Walkability: Which Measure to Choose, Where to Measure It, and How?', *Transportation Research Record*, 2672(35), pp. 139–150. Available at: <https://doi.org/10.1177/0361198118787095>.

Leicester City Council (2020) 'Leicester Street Design Guide'. Available at: <https://www.leicester.gov.uk/media/186708/leicester-street-design-guide-first-edition.pdf> (Accessed: 26 September 2023).

Li, Y., Yabuki, N. and Fukuda, T. (2022) 'Measuring visual walkability perception using panoramic street view images, virtual reality, and deep learning', *Sustainable Cities and Society*, 86, p. 104140. Available at: <https://doi.org/10.1016/j.scs.2022.104140>.

Li, Y., Yabuki, N. and Fukuda, T. (2023) 'Integrating GIS, deep learning, and environmental sensors for multicriteria evaluation of urban street walkability', *Landscape and Urban Planning*, 230, p. 104603. Available at: <https://doi.org/10.1016/j.landurbplan.2022.104603>.

Litman, T.A. (2003) 'Economic Value of Walkability', *Transportation Research Record*, 1828(1), pp. 3–11. Available at: <https://doi.org/10.3141/1828-01>.

Lu, Y. (2018) 'The association of urban greenness and walking behavior: Using google street view and deep learning techniques to estimate residents' exposure to urban greenness', *International Journal of Environmental Research and Public Health*, 15(8). Available at: <https://doi.org/10.3390/ijerph15081576>.

MacQueen, J. (1967) 'Some methods for classification and analysis of multivariate observations', *Proceedings of the Berkeley Symposium on Mathematical Statistics and Probability.*, 1(14), p. 281.

Mauri, M. et al. (2017) 'RAWGraphs: A Visualisation Platform to Create Open Outputs', in *Proceedings of the 12th Biannual Conference on Italian SIGCHI Chapter*. New York, NY, USA: Association for Computing Machinery (CHItaly '17), pp. 1–5. Available at: <https://doi.org/10.1145/3125571.3125585>.

Nagata, S. et al. (2020) 'Objective scoring of streetscape walkability related to leisure walking: Statistical modeling approach with semantic segmentation of Google Street View images', *Health & Place*, 66, p. 102428. Available at: <https://doi.org/10.1016/j.healthplace.2020.102428>.

Nutsford, D., Pearson, A.L. and Kingham, S. (2013) 'An ecological study investigating the association between access to urban green space and mental health', *Public Health*, 127(11), pp. 1005–1011. Available at: <https://doi.org/10.1016/j.puhe.2013.08.016>.

ONS (2022) *How the population changed in Leicester, Census 2021*. Available at: <https://www.ons.gov.uk/visualisations/censuspopulationchange/E06000016/> (Accessed: 26 September 2023).

OpenStreetMap (2023) *OpenStreetMap*, *OpenStreetMap*. Available at: <https://www.openstreetmap.org/> (Accessed: 12 October 2023).

Park, S., Deakin, E. and Lee, J.S. (2014) 'Perception-Based Walkability Index to Test Impact of Microlevel Walkability on Sustainable Mode Choice Decisions', *Transportation Research Record*, 2464(1), pp. 126–134. Available at: <https://doi.org/10.3141/2464-16>.

Pliakas, T. et al. (2017) 'Optimising measurement of health-related characteristics of the built environment: Comparing data collected by foot-based street audits, virtual street audits and routine secondary data sources', *Health & Place*, 43, pp. 75–84. Available at: <https://doi.org/10.1016/j.healthplace.2016.10.001>.

Rousseeuw, P.J. (1987) 'Silhouettes: A graphical aid to the interpretation and validation of cluster analysis', *Journal of Computational and Applied Mathematics*, 20, pp. 53–65. Available at: [https://doi.org/10.1016/0377-0427\(87\)90125-7](https://doi.org/10.1016/0377-0427(87)90125-7).

Shannon, C. (1948) 'A mathematical theory of communication', *The Bell System technical journal.*, 27(3), p. 379.

Simons, G. (2023) 'The cityseer Python package for pedestrian-scale network-based urban analysis', *Environment and Planning B: Urban Analytics and City Science*, 50(5), pp. 1328–1344. Available at: <https://doi.org/10.1177/23998083221133827>.

Southworth, M. (2005) 'Designing the Walkable City', *Journal of Urban Planning and Development*, 131(4), pp. 246–257. Available at: [https://doi.org/10.1061/\(ASCE\)0733-9488\(2005\)131:4\(246\)](https://doi.org/10.1061/(ASCE)0733-9488(2005)131:4(246)).

Su, J.-C. et al. (2020) 'Active Adversarial Domain Adaptation'. arXiv. Available at: <https://doi.org/10.48550/arXiv.1904.07848>.

Thorndike, R. (1953) 'Who belongs in the family?', *Psychometrika*, 18(4), pp. 267–276.

Uber Technologies Inc (2018) 'H3: Uber's Hexagonal Hierarchical Spatial Index', 27 June. Available at: <https://www.uber.com/en-GB/blog/h3/> (Accessed: 15 August 2023).

Villeneuve, P.J. et al. (2018) 'Comparing the normalized difference vegetation index with the google street view measure of vegetation to assess associations between greenness, walkability, recreational physical activity, and health in Ottawa, Canada', *International Journal of Environmental Research and Public Health*, 15(8). Available at: <https://doi.org/10.3390/ijerph15081719>.

Wen, R. (2019) 'google_streetview', 6 March. Available at: https://github.com/rrwen/google_streetview.

Xie, E. et al. (2021) 'SegFormer: Simple and Efficient Design for Semantic Segmentation with Transformers'. Available at: <https://doi.org/10.48550/ARXIV.2105.15203>.

Yin, L. and Wang, Z. (2016) 'Measuring visual enclosure for street walkability: Using machine learning algorithms and Google Street View imagery', *Applied Geography*, 76, pp. 147–153. Available at: <https://doi.org/10.1016/j.apgeog.2016.09.024>.

Zachary, D. and Dobson, S. (2021) 'Urban Development and Complexity: Shannon Entropy as a Measure of Diversity', *Planning Practice & Research*, 36(2), pp. 157–173. Available at: <https://doi.org/10.1080/02697459.2020.1852664>.

Zhou, H. et al. (2019) 'Social inequalities in neighborhood visual walkability: Using street view imagery and deep learning technologies to facilitate healthy city planning', *Sustainable Cities and Society*, 50, p. 101605. Available at: <https://doi.org/10.1016/j.scs.2019.101605>.

Appendices

Appendix A: Python Code.....	91
Appendix A-1: Required Libraries.....	91
Appendix A-2: Obtaining Points from Graph	92
Appendix A-3: Obtaining the Street View Images.....	93
Appendix A-4: Performing Semantic Segmentation on the SVI.....	96
Appendix B: Mean Subindicator Values per Hexagon	103
Appendix C: OpenStreetMap Amenities	105
Appendix C-1: Table of Amenity Types from OpenStreetMap	105
Appendix C-2: Map of Amenities from OpenStreetMap	110

Appendix A: Python Code

The complete code is available on GitHub at: <https://github.com/adhibsyed/walkability>

Appendix A-1: Required Libraries

```
# Libraries for data processing and manipulation
from os import path, makedirs, listdir
import pandas as pd
import numpy as np
import json
import re
from tqdm import tqdm
from concurrent.futures import ThreadPoolExecutor
import time
import requests
import zipfile
import jenksipy

# Libraries for streetview
import google_streetview.api

# Libraries for graph and geospatial functions
import osmnx as ox
from cityseer.tools import graphs, plot, io
import geopandas as gpd
import pyproj
from shapely.geometry import Point, Polygon
import h3
import contextily as ctx

# Libraries for deep learning
from transformers import SegformerFeatureExtractor,
SegformerForSemanticSegmentation
import torch

# Clustering
from sklearn.cluster import KMeans
import skfda
from skfda.ml.clustering import FuzzyCMeans
from scipy.special import boxcox
from sklearn.metrics import silhouette_score

# Libraries for image processing and visualisation
from PIL import Image
import matplotlib.pyplot as plt
import seaborn as sns
from matplotlib.colors import ListedColormap
from matplotlib.ticker import MaxNLocator
```

```

from matplotlib_scalebar.scalebar import ScaleBar
from matplotlib.offsetbox import OffsetImage, AnnotationBbox

Appendix A-2: Obtaining Points from Graph

# Obtaining points via graphs

# Load OSMnx graph
leicester_osmnx_graph =
ox.io.load_graphml(r"Z:\Dissertation\project\files\graph\leicester-
1864.graphml")
leicester_osmnx_graph_prj = ox.project_graph(leicester_osmnx_graph)

# Getting undirected to exclude multiple nodes for roads that are one way
leicester_ud = ox.get_undirected(leicester_osmnx_graph_prj)

# Transform Leicester graph to cityseer format
L = io.nx_from_osm_nx(ox.project_graph(leicester_ud, to_crs=27700))
plot.plot_nx(graphs.nx_simple_geoms(L), plot_geoms=True, labels=False,
dpi=200, figsize=(16, 16))

# Decompose street segments to 50 meters
le_simple = graphs.nx_simple_geoms(L)
le_decomp = graphs.nx_decompose(le_simple, 50)
plot.plot_nx(le_decomp, plot_geoms=True, labels=False, dpi=200, figsize=(16,
16))

# Obtaining a geodataframe and network structure
le_gdf_nx = graphs.network_structure_from_nx(le_decomp, crs=27700)

# Selecting the geodataframe specifically to obtain points
le_gdf = le_gdf_nx[0]
le_gdf.reset_index(inplace=True)

# Cleaning up the geodataframe
index_column_name = 'node_key'
le_gdf.rename(columns={'index': index_column_name}, inplace=True)

le_gdf.head()

```

Appendix A-3: Obtaining the Street View Images

```
# Splitting the dataframe into 4 batches before downloading images
num_records = len(le_gdf)
records_per_df = num_records // 4

le_df_1 = le_gdf[:records_per_df]
le_df_2 = le_gdf[records_per_df:2 * records_per_df]
le_df_3 = le_gdf[2 * records_per_df:3 * records_per_df]
le_df_4 = le_gdf[3 * records_per_df:]

le_df_test = le_gdf.head(200)

def download_image(url, file_path, max_retries=3):
    retries = 0
    while retries < max_retries:
        try:
            response = requests.get(url, stream=True)
            response.raise_for_status()

            with open(file_path, 'wb') as out_file:
                for chunk in response.iter_content(1034):
                    out_file.write(chunk)
            return Image.open(file_path)
        except Exception as e:
            print(f"Error opening image '{file_path}': {e}")
            retries += 1
            if retries < max_retries:
                wait_time = 2** retries
                print(f"Retrying in {wait_time} seconds...")
                time.sleep(wait_time)
            else:
                print("Max retries exceeded")
                return None

def process_coordinates_batch(heading, coordinate_batch, base_folder,
                           executor):
    heading_folder = path.join(base_folder, f'images_{heading}')
    metadata_folder = path.join(base_folder, f'metadata_{heading}')
    makedirs(heading_folder, exist_ok=True)
    makedirs(metadata_folder, exist_ok=True)

    all_futures = []
    for index, row in coordinate_batch.iterrows():

        latitude = row['latitude']
        longitude = row['longitude']
```

```

parameters = [
    **common_parameters,
    'location': f'{latitude},{longitude}',
    'heading': str(heading)
]

results = google_streetview.api.results(parameters)
metadata = results.metadata

# Create a list to store the futures for image downloads
futures = []

for i, url in enumerate(results.links):
    if metadata[i]['status'] == 'OK':
        pano_id = metadata[i].get('pano_id')
        if pano_id not in unique_pano_ids:
            unique_pano_ids.add(pano_id)
            location = metadata[i].get('location')

            if location:
                lat = location.get('lat')
                lng = location.get('lng')
                if lat is not None and lng is not None and pano_id is
not None:
                    file_name = f"gsv_{lat}_{lng}_{pano_id}.jpg"
                    metadata[i]['_file'] = file_name

                    file_path = path.join(heading_folder, file_name)

                    # Use ThreadPoolExecutor for parallel image
                    downloads
                    future = executor.submit(download_image, url,
                    file_path)
                    futures.append((future, file_path))

                    metadata_list.append(metadata[i])
                else:
                    print(f"Metadata for image {i} is missing location
information.")

all_futures.extend(futures)

# writing the list of metadata dictionaries to a single file
metadata_file_path = path.join(metadata_folder,
f"metadata_{heading}_batch{df_batch}.json")
with open(metadata_file_path, 'w') as out_file:
    json.dump(metadata_list, out_file)

```

```

    return all_futures

base_folder = r'D:\University\Dissertation\project\files\test2'
headings = [240]
df_batch = "4"
common_parameters = {
    'size': '640x640',
    'fov': '120',
    'key': 'abc' # Insert Google Maps API Key here
}

# Split coordinates into batches
batch_size = 10
coordinate_batches = [le_df_4.iloc[i:i + batch_size] for i in range(0,
len(le_df_4), batch_size)]

# Process each heading and coordinate batch
with ThreadPoolExecutor(max_workers=5) as executor:
    all_batch_futures = []
    metadata_list = []
    unique_pano_ids = set()
    for heading in tqdm(headings, desc="Processing Headings"):
        for coordinate_batch in tqdm(coordinate_batches, desc="Processing
Batches"):
            batch_futures = process_coordinates_batch(heading,
coordinate_batch, base_folder, executor)
            all_batch_futures.extend(batch_futures)

```

Appendix A-4: Performing Semantic Segmentation on the SVI

```
# Setting up some requirements

# Check if GPU is available and set the device accordingly
device = torch.device("cuda" if torch.cuda.is_available() else "cpu")

# Load the pre-trained SegFormer-B5 model and feature extractor
feature_extractor =
SegformerFeatureExtractor.from_pretrained("nvidia/segformer-b5-finetuned-
cityscapes-1024-1024")
model = SegformerForSemanticSegmentation.from_pretrained("nvidia/segformer-b5-
finetuned-cityscapes-1024-1024")
model.to(device) # Move the model to GPU

torch.cuda.empty_cache()

print(torch.cuda.memory_summary(device=None, abbreviated=False))

# Defining label names
label_names = {
    0: "road",
    1: "sidewalk",
    2: "building",
    3: "wall",
    4: "fence",
    5: "pole",
    6: "traffic_light",
    7: "traffic_sign",
    8: "vegetation",
    9: "terrain",
    10: "sky",
    11: "person",
    12: "rider",
    13: "car",
    14: "truck",
    15: "bus",
    16: "train",
    17: "motorcycle",
    18: "bicycle",
    19: "unknown"
}

label_names_perc = {
    0: "perc_road",
    1: "perc_sidewalk",
    2: "perc_building",
    3: "perc_wall",
```

```

4: "perc_fence",
5: "perc_pole",
6: "perc_traffic_light",
7: "perc_traffic_sign",
8: "perc_vegetation",
9: "perc_terrain",
10: "perc_sky",
11: "perc_person",
12: "perc_rider",
13: "perc_car",
14: "perc_truck",
15: "perc_bus",
16: "perc_train",
17: "perc_motorcycle",
18: "perc_bicycle",
19: "perc_unknown"
}

# Defining color palette for label names (# https://mokole.com/palette.html)
label_colors = {
    "road": (255, 140, 0), #ff8c00 darkorange
    "sidewalk": (255, 215, 0), #ffd700 gold
    "building": (0, 191, 255), #00bfff deepskyblue
    "wall": (250, 128, 114), #fa8072 salmon
    "fence": (47, 79, 79), #2f4f4f darkslategray
    "pole": (154, 205, 50), #9acd32 yellowgreen
    "traffic_light": (0, 0, 139), #00008b darkblue
    "traffic_sign": (143, 188, 143), #8fbcc8f darkseagreen
    "vegetation": (147, 112, 219), #9370db mediumpurple
    "terrain": (0, 100, 0), #006400 darkgreen
    "sky": (0, 250, 154), #00fa9a mediumspringgreen
    "person": (255, 0, 0), #ff0000 red
    "rider": (0, 0, 255), #0000ff blue
    "car": (127, 0, 0), #7f0000 maroon2
    "truck": (216, 191, 216), #d8bfd8 thistle
    "bus": (0, 255, 0), #00ff00 lime
    "train": (255, 0, 255), #ff00ff fuchsia
    "motorcycle": (255, 105, 180), #ff69b4 hotpink
    "bicycle": (0, 255, 255), #00ffff aqua
    "unknown": (255, 255, 255) #white
}

# Creating a dataframe for the results for each heading
df_results_0 = pd.DataFrame(columns=['latitude', 'longitude', 'pano_id'] +
list(label_names.values()) + list(label_names_perc.values()))
df_results_120 = pd.DataFrame(columns=['latitude', 'longitude', 'pano_id'] +
list(label_names.values()) + list(label_names_perc.values()))

```

```

df_results_240 = pd.DataFrame(columns=['latitude', 'longitude', 'pano_id'] +
list(label_names.values()) + list(label_names_perc.values()))
df_results_test = pd.DataFrame(columns=['latitude', 'longitude', 'pano_id'] +
list(label_names.values()) + list(label_names_perc.values()))

# Regular expression pattern to extract latitude and longitude from the file
# name
# pattern = r"gsv_([-+]?[0-9]+\.[0-9]+)([-+]?[0-9]+\.[0-9]+)_joined.jpg"
pattern = r"gsv_([-+]?[0-9]+\.[0-9]+)([-+]?[0-9]+\.[0-9]+)(.*?)\.[^?]*"

# Define the path to the folder containing the images
images_folder_0 = r"Z:\Dissertation\project\files\test2\images_0"
images_folder_120 = r"Z:\Dissertation\project\files\test2\images_120"
images_folder_240 = r"Z:\Dissertation\project\files\test2\images_240"
images_folder_test =
r"Z:\Dissertation\project\files\test2\overlaided_images_test"

# Define the path to the folder containing the images
overlaided_images_folder_0 =
r"Z:\Dissertation\project\files\test2\overlaided_images_0"
makedirs(overlaided_images_folder_0, exist_ok=True)
overlaided_images_folder_120 =
r"Z:\Dissertation\project\files\test2\overlaided_images_120"
makedirs(overlaided_images_folder_120, exist_ok=True)
overlaided_images_folder_240 =
r"Z:\Dissertation\project\files\test2\overlaided_images_240"
makedirs(overlaided_images_folder_240, exist_ok=True)
overlaided_images_folder_test =
r"Z:\Dissertation\project\files\test2\overlaided_images_test"
makedirs(overlaided_images_folder_test, exist_ok=True)

def image_generator(image_files, images_folder, seg_batch_size):
    batch_images = []
    batch_metadata = []

    for image_file in image_files:
        match = re.search(pattern, image_file)
        latitude = float(match.group(1))
        longitude = float(match.group(2))
        pano_id = match.group(3)

        image_path = os.path.join(images_folder, image_file)
        image = Image.open(image_path)

        batch_images.append(image)
        batch_metadata.append((latitude, longitude, pano_id))

    if len(batch_images) >= seg_batch_size:

```

```

yield batch_images, batch_metadata
batch_images = []
batch_metadata = []

if len(batch_images) > 0:
    yield batch_images, batch_metadata

def process_images(images_folder, overlayed_images_folder, df_results,
seg_batch_size):
    image_files = [f for f in listdir(images_folder) if f.endswith(".jpg")]

    results_list=[]
    batch_counter = 0

    for batch_images, batch_metadata in tqdm(image_generator(image_files,
images_folder, seg_batch_size), total=len(image_files) // seg_batch_size):
        batch_logits = []

        for batch_image in batch_images:
            inputs = feature_extractor(images=batch_image,
return_tensors="pt")
            inputs.to(device)

        model.eval()

        with torch.no_grad():
            outputs = model(**inputs)
            logits = outputs.logits

        batch_logits.append(logits)

        image_height = batch_image.size[1]
        image_width = batch_image.size[0]

    for idx, (latitude, longitude, pano_id) in enumerate(batch_metadata):
        try:
            image = batch_images[idx]
            logits = batch_logits[idx]

            # Calculating the percentage or number of pixels for each
segmented object
            num_labels = logits.shape[1]
            processed_image_height = logits.shape[2]
            processed_image_width = logits.shape[3]

            segmentation_results = []
            for label_index in range(num_labels):

```

```

        # Get the logits for the current label
        label_logits = logits[0, label_index] # Assuming
batch_size = 1

        # Calculating the percentage of pixels for the current
label
        label_pixels = (label_logits > 0).sum().item()
        label_percentage = (label_pixels / (processed_image_height
* processed_image_width)) * 100

        # Storing the segmentation result in a table or data
structure
        segmentation_results.append({
            'label_index': label_index,
            'label_percentage': label_percentage,
            'label_pixels': label_pixels
        })

        # Normalise the percentages
        total_percentage = sum(result['label_percentage'] for result
in segmentation_results)
        for result in segmentation_results:
            result['label_percentage'] = result['label_percentage'] /
total_percentage * 100

        # Obtaining the predicted labels with the highest probability
        predicted_labels = torch.argmax(logits,
dim=1).squeeze().detach().cpu().numpy()
        resized_labels =
np.array(Image.fromarray(predicted_labels.astype(np.uint8)).resize((image_widt
h, image_height)))

        # Create a color mask for each label
        color_mask = np.zeros((image_height, image_width, 3),
dtype=np.uint8)
        for label_index in np.unique(resized_labels):
            label_name = label_names.get(label_index, "unknown") #
Use "unknown" as default label name
            color = label_colors[label_name]
            mask = (resized_labels == label_index)
            color_mask[mask] = color

        # Convert the color mask to a PIL image
        color_mask_image = Image.fromarray(color_mask)

        # Combine the color mask with the original image using alpha
blending

```

```

        alpha = 0.5 # Adjust the alpha value for transparency
        overlayed_image = Image.blend(image, color_mask_image, alpha)

        # Save the overlayed image
        overlayed_image.save(path.join(overlayed_images_folder,
f"overlay_{latitude}_{longitude}_{pano_id}.jpg"))

        # Create dictionaries with the results for the current image
        result_dict_percentage = {'latitude': latitude, 'longitude':
longitude, 'pano_id': pano_id}
        result_dict_pixels = {}

        for result in segmentation_results:
            label_index = result['label_index']
            label_percentage = result['label_percentage']
            label_pixels = result['label_pixels']

            label_name_percentage = label_names_perc[label_index] # Use label_names_perc for percentage column names
            result_dict_percentage[label_name_percentage] =
label_percentage

            label_name_pixels = label_names[label_index] # Use label_names for pixel count column names
            result_dict_pixels[label_name_pixels] = label_pixels

        # Combine the two dictionaries and append the combined
        dictionary to the list
        result_dict_combined = {**result_dict_percentage,
**result_dict_pixels}
        results_list.append(result_dict_combined)

    except Exception as e:
        print(f"Error processing image: {image_files[idx]}")
        print(e)
        continue

    torch.cuda.empty_cache()
    batch_counter += 1

    if batch_counter % 15 == 0:
        print(f"Pausing for 30 seconds after {batch_counter} batches...")
        time.sleep(30)

df_results = pd.DataFrame(results_list)

return df_results

```

```
# Running the SegFormer model and obtaining percentages of pixels of different
# objects in the images (heading 0)
df_results_0 = process_images(images_folder_0, overlayed_images_folder_0,
df_results_0, seg_batch_size=50)

# Running the SegFormer model and obtaining percentages of pixels of different
# objects in the images (heading 120)
df_results_120 = process_images(images_folder_120,
overlayed_images_folder_120, df_results_120, seg_batch_size=75)

# Running the SegFormer model and obtaining percentages of pixels of different
# objects in the images (heading 240)
df_results_240 = process_images(images_folder_240,
overlayed_images_folder_240, df_results_240, seg_batch_size=75)
```

Appendix B: Mean Subindicator Values per Hexagon

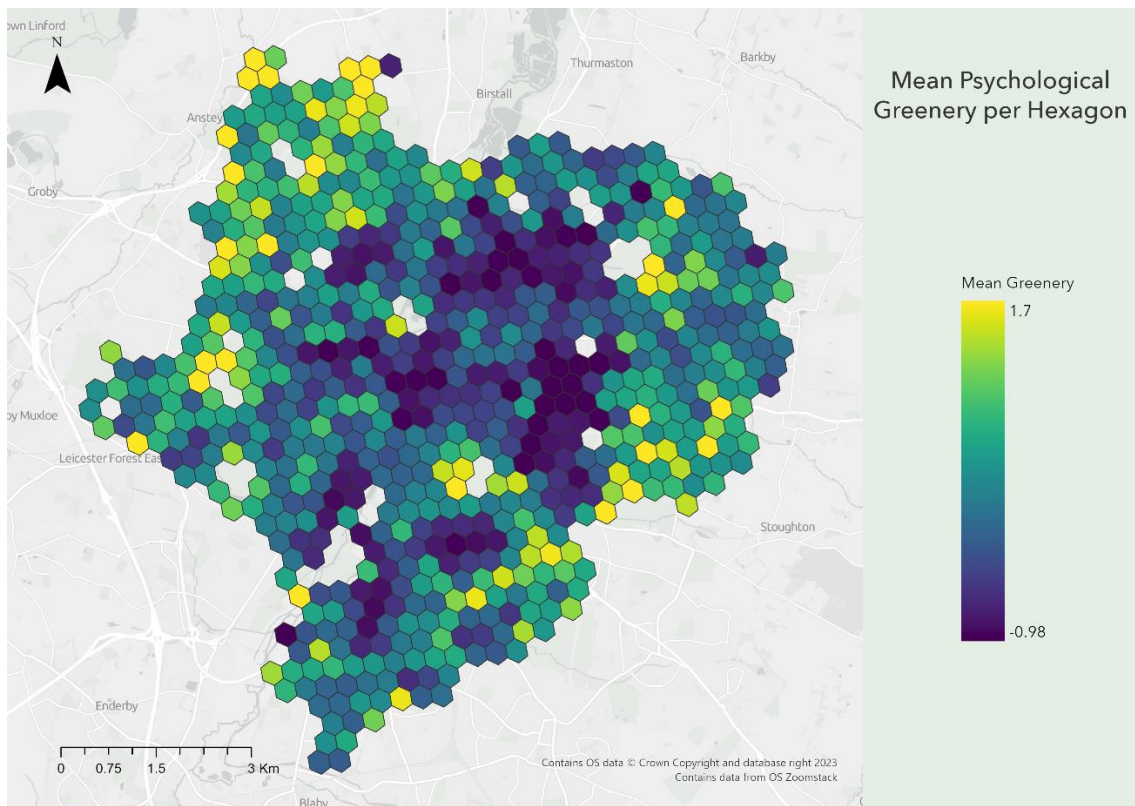


Figure B-1: Mean Psychological Greenery per Hexagon (Map scale: 1:60000).

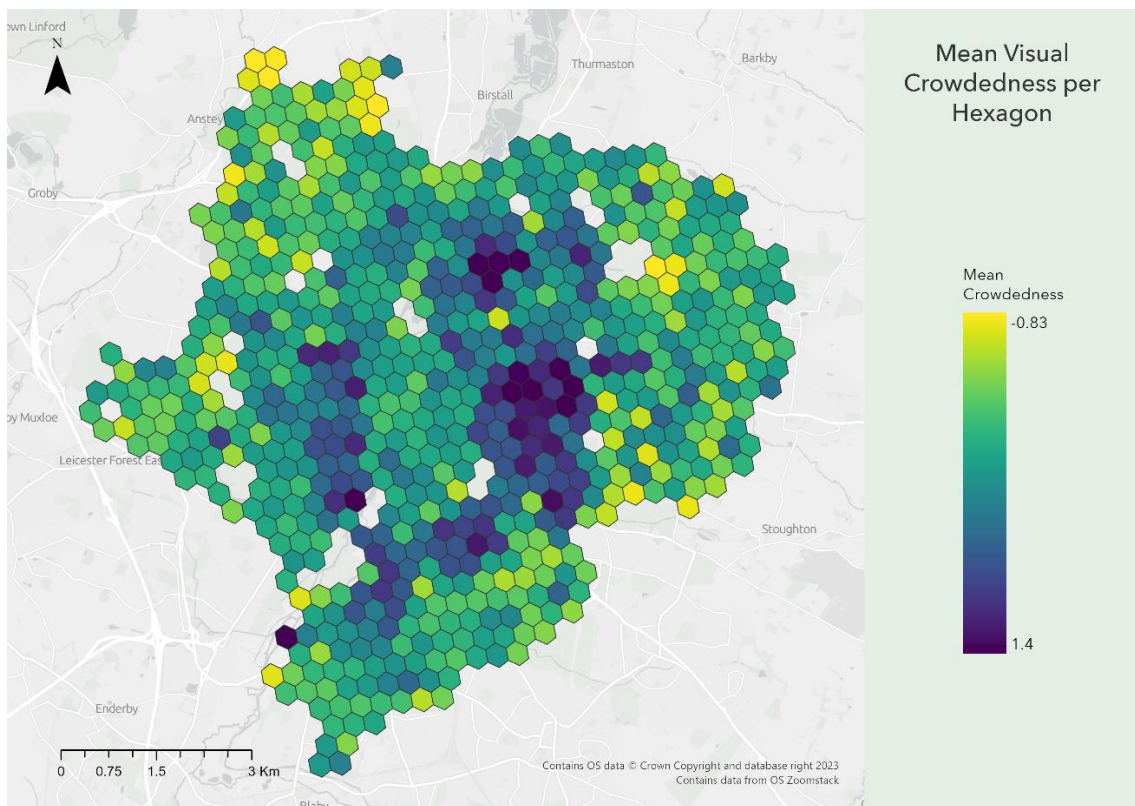


Figure B-2: Mean Visual Crowdedness per Hexagon (Map scale: 1:60000).

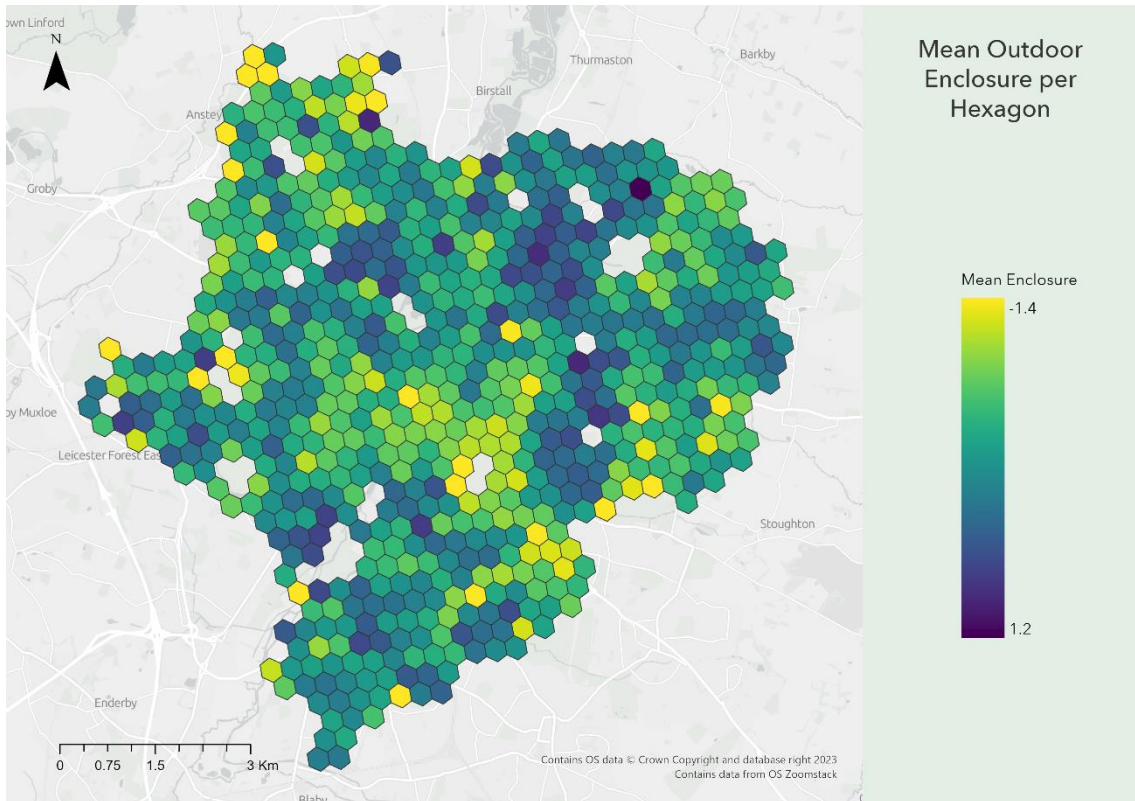


Figure B-3: Mean Outdoor Enclosure per Hexagon (Map scale: 1:60000).

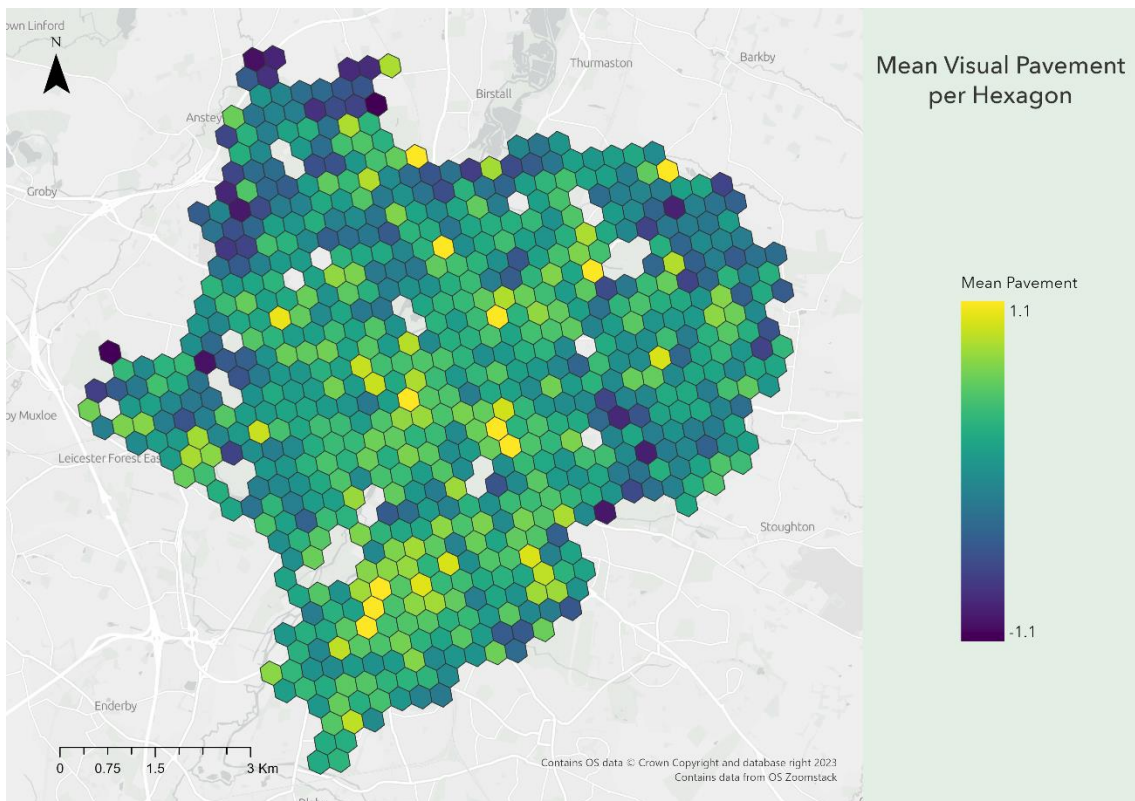


Figure B-4: Mean Visual Pavement per Hexagon (Map scale: 1:60000).

Appendix C: OpenStreetMap Amenities

Appendix C-1: Table of Amenity Types from OpenStreetMap

POI Type	Count
archaeological	2
arts_centre	1
artwork	21
atm	63
attraction	13
bakery	11
bank	38
bar	30
beauty_shop	13
bench	202
beverages	12
bicycle_rental	38
bicycle_shop	6
bookshop	8
bus_station	2
bus_stop	208
butcher	12
cafe	102
camera_surveillance	3
car_dealership	26
car_rental	4
car_wash	17
caravan_site	2
castle	1
chemist	9
Christian (place of worship)	61

christian_anglican (place of worship)	33
christian_catholic (place of worship)	11
christian_evangelical (place of worship)	1
christian_methodist (place of worship)	9
cinema	5
clinic	8
clothes	52
college	14
comms_tower	4
community_centre	44
computer_shop	3
convenience	133
courthouse	2
dentist	16
department_store	5
doctors	28
doityourself	17
drinking_water	1
fast_food	177
fire_station	4
florist	8
fountain	1
fuel	17
furniture_shop	9
garden_centre	1
general	1

gift_shop	13
golf_course	5
graveyard	7
greengrocer	2
guesthouse	3
hairdresser	56
helipad	1
Hindu (place of worship)	16
hospital	10
hotel	25
jeweller	10
Jewish (place of worship)	2
kindergarten	3
kiosk	1
laundry	11
library	22
mall	3
marina	1
market_place	2
memorial	20
mobile_phone_shop	13
monument	6
museum	9
Muslim (place of worship)	38
muslim_shia (place of worship)	3
muslim_sunni (place of worship)	23
newsagent	22
nightclub	2
nursing_home	1

optician	15
outdoor_shop	3
park	106
parking	629
parking_bicycle	13
parking_multistorey	11
pharmacy	42
picnic_site	3
pier	7
pitch	229
playground	157
police	10
post_box	139
post_office	41
prison	2
pub	118
public_building	2
railway_station	4
recycling	19
recycling_glass	6
recycling_metal	1
recycling_paper	1
restaurant	142
ruins	2
school	131
shelter	7
shoe_shop	10
Sikh (place of worship)	7
sports_centre	30
sports_shop	3

stadium	5
stationery	2
supermarket	53
swimming_pool	2
taxi	5
telephone	30
theatre	6
toilet	34
tourist_info	57
tower	4
town_hall	2
toy_shop	3
track	5
travel_agent	9
university	33
vending_any	1
vending_machine	4
vending_parking	2
viewpoint	1
waste_basket	107
water_well	1
zoo	1

Appendix C-2: Map of Amenities from OpenStreetMap

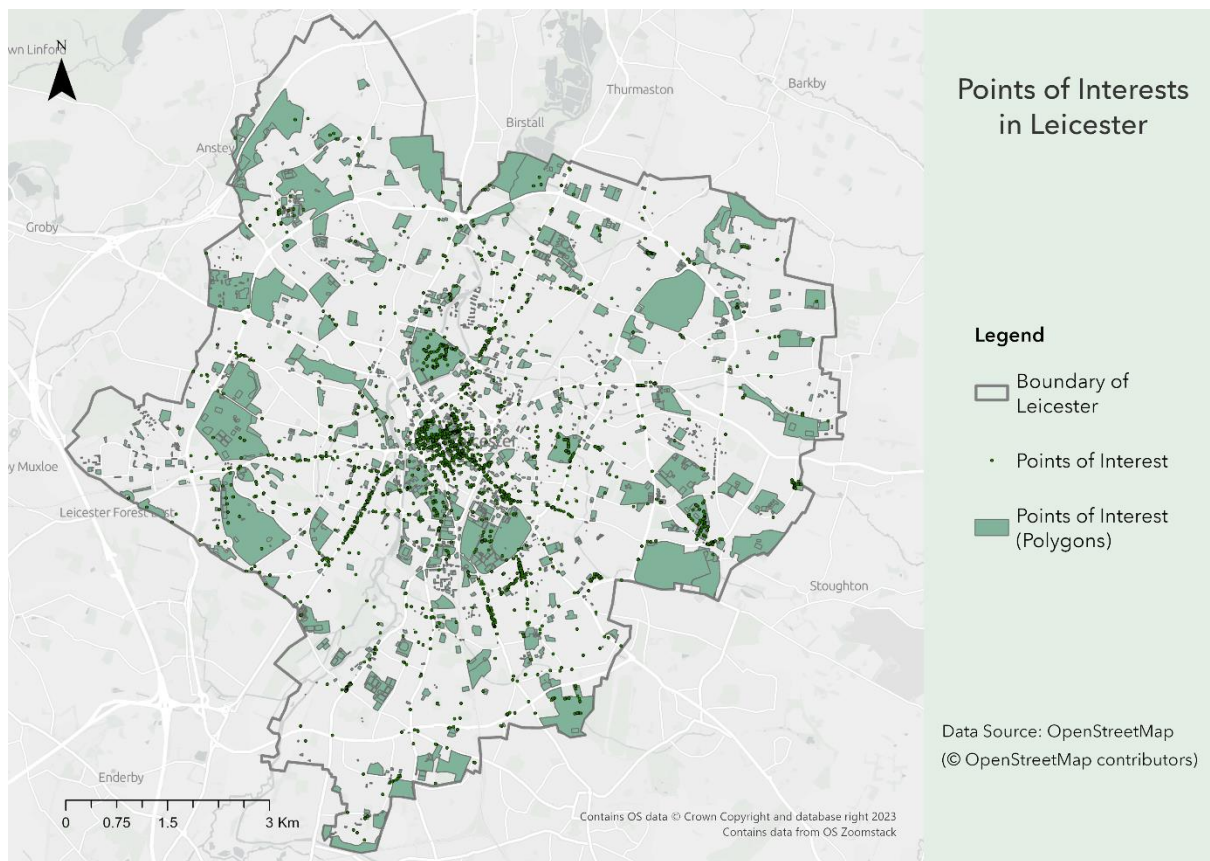


Figure C-1: Points of Interest in Leicester (Map scale: 1:60000).